

Susanne Kirchhof

Diels Alder Hydrogels as Intraocular Drug Delivery Systems for Antibodies

Diels Alder Hydrogels as Intraocular Drug Delivery Systems for Antibodies

DISSERTATION ZUR ERLANGUNG DES DOKTORGRADES
DER NATURWISSENSCHAFTEN (DR. RER. NAT.)
DER FAKULTÄT FÜR CHEMIE UND PHARMAZIE
DER UNIVERSITÄT REGENSBURG



vorgelegt von
Susanne Kirchhof
aus Bobingen

Juli 2015

Diese Arbeit entstand in der Zeit von August 2010 bis Juli 2015 am Lehrstuhl für Pharmazeutische Technologie an der Universität Regensburg.

Die Arbeit wurde von Herrn Prof. Dr. Achim Göpferich angeleitet.

Promotionsgesuch eingereicht am: 31. Juli 2015

Datum der mündlich Prüfung: 09. Oktober 2015

Prüfungsausschuss:

- Prof. Dr. Jens Schlossmann (Vorsitzender)
- Prof. Dr. Achim Göpferich (Erstgutachter)
- PD Dr. Rainer Müller (Zweitgutachter)
- Prof. Dr. Sigurd Elz (Drittprüfer)

Diels Alder Hydrogels as Intraocular Drug Delivery Systems for Antibodies

Die Wissenschaft fängt eigentlich erst da an, interessant zu werden, wo sie aufhört.

Justus von Liebig

Table of Contents

1	Introduction and Goal of the Thesis	1
1.1	Introduction.....	2
1.2	Goal of the thesis.....	4
2	Hydrogels in Ophthalmic Applications.....	9
2.1	Introduction.....	11
2.2	Methods of hydrogel preparation and properties of hydrogels	13
2.3	Design criteria for hydrogels and challenges associated with their preparation	15
2.4	Ophthalmic applications of hydrogels	16
2.4.1	In situ forming hydrogels for ophthalmic drug delivery.....	16
2.4.2	Drug-eluting contact lenses.....	18
2.4.3	Tissue adhesives for ocular wound repair	21
2.4.4	Intraocular lenses.....	22
2.4.5	Hydrogel-based vitreous substitutes	23
2.4.6	Intravitreal drug delivery systems	25
2.4.7	Cell-based approaches.....	27
2.5	Limitations of hydrogel-based drug delivery systems.....	29
2.6	Concluding remarks and future perspectives	31
3	Investigation of the Diels-Alder Reaction as a Cross-Linking Mechanism for Degradable Poly(ethylene glycol) Based Hydrogels.....	33
3.1	Introduction.....	35

3.2	Experimental Section	36
3.2.1	General procedure.....	36
3.2.2	Materials.....	36
3.2.3	Synthesis of branched PEG-amines	37
3.2.4	Synthesis of furyl-substituted four-armed PEG	37
3.2.5	Synthesis of furyl-substituted eight-armed PEG, molecular weight 10 kDa	38
3.2.6	Synthesis of furyl-substituted eight-armed PEG, molecular weight 20 kDa	38
3.2.7	Synthesis of 3,6-epoxy-1,2,3,6-tetrahydrophthalimide (ETPI).....	38
3.2.8	Synthesis of ETPI-substituted four-armed PEG	39
3.2.9	Synthesis of 4armPEG10k-maleimide	39
3.2.10	Synthesis of 8armPEG10k-maleimide	40
3.2.11	Synthesis of 8armPEG20k-maleimide	40
3.2.12	Preparation of Diels-Alder hydrogels.....	40
3.2.13	Rheological characterization of Diels-Alder hydrogels.....	41
3.2.14	Calculation of hydrogel network mesh size.....	41
3.2.15	Swelling and degradation of Diels-Alder hydrogels.....	42
3.3	Results and discussion.....	43
3.3.1	Synthesis of furyl- and maleimide-substituted PEG-derivatives	43
3.3.2	Rheological characterization of Diels-Alder hydrogels.....	43
3.3.3	Calculation of hydrogel network mesh size.....	46
3.3.4	Swelling and degradation of Diels-Alder hydrogels.....	48
3.4	Conclusion	51
4	New Insights into the Cross-Linking and Degradation Mechanism of Diels-Alder Hydrogels	53
4.1	Introduction.....	55
4.2	Experimental section.....	57
4.2.1	Materials.....	57
4.2.2	Hydrolytic stability of 8armPEG10k-maleimide.....	57
4.2.3	Rheological characterization of DA hydrogels.....	58
4.2.4	Swelling and degradation of DA hydrogels.....	58
4.2.5	Molecular modeling studies.....	59
4.2.6	Statistical analysis	59
4.3	Results and discussion.....	60
4.3.1	Hydrolytic stability of 8armPEG10k-maleimide.....	60
4.3.2	Rheological characterization of DA hydrogels.....	61
4.3.3	Swelling and degradation of DA hydrogels.....	64

4.3.4	Molecular modeling studies.....	67
4.4	Conclusion.....	70
5	Diels-Alder Hydrogels for Controlled Antibody Release: Correlation between Mesh Size and Release Rate	71
5.1	Introduction.....	73
5.2	Materials and methods	74
5.2.1	Materials.....	74
5.2.2	Swelling studies.....	75
5.2.3	Rheological characterization.....	76
5.2.4	Low field NMR measurements.....	76
5.2.5	In vitro release of fluorescein isothiocyanate-labeled dextran	78
5.2.6	In vitro release of bevacizumab.....	78
5.3	Results and discussion.....	79
5.3.1	Determination of the network mesh size.....	79
5.3.2	In vitro release of fluorescein isothiocyanate labeled dextran.....	86
5.3.3	In vitro release of bevacizumab.....	90
5.4	Conclusion.....	91
6	Diels-Alder Hydrogels with Enhanced Stability: First Steps Towards Controlled Release of Bevacizumab.....	93
6.1	Introduction.....	95
6.2	Materials and methods	97
6.2.1	General procedure.....	97
6.2.2	Materials.....	97
6.2.3	Synthesis of macromonomers.....	97
6.2.4	Hydrolytic stability of maleimides.....	98
6.2.5	Kinetics of the Diels-Alder reaction	98
6.2.6	Characterization of Diels-Alder hydrogels.....	99
6.2.7	In vitro release of bevacizumab.....	99
6.2.8	Statistical analysis	100
6.3	Results and discussion.....	100
6.3.1	Synthesis of macromonomers.....	100
6.3.2	Hydrolytic stability of maleimides.....	101
6.3.3	Gelation kinetics of Diels-Alder hydrogels.....	102
6.3.4	Rheological characterization of Diels-Alder hydrogels.....	105
6.3.5	Determination of the average mesh size.....	106

6.3.6 Swelling and degradation of Diels-Alder hydrogels.....	107
6.3.7 In vitro release of bevacizumab.....	109
6.4 Conclusion.....	111
6.5 Supplements.....	112
6.5.1 Synthesis of 8armPEG20k-NH ₂ (1), 8armPEG20k-Fur (2a) and 8armPEG20k-Mal (2b).....	112
6.5.2 Synthesis of compound 3.....	112
6.5.3 Synthesis of compound 4.....	113
6.5.4 Synthesis of compound 8armPEG20k-Ahx-Fur (5a).....	114
6.5.5 Synthesis of compound 8armPEG20k-Ahx-Mal (5b).....	114
6.5.6 Synthesis of compound 6.....	115
6.5.7 Synthesis of compound 7.....	115
6.5.8 Synthesis of compound 8.....	116
6.5.9 Synthesis of compound 9.....	116
6.5.10 Synthesis of compound 8armPEG20k-Lys-Ahx-Fur ₂ (10a).....	117
6.5.11 Synthesis of compound 8armPEG20k-Lys-Ahx-Mal ₂ (10b).....	117
7 Summary and Conclusion.....	119
7.1 Summary.....	120
7.2 Conclusion and outlook.....	122
References.....	125
List of Figures.....	153
List of Schemes.....	155
List of Tables.....	157
Appendix.....	158

Chapter 1

Introduction and Goal of the Thesis

1.1 Introduction

In recent years, the therapeutic use of antibodies has become a powerful new treatment option for various serious diseases including asthma, rheumatoid arthritis, Crohn's disease, different types of cancer and wet age related macular degeneration (AMD) [1–5]. Since the market launch of the first antibody muromonab-CD3 in 1986, the number of therapeutically successful antibodies has increased continuously. Nowadays, antibodies, antibody fragments, conjugates, and fusion proteins represent the most important and valuable product class within the biopharmaceutical market. These antibody products can be applied either systemically or locally. Although the systemic application of antibodies is associated with several disadvantages, including high dosing and severe side effects, most antibodies are currently administered by intravenous injections. The mentioned drawbacks can be overcome by local application in order to achieve higher drug concentrations at the application site. This results in lower required drug dosages and improved therapeutic effects. Moreover, the systemic antibody exposure is reduced causing less systemic side effects. Currently, a variety of potential, local antibody application sites are investigated or have already been established. For instance, antibodies are directly administered at the tumor site for anti-cancer application, are intraarticularly injected for the treatment of arthritic joint diseases or are being used to minimize or even cure injuries of the central nervous system after intrathecal delivery [6–8]. The most used method for local antibody delivery is the intravitreal administration of anti-vascular endothelial growth factor (VEGF) antibodies for the therapy of diseases at the posterior segment of the eye, such as AMD and proliferative diabetic retinopathy (PDR) [5,9]. In this case the blood-retina-barrier represents an insurmountable obstacle for the systemic application of macromolecules, such as antibodies. Thus, intraocular injections are essential for a successful antibody therapy (Figure 1.1).

However, there are several limitations minimizing the success of those strategies: short drug residence times at the application site and hence frequent antibody administration as well as side effects of injections, such as pain and inflammation, reduce the compliance [10]. Consequently, suitable drug delivery systems for sustained antibody delivery are required to overcome these limitations and enable more effective therapies [11]. During the last decades different types of drug delivery systems based on

microparticles, nanoparticles, liposomes and hydrogels were investigated [12,13]. These drug delivery systems lower drug dosage and enhance drug efficacy while reducing systemic side effects.

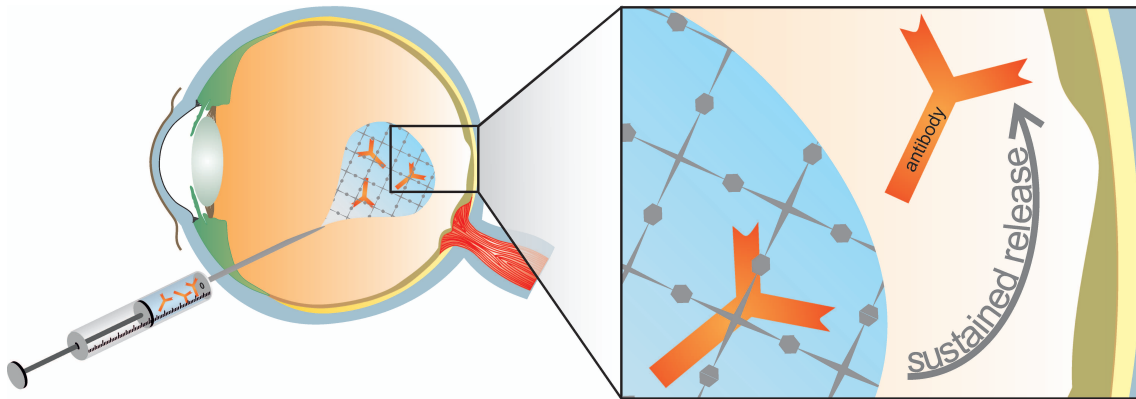


Figure 1.1. Sustained release of entrapped antibodies at the posterior segment of the eye after intraocular injection of an *in situ* gelling hydrogel.

The use of hydrogels for antibody delivery offers several advantages, such as reduced antibody degradation [13,14]. Generally, hydrogels are regarded to be biocompatible because of their high water content and soft nature similar to the extracellular matrix. Their porous structure is extremely suitable to accommodate high loads of water-soluble proteins either by post-fabrication partitioning or *in situ* encapsulation [14,13]. The simple preparation procedures in aqueous medium at room temperature contribute to preserving protein stability. Moreover, the entrapped antibodies have limited mobility in hydrogel networks with high cross-linking density resulting in sustained release controlled by the swelling and degradation behavior of the gels. Finally, *in situ* gelling hydrogels can be easily injected and form drug delivery systems at the application site.

Important for the success of the system is a precise control over the cross-linking density and hence the mechanical properties, the swelling capacity, the degradation behavior of the hydrogel and the release profile of entrapped antibodies [15]. However, it is more or less impossible to obtain a defined network structure through widespread radical photopolymerization [16]. Moreover, the use of photoinitiators generates free radicals during cross-linking, which may induce toxicity and affect the bioactivity and availability of proteins [14,17,18]. Additionally, a lower cross-linking conversion due to un-reacted functional groups and network non-idealities may negatively influence antibody release. Therefore, alternative cross-linking reactions have to be developed for the successful utilization of antibody release systems based on hydrogels. An appropriate reaction

should occur in water at body temperature without using any catalyst or initiator. A cross-linking reaction that meets the criteria is the Diels-Alder (DA) click reaction. This [4 + 2] cyclo-addition is a highly effective reaction between electron-rich diens and dienophiles. Despite being widely used in organic chemistry for the synthesis of steroid hormones and six-membered rings, its application for hydrogel preparation is less common [19,20]. Nevertheless, few examples have been described in literature using natural polymers in combination with relatively short cross-linkers, which results in rather undefined networks [21,22]. Although natural polymers are regarded to be non-toxic and principally biodegradable, they are less suitable for hydrogel preparation due to their non-reproducible chemical and physical properties. Therefore, synthetic polymers are favored for hydrogel preparation. Especially hydrogels based on poly(ethylene glycol) (PEG) are widespread because of their favorable polymer properties, such as high solubility, excellent biocompatibility and broad acceptance by regulatory agencies [14,23].

1.2 Goal of the thesis

This thesis is focused on the development and characterization of DA hydrogels as injectable drug delivery system for the intraocular application of antibodies.

Currently, hydrogels are already used for a number of different applications in ophthalmology. For instance, they are used as *in situ* gelling eye drops, soft contact lenses (SCL), intraocular lenses (IOL) and adhesives for ocular wound repair or are investigated as vitreous substitutes and intravitreal drug delivery systems (**Chapter 2**). Although significant progress has been made in the field of SCL, *in situ* gelling eye drops and adhesives for ocular wound repair, many challenges remain to improve the safety and clinical performance of intraocularly applied hydrogels. More research is particularly needed to improve hydrogels as intravitreal drug delivery systems for the treatment of severe, vision-threatening diseases, such as AMD or PDR.

There are a number of general requirements that intraocularly applied hydrogels must fulfill. Ideally, these hydrogels are injectable and offer sustained drug release over several weeks. So-called *in situ* gelling hydrogels, which are injected prior to gelation and form a semi-solid drug depot at the application site, offer such characteristics. After gelation the mechanical properties of the resulting hydrogel should be comparable to those of the environment in order to cause no foreign body sensation. Moreover, the hydrogel should be designed for simple and effective drug loading procedures, especially for proteins and

antibodies. Therefore, suitable cross-linking processes are necessary to permit fast gelation without inactivating the entrapped proteins. Besides appropriate loading procedures, a complete, yet sustained release of still active drugs is of particular importance. One of the main challenges of hydrogels is the control of drug release over several weeks due to their high water content. After complete drug release, the hydrogel should degrade without releasing any toxic degradation product. Although, a multitude of polymers and cross-linking possibilities have already been tested, there is no product commercially available until today. Promising materials are chemically cross-linked PEG-based hydrogels. Due to their excellent biocompatibility they are used for several biomedical applications. As *in situ* gelling systems they can be easily injected by minimally invasive techniques and hold great promise as drug delivery systems. Nevertheless, most established cross-linking mechanisms are associated with significant disadvantages, such as the formation of potentially harmful radicals or unwanted side reactions with incorporated protein drugs.

To overcome these limitations, new cross-linking reactions for PEG-based hydrogels have to be developed. Since the DA reaction proceeds in water without any initiator or metal catalyst, it is considered as an effective and non-toxic cross-linking possibility (**Chapter 3**). For the hydrogel preparation, two complementary macromonomers were synthesized by functionalizing star-shaped PEG with furyl and maleimide groups (Figure 1.2).

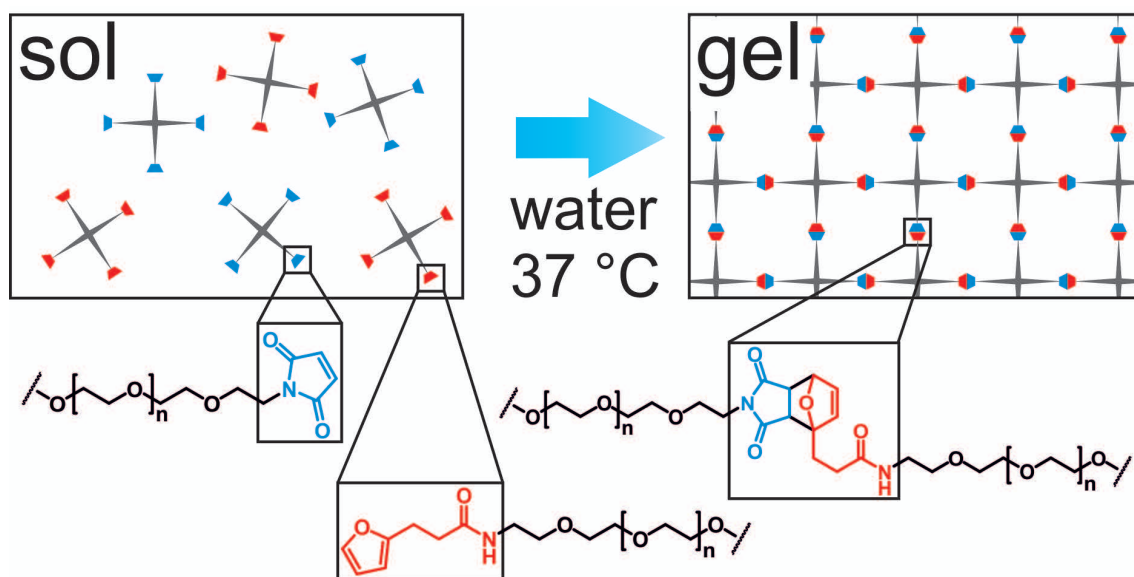


Figure 1.2. Principle of DA reaction for *in situ* hydrogel formation. Furyl- and maleimide functionalized star shaped PEG were dissolved in water and combined, e.g. by using a two-chamber syringe. Directly after mixing both components the formation of highly elastic hydrogels is initiated.

The influence of the macromonomer concentration, molecular weight and branching factor on gel characteristics, such as rheology and swelling behavior, were investigated. Surprisingly, the covalently cross-linked hydrogels dissolved within days to weeks. To investigate this unexpected degradation behavior of PEG-based DA hydrogels in detail, further experiments were performed (**Chapter 4**). UV spectroscopy was used to analyze the hydrolytic stability of maleimide functionalized star-shaped PEG as a function of temperature and pH. Finally, molecular modeling studies of DA and retro-Diels-Alder (rDA) moieties were performed to investigate the influence of these reactions for the degradation process.

Besides the degradability, the permeability of entrapped drugs, such as proteins or antibodies, is crucial for success or failure of the system. The mesh size or correlation length ξ is an important parameter that characterizes the permeability. It is defined as “the average distance between consecutive cross-links” and indicates the maximum size of solutes that can pass through the gel network. In **Chapter 5** swelling studies, rheology and low field NMR spectroscopy were used to calculate ξ of the prepared DA hydrogels. The knowledge of ξ , in combination with the size of the entrapped molecule, allows the estimation of the drug release rate and the evaluation of the general suitability of the resulting hydrogels for controlled release of entrapped, therapeutic antibodies. As a proof of concept, fluorescein-labeled dextrans of different molecular weight were entrapped into the hydrogel and release studies were performed. Finally, the data of those *in vitro* studies were compared to theoretical predictions.

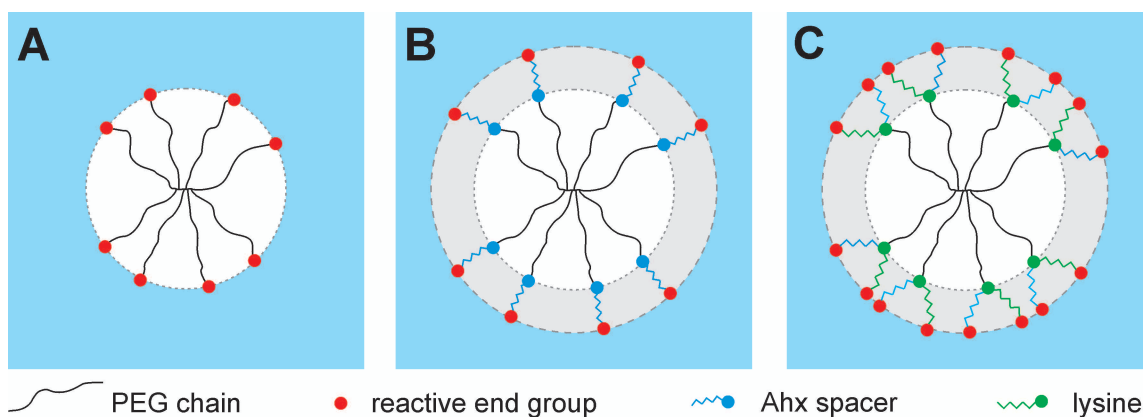


Figure 1.3 Modification of eight-armed PEG (A) by introducing Ahx spacer between PEG and reactive end-groups to increase hydrolytic stability (B). Modification with Lys and Ahx yields in doubled number of reactive end-groups and increased hydrolytic stability (C).

However, slow gelation and comparatively fast degradation may limit the application of DA hydrogels as injectable drug delivery systems. To overcome these limitations the macromonomers were modified with lysine (Lys) and/or 6-aminohexanoic acid residues (Ahx) in order to increase the hydrolytic stability of maleimide and to double the number of reactive groups per macromonomer (**Chapter 6**) (Figure 1.3).

To prove the feasibility of the optimized DA hydrogels as drug delivery systems, the gels were loaded with bevacizumab, a VEGF-neutralizing antibody used in the treatment of AMD. Afterwards, the release profiles of the entrapped antibody were determined by fluorescence spectroscopy.

Chapter 2

Hydrogels in Ophthalmic Applications

This chapter was published as: S. Kirchhof, A. M. Goepferich and F. P. Brandl, *Eur. J. Pharm. Biopharm.* (2015), doi: [org/10.1016/j.ejpb.2015.05.016](https://doi.org/10.1016/j.ejpb.2015.05.016)

Abstract

More and more people worldwide are affected by severe eye diseases eventually leading to visual impairment or blindness. In most cases, the treatment involves the application of ophthalmic dosage forms such as eye drops, suspensions or ointments. Unfortunately, some of the therapeutic approaches have major shortcomings, especially in the treatment of the posterior segment of the eye, where many vision-threatening diseases originate. Therefore, research focuses on the development of new materials (e.g., for vitreous substitution) and more advanced drug delivery systems. Hydrogels are an extremely versatile class of materials with many potential applications in ophthalmology. They found widespread application as SCL, foldable IOL, *in situ* gelling formulations for ophthalmic drug delivery and ocular adhesives for wound repair; their use as vitreous substitutes and intravitreal drug delivery systems is currently under investigation. In this article, we review the different applications of hydrogels in ophthalmology with special emphasis placed on the used polymers and their suitability as ocular drug delivery systems.

2.1 Introduction

More and more people worldwide are affected by severe eye diseases, such as glaucoma, PDR and AMD [24–27]. Without adequate treatment, these diseases will eventually lead to severe visual impairment or blindness. Today, two major strategies for the treatment and management of ocular disorders can be identified: (1) the attempt to specifically deliver drug molecules to diseased ophthalmic tissues and (2) surgical procedures to repair or replace damaged tissues, such as the lens or the vitreous body [28–30]. Unfortunately, most currently available therapeutic approaches have major shortcomings, especially in the treatment of the posterior segment of the eye, where most vision-threatening diseases originate. The main challenges are as follows: (1) poor adherence of patients to the currently available therapeutic regimens, (2) maintaining effective drug levels over extended time periods and extending the required dosing intervals, (3) the delivery of drug molecules to the posterior segment of the eye, (4) the administration of therapeutic proteins and nucleic acids, and (5) the repair or substitution of dysfunctional cells or tissues. For example, over 50% of 500 surveyed glaucoma patients were found to be either non-adherent to their therapeutic regimens or demonstrated improper administration techniques [31]. While patients can be educated on the importance of adherence and instructed on proper eye drop administration, the inherent shortcomings of eye drops, such as low ocular bioavailability of the applied drug, are less easy to overcome. For example, it has been shown that less than 5% of the administered dose reaches the target tissue due to drainage and limited corneal permeability [32–34]. Moreover, only the anterior segment of the eye can be treated by eye drop installation, whereas different application routes (e.g., intravitreal injections) and/or more complex drug delivery systems (e.g., intraocular implants) may be required to reach the posterior segment [35–38]. For example, the development of anti-VEGF drugs, such as monoclonal antibodies or antibody fragments, revolutionized the therapy of neovascular AMD and other vision-threatening diseases [5,9,39]. However, the required intravitreal injections are associated with significant discomfort and complications including endophthalmitis, retinal tears or detachment, and cataract [10]. It is obvious that sustained delivery systems for anti-VEGF drugs would make the current therapeutic regimens more patient-friendly and cost-effective.

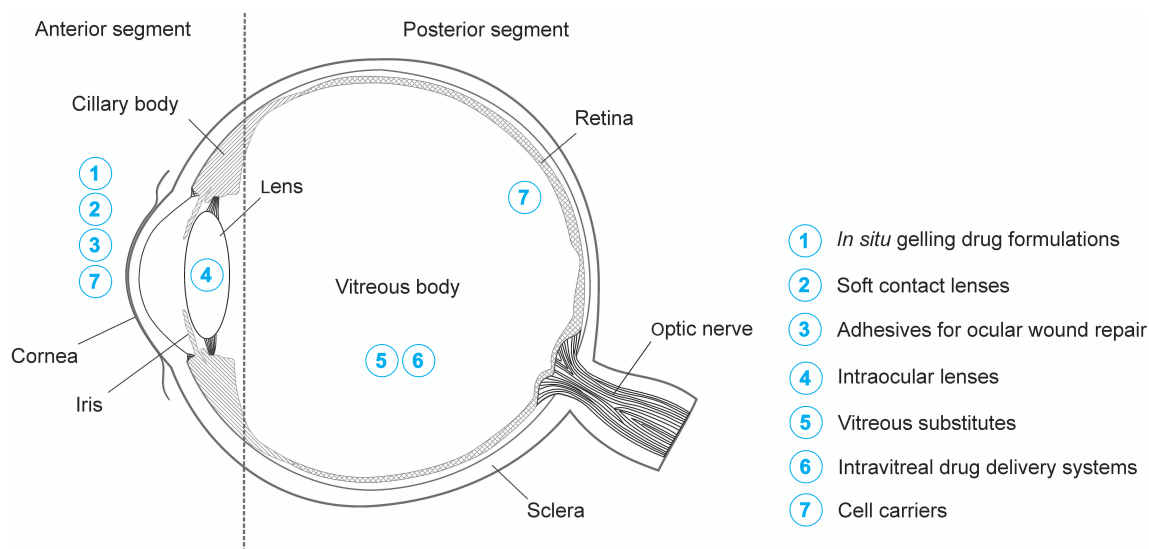


Figure 2.1. Application sites of hydrogels in ophthalmology.

The given examples illustrate the need for new developments in the field of ophthalmic drug delivery, and indicate the great market potential of those drug delivery systems. Compared to the different materials and dosage forms that have been developed for ophthalmic applications, such as colloidal drug delivery systems [40–42] or polymeric implants [43], hydrogels may offer several advantages. For example, the mild preparation conditions and high water content of hydrogels are beneficial in preserving the activity of biopharmaceuticals such as peptides, proteins or nucleic acids [13,14,44]. Moreover, many hydrogels, such as temperature-responsive or *in situ* chemically cross-linked systems, can be administered by minimally invasive methods [13,14,44,45]. Hydrogels have already been approved for several ophthalmic applications, with many more currently being under investigation. For instance, they are successfully marketed as corrective SCL [46], foldable IOL [47,48], or *in situ* gelling vehicles for ophthalmic drug delivery [49,50]. Most research efforts currently aim at improving existing formulations for antibiotics, anti-inflammatory drugs or β -blockers, or at developing sustained release formulations for therapeutic proteins and nucleic acids. Furthermore, hydrogels are investigated as adhesives for ocular wound repair [51] or potential vitreous substitutes [29,30]. A graphical overview on possible ophthalmic applications of hydrogels is given in Figure 2.1.

In most of these applications, hydrogels are used because of their favorable physicochemical properties (e.g., transparency, high water content, and mechanical flexibility) or in combination with active pharmaceutical ingredients. In this review article, we present a general overview on ophthalmic applications of hydrogels with

special emphasis on drug delivery systems for the posterior segment of the eye. We particularly focus on the different gel-forming polymers, the physicochemical properties of the resulting hydrogels, and the challenges associated with the preparation of hydrogel-based drug delivery systems. Recent developments in the field of ophthalmic drug delivery are presented and critically reviewed regarding the potential therapeutic benefits.

2.2 Methods of hydrogel preparation and properties of hydrogels

Before discussing the diverse applications of hydrogels in ophthalmology, a short review on the different methods of hydrogel preparation will be presented along with an overview on the characteristic properties of hydrogels. According to the definition by the International Union of Pure and Applied Chemistry, a hydrogel is a polymer network that is expanded throughout its whole volume by water [52]. A wide range of natural, semisynthetic and synthetic polymers can be used as starting materials for hydrogels. Typical examples for polymers of natural origin include alginate, collagen, and hyaluronic acid (HA) (Figure 2.2). PEG, poly(vinyl alcohol) (PVA), polymers based on acrylate monomers, and siloxanes are important examples for synthetic gel-forming materials (Figure 2.3) [13,44,53–55].

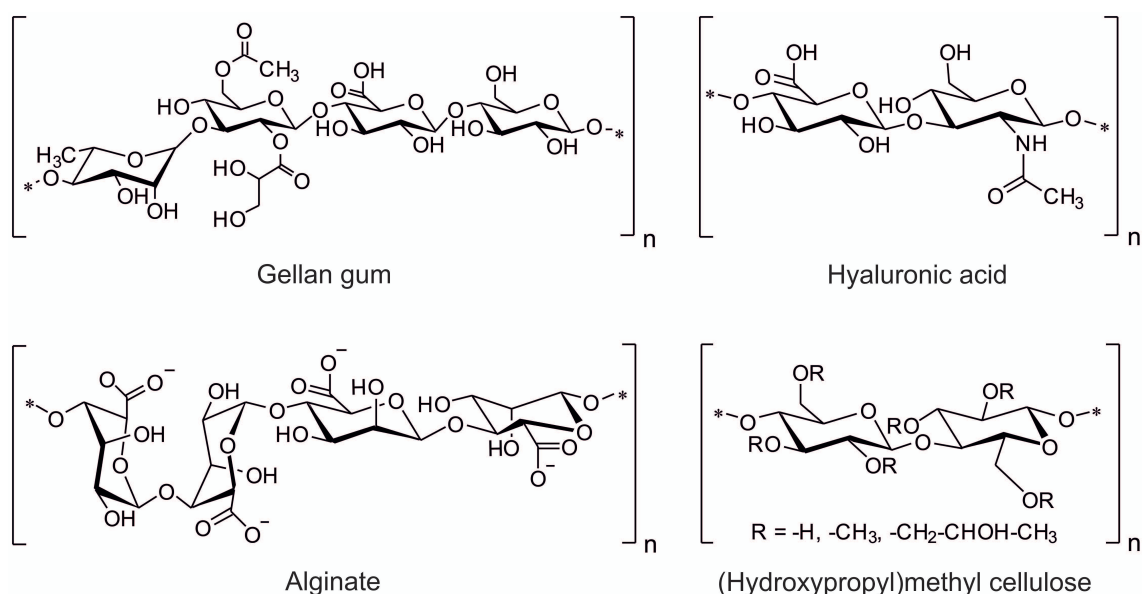


Figure 2.2. Chemical structures of selected polymers from natural sources commonly used for the preparation of hydrogels.

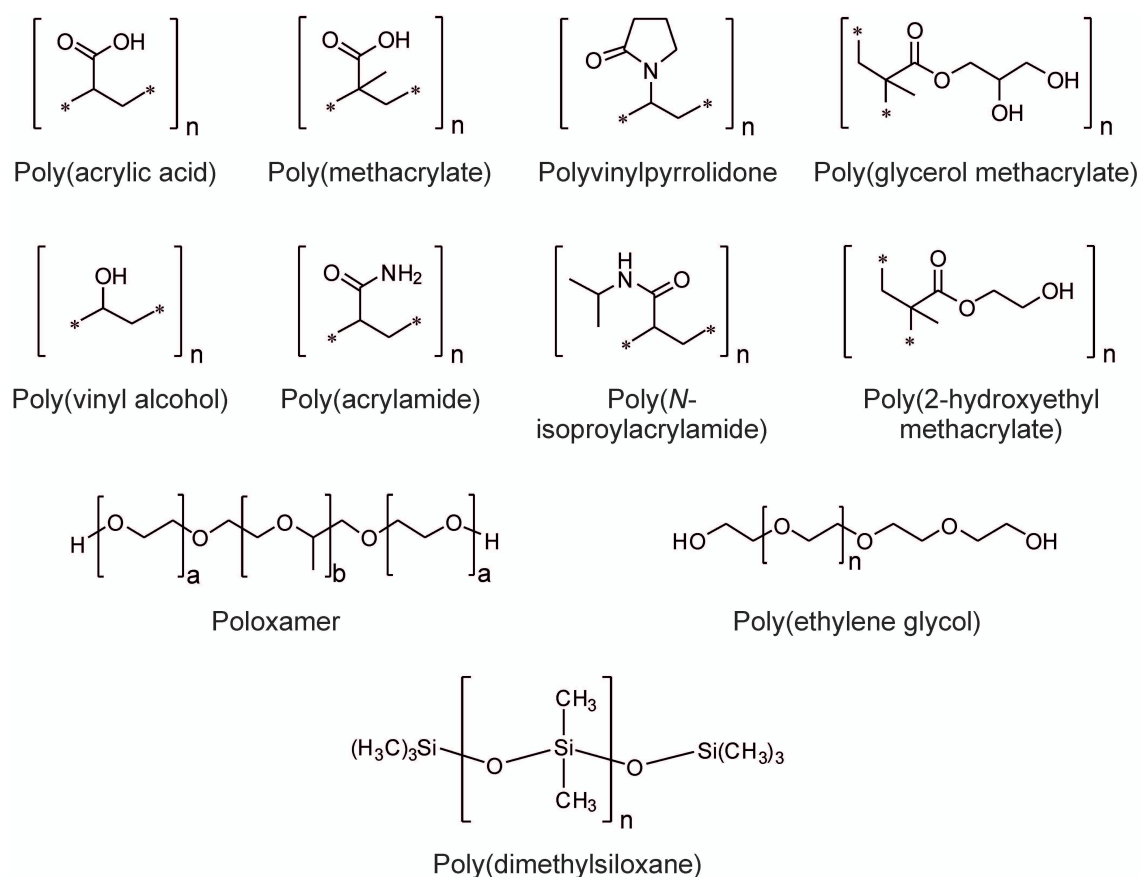


Figure 2.3. Chemical structures of synthetic polymers commonly used for the preparation of hydrogels.

Polymers of natural origin usually have the advantage of being non-toxic and biodegradable. Furthermore, natural polymers often interact with proteins and cells through non-specific or specific binding, which can be desired in hydrogel-based sustained release systems or cell carriers. However, hydrogels made from natural polymers may suffer from weak mechanical strength, high batch-to-batch variability, and immunogenicity. Synthetic polymers, on the other hand, allow for the preparation of hydrogels with well-defined network architecture, tunable mechanical properties, and prolonged stability. However, many synthetic polymers, such as PEG or PVA, do not inherently interact with proteins or cells; furthermore, biocompatibility and biodegradability must be carefully evaluated.

Hydrogels can be further classified into physical and chemical gels, depending on how the polymer networks are formed [13,44,53–55]. In physical or reversible hydrogels, the networks are formed by physical aggregation of polymer chains, caused by molecular entanglements, hydrogen bonds, hydrophobic interactions, ionic bonding, or complexation. All of these interactions are reversible, and the stability of the formed hydrogels is susceptible to changes in the ionic strength, pH, temperature, or the application of mechanical stress. Chemical or permanent hydrogels, on the other hand,

contain covalently cross-linked polymer networks with tunable physicochemical properties such as equilibrium water content, permeability, mechanical strength, and degradability. Covalently cross-linked networks can be formed by radical polymerization of water-soluble monomers (e.g., 2-hydroxyethyl methacrylate or acrylamide) and suitable cross-linking agents (e.g., PEG diacrylate or bisacrylamide). Alternatively, pre-formed polymers (e.g., HA or star-shaped PEG) can be functionalized with reactive groups suitable for polymerization and cross-linked via Schiff base formation, Michael-type addition reaction, azide-alkyne cycloaddition, or DA reaction [13,14,44,45,56]. For a more comprehensive overview on the different hydrogel-forming polymers and cross-linking mechanisms, the reader is referred to several excellent review articles [13,14,44,45,53–56].

2.3 Design criteria for hydrogels and challenges associated with their preparation

Cross-linked hydrogels are extremely versatile materials with many favorable properties such as transparency, high water content, good biocompatibility and mechanical flexibility. Consequently, hydrogels found widespread application in ophthalmology as SCL, foldable IOL, *in situ* gelling vehicles for ophthalmic drug delivery, and adhesives for ocular wound repair; their use as vitreous substitutes and intravitreal drug delivery systems is currently under investigation. All ophthalmic formulations must meet strict requirements regarding sterility and biocompatibility; however, the biocompatibility standards for topically or intraocularly applied hydrogels may be different. Besides these fundamental requirements, hydrogels used in ophthalmology must meet further criteria, which often depend on their specific applications. In the following section, we will discuss general design criteria for hydrogel-based drug delivery systems such as *in situ* forming hydrogels for topical drug delivery, drug-eluting SCL and intravitreal drug delivery systems. Design criteria for specific applications, such as ocular wound repair, vitreous substitution or cell transplantation, are separately discussed later in this article. When developing hydrogels for ophthalmic drug delivery, two major design criteria can be identified: availability and stability of the active ingredients [13,14,44]. Availability relates to the capability of delivering therapeutics at the right dosage; it depends on the method of drug loading, the type and molecular weight of the polymer, the polymer concentration, the cross-linking density, the hydrogel degradation rate, and the affinity of

the payload for the carrier. The stability of the active ingredients is again influenced by the method of drug loading, the type of the polymer, the cross-linking mechanism, the type and concentration of the initiator, and the use of stabilizing agents. Drugs can be loaded into hydrogels by incubating cross-linked gels in concentrated drug solutions (post-fabrication partitioning) or by *in situ* encapsulation, a method in which drug loading and cross-linking are carried out simultaneously [14]. The former method has the advantage of preserving drug stability, but offers less control over the amount of drug loading. On the other hand, *in situ* encapsulation permits the preparation of hydrogels loaded with large quantities of drugs in a fast and reproducible way. However, the polymerization reaction may induce undesired reactions between the encapsulated molecules and the polymer network, which negatively affects drug availability and stability [13,14,17,44]. Aside from the above-mentioned methods, drugs can be incorporated within gel matrices through tethering via pH- or enzyme-sensitive linkers, or through the addition of drug-loaded micro- or nanoparticles [13,14,44,57]. The drug release rate is mostly defined by the molecular weight of the active ingredient, the polymer concentration, the cross-linking density of the hydrogel, and the affinity of the active ingredient for the polymer network [13,14,44,58,59]. For example, the release of synthetic drugs, peptides, and small proteins is often diffusion-controlled. On the other hand, the release of large proteins, such as whole antibodies, may be swelling-controlled or chemically controlled if the gel matrix degrades. The release kinetics can be modulated to some degree by varying the concentration of the gel-forming polymers, by carefully adjusting the cross-linking density, by varying the molecular weight of the gel-forming polymers, or by altering the degradation rate. However, it should be kept in mind that this process may also change other parameters of the drug delivery system such as mechanical properties, biocompatibility, and drug stability.

2.4 Ophthalmic applications of hydrogels

2.4.1 In situ forming hydrogels for ophthalmic drug delivery

Liquid ophthalmic formulations usually show low bioavailability because of constant lachrymation and fast nasolacrimal drainage [34,60]. As a result, short dosing intervals and high drug concentrations are needed to reach effective therapeutic levels. This may result in non-adherence of patients [31]; moreover, absorption of the drug drained through

the nasolacrimal canal may cause systemic side effects. To extend the precorneal residence time of the applied therapeutics, various vehicles, such as suspensions, ointments and inserts, have been developed [38,40,42,61]. Even though some improvements over conventional liquid dosage forms have been reached, these drug delivery systems did not become widely accepted because of blurred vision and foreign body sensation. With regard to patient acceptability, liquid dosage forms that remain in contact with the cornea and sustain drug release over extended periods of time would be ideal. Such a behavior can be achieved by delivery systems that show a sol-gel phase transition due to changes in the pH, temperature, or ionic strength [38,49,50]. These *in situ* forming hydrogels are instilled in liquid form and shift to the gel phase once in the cul-de-sac of the eye. Cellulose acetate phthalate, which was first introduced in the 1980s, and poly(acrylic acid) (PAA, Carbomer, or Carbopol®) are among the polymers that reversibly gel in response to variations in the pH [62–65]. PAA exhibits a distinct sol-gel phase transition as the pH of the solution is raised above its pKa of about 5.5. Viscosity enhancing polymers, such as (hydroxypropyl)methyl cellulose (HPMC), can be added to reduce the irritant effect of highly concentrated PAA hydrogels [66,67]. Alternatively, temperature-responsive polymers, such as poloxamers (Pluronic®), poly(*N*-isopropylacrylamide) (PNIPAAm), or polysaccharides, can be used to develop *in situ* gelling formulations. Poloxamers are triblock copolymers composed of a hydrophobic poly(propylene oxide) central block flanked by two hydrophilic poly(ethylene oxide) blocks; they exhibit a reversible sol-gel phase transition, with the phase transition temperature depending on the concentration, molecular weight and poly(ethylene oxide) : poly(propylene oxide) weight ratio. Poloxamer-based formulations were evaluated in multiple studies; the developed systems provided sustained release of timolol and pilocarpine over several hours [68–70]. The combination of pH and temperature-responsive polymers is another promising approach to formulate *in situ* gelling delivery systems. For example, Lin and Sung [71] showed that physical mixtures of 0.3% Carbopol® and 14% Pluronic® F-127 gave *in situ* forming hydrogels. A similar formulation was shown to provide sustained release of puerarin over 8 h [72]. In addition to physical mixtures of poloxamers and PAA, graft copolymers of Pluronic® F-127 and PAA were proposed as *in situ* gelling vehicles for ophthalmic drug delivery [73]. Aqueous solutions of PNIPAAm also show a temperature-dependent sol-gel phase transition and may have therapeutic benefits in the treatment of glaucoma [74]. Cao *et al.* [75] developed a novel PNIPAAm-chitosan copolymer for potential use in ophthalmic

drug delivery. In comparison with conventional timolol eye drops, the *in situ* gelling formulation showed improved pharmacokinetic parameters such as maximum plasma concentration (C_{max}), time to reach C_{max} , and area under the curve; it had a stronger capacity to reduce the intraocular pressure over a period of 12 h. Besides PAA, poloxamer and PNIPAAm-based formulations, temperature-responsive materials of natural origin have been investigated as potential alternative. For example, Miyazaki *et al.* [76] developed a temperature-sensitive system containing 1.5% xyloglucan for the sustained release of pilocarpine, which showed a miotic response similar to hydrogels containing 25% Pluronic® F-127. Despite this success, there are currently no pH or temperature-sensitive hydrogels approved for human use. Among all stimuli-responsive systems, hydrogels sensitive to the ionic strength are most widespread and have proven to be most successful. Aqueous solutions of certain polymers, such as gellan gum (Gelrite®) or alginate, form hydrogels after instillation into the conjunctival sac through the presence of cations in the tear fluid. Gellan gum is a linear, anionic heteropolysaccharide consisting of glucose, glucuronic acid and rhamnose [77]. A solution of 0.6% gellan gum was demonstrated to enhance the precorneal residence time and, hence, the bioavailability of timolol [78]. These formulations proved to be extremely successful and resulted in the approval of two products (Timoptol® XE and Timoptic® XE). Moreover, delivery systems based on gellan gum were developed for methylprednisolone [79], and the two antibiotics ciprofloxacin [80] and pefloxacin [81]. Similar to gellan gum, alginate forms hydrogels at physiological levels of cations. Alginate was used in combination with HPMC as viscosity-enhancing agent to develop sustained release systems for antibiotics [82,83]. The fluoroquinolone antibiotic gatifloxacin was released from alginate/HPMC hydrogels over a period of 8 h with excellent ocular tolerance [83]. Mixtures of gellan gum and alginate could further improve the bioavailability of matrine [84]. Furthermore, combinations of alginate and Pluronic® have been described for the ophthalmic delivery of pilocarpine [85].

2.4.2 Drug-eluting contact lenses

Corrective SCL are without doubt the most common and most successful commercial application of hydrogels. The idea of using poly(2-hydroxyethyl methacrylate) (pHEMA) hydrogels for corrective SCL was first reported in 1960 by Otto Wichterle [86]. Since that time, new developments have occurred and further improvements of existing materials have been made [46]. Selected hydrogel materials used for the manufacture of

corrective SCL are listed in Table 2.1. Most research efforts currently aim at improving the oxygen permeability and wearing comfort of SCL [87,88]. Another field of activity is the development of new polymers with antifouling properties to reduce the adsorption of proteins and cells on the lens surface [89]. This may help to improve the biocompatibility of SCL, especially during long-term wear. The second major innovation has been the development of poly(dimethyl siloxane) (PDMS) based lens materials (Table 2.2) [46]. These silicone hydrogels combine the extremely high oxygen permeability of PDMS and the wearing comfort of conventional pHEMA hydrogels. Besides their application as corrective lenses, SCL may serve as drug delivery system for the anterior segment of the eye [90–93], or as protective devices or “bandage lenses” for the treatment of corneal injuries [94]. Although there are currently no approved products on the market, the use of SCL as drug delivery system is an interesting yet challenging approach. The main challenge is to reach adequate levels of drug loading while ensuring controlled drug release at the same time. To achieve this goal, different possibilities of drug loading have been investigated. The applied techniques range from simply soaking the lenses in concentrated drug solutions to more sophisticated approaches such as molecular imprinting, piggybacking of drug-polymer films on SCL, loading with liposomes, surface modification with nanoparticles, and the use of ionic ligands [90–93]. Although most studies used commercial SCL, the development of new lens materials has been described as well. For example, Ribeiro *et al.* [95] reported the synthesis of bio-inspired pHEMA-based hydrogels for potential application as drug-eluting SCL. By copolymerizing HEMA, 4-vinylimidazole, and zinc methacrylate, hydrogels with high affinity for carbonic anhydrase inhibitors were obtained. In comparison with plain pHEMA hydrogels, the bio-inspired hydrogels showed a higher drug loading efficiency and 50% lower release rates for acetazolamide and ethoxzolamide. However, further aspects such as optical transparency, influence of the thickness on drug release, and long-term stability of the drug-polymer interactions, need to be studied to evaluate the applicability of bio-inspired hydrogels as drug-eluting SCL. The given example illustrates the challenges researchers face in the development of drug-eluting SCL. Even though well-established polymers are used, biocompatibility, transparency, and oxygen permeability of drug-loaded SCL have to be proven again. However, finding effective ways of drug loading and maintaining therapeutic drug concentrations over extended time periods are by far the greatest challenge. Exhaustive *in vitro* and *in vivo* studies will be required to prove the safety and efficacy of the developed drug delivery system.

Table 2.1. Conventional hydrogel materials used for the preparation of corrective SCL (Sources: USAN dictionary, data from the manufactures).

USAN ^a name	Main components	Water content / %	Dk value / barrers ^b	Examples of trade names
Etafilcon A	HEMA/SMA/TRIM	58	28	ACUVUE [®] 2 [®]
Hilafilcon B	HEMA/EGDMA/AMA/NVP	59	22	SofLens [®] 59
Nelfilcon A	PVA, partially acetalized with <i>N</i> -(formylmethyl)acrylamide	69	26	DAILIES [®] AquaComfort Plus [®]
Nesofilcon A	HEMA/NVP/EGDMA/AMA/PEPGDMA/TBHMA/MAEBTP	78	42	Biotrue [®] ONEday
Ocufilcon D	HEMA/MAA/EGDMA	55	20	Biomedics [®] 1 Day extra
Omafilcon A	HEMA/MPC/EGDMA	62	33	Proclear [®]
Polymacon B	HEMA/EGDMA	38	9	SofLens [®] 38

^a USAN: United States adopted name^b Dk represents the oxygen permeability (barrers = 10⁻¹¹ cm² O₂ s⁻¹ mmHg)

AMA: allyl methacrylate; EGDMA: ethylene glycol dimethacrylate; HEMA: 2-hydroxyethyl methacrylate; MAA: methacrylic acid; MAEBTP: 4-(2-methacryloyloxyethyl)-2-(2H-benzotriazol-2-yl)phenol; MPC: 2-methacryloyloxyethyl phosphorylcholine; NVP: *N*-vinylpyrrolidone; PEPGDMA: poly(ethylene propylene glycol) dimethacrylate; PVA: poly(vinyl alcohol); TBHMA: 4-tert-butyl-2-hydroxycyclohexyl methacrylate; SMA: sodium methacrylate; TRIM: 1,1,1-tris(hydroxymethyl)propane trimethacrylate

Table 2.2. Silicone hydrogels used for the preparation of corrective SCL (Sources: USAN dictionary, data from the manufactures).

USAN ^a name	Main components	Water content / %	Dk value / barrers ^b	Examples of trade names
Balafilcon A	PBVC/NCVE/TPVC/NVP	36	99	Pure Vision [®] 2
Galyfilcon A	mPDMS/SiGMA/HEMA/DMAA/EGDMA/NVP	47	60	ACUVUE [®] ADVANCE [®]
Lotrafilcon A	siloxane macromere/TRIS/DMAA	24	140	AIR OPTIX [®] Night & Day [®]
Lotrafilcon B	siloxane macromere/TRIS/DMAA	33	110	AIR OPTIX [®] AQUA
Narafilcon A	mPDMS/DMAA/HEMA/TEGDMA/NVP	46	100	1-DAY ACUVUE [®] TruEye [®]
Senofilcon A	mPDMS/SiGMA/HEMA/DMAA/TEGDMA/NVP	38	103	ACUVUE [®] OASYS [®]
Sifilcon A	siloxane macromere/DMAA/TRIS/styrene	32	82	AIR OPTIX [®] INDIVIDUAL

^a USAN: United States adopted name^b Dk represents the oxygen permeability (barrers = 10⁻¹¹ cm² O₂ s⁻¹ mmHg)

EGDMA: ethylene glycol dimethacrylate; DMAA: *N,N'*-dimethyl acrylamide; HEMA: 2-hydroxyethyl methacrylate; mPDMS: monofunctional polydimethylsiloxane; NCVE: *N*-carboxyvinyl ester; NVP: *N*-vinylpyrrolidone; PBVC: poly(dimethylsiloxyl)di-(silylbutanol)bis-(vinyl carbamate); SiGMA: methylbis-(trimethylsiloxy)silylpropylglyceryl methacrylate; TEGDMA: tetraethylene glycol dimethacrylate; TPVC: tris(trimethylsiloxy)silylpropylvinyl carbamate; TRIS: methacryloxypropyl tris(trimethylsiloxy silane)

2.4.3 Tissue adhesives for ocular wound repair

Another possible application for hydrogels is in the treatment of surgical or traumatic ocular wounds that are routinely sutured with thin nylon threads. Unfortunately, this standard treatment is associated with several disadvantages including infections, inflammation, corneal neovascularization, and impaired wound healing. To overcome the drawbacks of ocular sutures, tissue adhesives have been developed [96]. Tissue adhesives are materials, which are able to glue tissue surfaces together, either by mechanical adhesion or by forming chemical bonds. Soft and flexible hydrogels are among the most promising materials that are currently suggested as ophthalmic adhesives [97]. Many different polymers, either of natural or of synthetic origin, have been investigated for their suitability as ophthalmic sealants [51]. For example, hydrogels were prepared from polysaccharides, such as HA or chondroitin sulfate, gelatin, and different derivatives of PEG. The applied cross-linking reactions were, among other reactions, photoactivated processes and nucleophilic substitutions. For an optimal performance, ophthalmic adhesives must meet a number of requirements. Based on the available literature, Oelker and Grinstaff [51] defined essential design requirements for ideal ophthalmic adhesives, including leak pressure (> 80 mmHg), cross-linking time (< 30 s), mechanical properties (5–200 kPa), swelling ($< 200\%$), diffusion coefficient ($2 \cdot 10^{-7} \text{ cm}^2 \text{ s}^{-1}$), refractive index (1.32–1.40), adhesion strength (> 0.1 kPa), viscosity (5–100 cP), and degradation time (1 week–6 months). Very recently, the U.S. Food and Drug Administration approved ReSure[®] Sealant; the *in situ* forming hydrogel is based on PEG and trilycine amine, has a water content of approximately 90% after polymerization, and has been approved for sealing corneal incisions after cataract surgery. Although most tissue adhesives were developed for sealing corneal incisions, a few studies investigated their intraocular use in retinal detachment surgery [98–100]. Moreover, the possibility of incorporating drug molecules into hydrogel-based tissue adhesives has been studied. In particular, doxycycline-loaded hydrogels were investigated for the treatment of corneal injuries resulting from exposure to chemical warfare agents, such as sulfur mustard and nitrogen mustard [101,102]. In comparison with equally dosed doxycycline solutions, *in situ* forming doxycycline-loaded PEG hydrogels could improve epithelial healing in a vesicant-exposed corneal organ culture model [101]. In a follow-up study, rabbit corneas were exposed to sulfur mustard *in vivo*; the instillation of doxycycline eye drops resulted in faster edema reduction, but the hydrogels significantly reduced neovascularization [102]. In addition, hydrogels loaded with epidermal growth factor

(EGF) were developed for the treatment of corneal epithelial wounds. As a first proof of concept, Sheardown *et al.* [103] examined the effects of EGF on corneal epithelial wound healing in rabbits. Compared to control gels without EGF, the treatment with EGF-loaded PAA hydrogels resulted in significant wound healing enhancement. More recently, sustained release of EGF from chemically cross-linked cationized gelatin hydrogels has been reported [104]. The applied hydrogels gradually degraded over 1 week with concomitant release of EGF; the controlled release of EGF accelerated corneal epithelial wound healing in comparison with topically applied EGF solutions. Compared to physically cross-linked hydrogels, such as hydrogels based on gellan gum or alginate, these chemically cross-linked hydrogels are advantageous because they offer a much more prolonged drug release. Furthermore, high levels of drug loading can be reached, which is an advantage over drug-eluting SCL.

2.4.4 Intraocular lenses

In addition to these topical applications, hydrogels may also serve as IOL, vitreous substitutes, or intravitreal drug delivery systems. These intraocular applications are particularly relevant since most vision-threatening diseases, such as cataract, PDR or AMD, originate from the lens or the posterior segment of the eye. In cataract surgery, which is the most frequently performed eye surgery worldwide, the impaired lens is removed and subsequently substituted with an artificial IOL [28]. The first IOL were manufactured from rigid poly(methyl methacrylate). Today, more flexible materials, including hydrophobic acrylate polymers, hydrophilic acrylate polymers (i.e., hydrogels), siloxanes, and collamer (i.e., a copolymer of collagen and HEMA with a water content of 34%), are generally preferred [47,105]. These highly elastic materials are used to manufacture foldable IOL, which can be implanted through smaller incisions. The most frequent complication of cataract surgery is posterior capsule opacification (PCO), which has been associated with the abnormal proliferation of residual lens epithelial cells in the capsular bag [48]. As a consequence, several strategies to prevent PCO have been developed. For example, coating the lens surface with PEG or “bioactive” polymers exhibiting sulfonate and carboxylate groups could successfully prevent cell adhesion and proliferation [106,107]. Surface modification with porphyrins, which generate cytotoxic singlet oxygen, may also improve the biocompatibility of IOL [108]. Another approach to improve the biocompatibility of IOL and reduce the risk for PCO is the incorporation and controlled release of drug molecules. The available studies on drug-loaded IOL have

been reviewed in two recent articles; the different approaches were compared with regard to the administered drug molecules, the used drug loading method, and potential therapeutic benefits [109,110]. In general, there are three possibilities for drug loading: soaking the lens in concentrated drug solutions, coating of the lens surface (e.g., by spraying or chemical modification), and coating of the haptics that hold the lens in place. Apart from the optical portion, IOL are not required to be fully transparent. For example, the haptics can be coated with non-transparent polymers, drug suspensions, or molecules that stain certain regions of the lens material [109]. Such drug-loaded IOL may have potential benefits in the prevention of endophthalmitis, a frequent complication of cataract surgery; they may prevent postoperative inflammation and reduce the risk for PCO. Nevertheless, there are no products approved for human use at the moment.

2.4.5 Hydrogel-based vitreous substitutes

Besides cataract, severe vitreoretinal diseases, such as diabetic retinopathy or retinal detachment, affect more and more people in industrialized nations. After surgical intervention and removal of the dysfunctional vitreous, the injection of vitreous substitutes may be required, either for short-term or for long-term treatment. Because of the complex function of the vitreous and delicate nature of the intraocular environment, potential vitreous substitutes have to meet particular requirements [111]. An ideal vitreous substitute should (1) be clear and transparent, (2) be biologically and chemically inert, (3) possess a refractive index and density comparable to those of the natural vitreous, (4) possess sufficient mechanical rigidity, (5) allow the transfer of metabolites, (6) be non-absorbable and non-biodegradable, (7) be hydrophilic, and (8) be injectable through small-gauge needles. At the moment, various materials are used in clinical practice, including gases (e.g., air, sulfur hexafluoride or perfluoropropane), perfluorocarbon liquids, fluorosilicone, and silicone oils [29,111–114]. However, none of these substances are ideal for long-term or permanent vitreous substitution due to their fast intraocular absorption, toxic reactions or other adverse effects, such as the formation of post-operative cataract or glaucoma. Therefore, alternative vitreous substitutes, based on natural, semisynthetic and synthetic polymers, have been investigated; the tested polymers included HPMC [115], ADCON-L [116], HA/gellan gum [117], pHEMA [118], poly(glycerol methacrylate) [119] Pluronic® [120], siloxanes [121], PVA [122] and poly(vinyl pyrrolidone) [123]. In the early days, uncross-linked polymer solutions were investigated; however, these substances had major drawbacks and adverse

effects, such as short retention time, opacification and inflammation, and were, therefore, not useful as long-term vitreous substitutes [29,111,113]. Today's experimental vitreous substitutes are mostly cross-linked hydrogels; these materials show an enhanced retention time in the eye and are capable to act as a tamponade agent. A comprehensive overview on these polymeric vitreous substitutes is given elsewhere and, therefore, not subject of this article [29]. Recently, new developments and improvements of existing hydrogel-based vitreous substitutes have been reported. For example, Leone *et al.* [124] reported the synthesis of PVA hydrogels through cross-linking with non-toxic trisodium trimetaphosphate (STMP). Using a STMP : PVA molar ratio of 1 : 8 resulted in rheological properties similar to those of the natural vitreous body. More importantly, these properties were preserved after injection. The developed PVA gel met the requirements for vitreous substitutes regarding transparency, swelling capacity, permeability, and cytotoxicity. However, *in vivo* studies to prove the long-term compatibility of this promising material remain to be done. Swindle-Reilly *et al.* [125] copolymerized acrylamide with bisacryloylcystamine. The disulfide-containing cross-linker was then reduced to give an injectable polymer solution; once inside the eye, the disulfide cross-links reformed by air oxidation to produce a stable hydrogel that matched the mechanical properties of the natural vitreous humor. One week after injection into the vitreous cavity of rabbits, slit lamp examination, dilated fundus examination, electroretinography, and histopathological examination showed no signs of inflammation. Although this pilot study has indicated the biocompatibility of the gel, further *in vivo* studies on the long-term compatibility and stability are required. A different cross-linking approach was pursued by Tao *et al.* [126]. A mixture of two reactive PEG derivatives was injected into vitrectomized eyes of rabbits; cross-links were introduced *in situ* by Michael-type addition reaction. The formed hydrogel was stable during the study period of 9 months; the mechanical and optical properties were very similar to the natural vitreous body. No adverse reactions were detected by measurement of the intraocular pressure (IOP), fundus fluorescein angiography, electroretinography, histopathological examination, and B-scan ultrasound. Altogether, this comprehensive study demonstrated that chemically cross-linked PEG hydrogels might be suitable as long-term vitreous substitute. Besides synthetic polymers, the use of natural polymers for vitreous replacement has been investigated in two recent studies. With HA being an essential part of the human vitreous body [127], the use of this polymer for vitreous substitution seems obvious, even though the injection of uncross-linked HA solutions has

proven to be unsuccessful [111]. Schramm *et al.* [128] compared two different HA hydrogels regarding their suitability as vitreous substitute; the cross-links were introduced either with adipic dihydrazide (ADH) and 1-ethyl-3-(3-dimethylaminopropyl)carbodiimide (EDC), or by photopolymerization of glycidyl methacrylate groups. In cell culture experiments, ADH/EDC cross-linked hydrogels induced mild cytotoxicity, whereas photopolymerized HA gels showed no toxicity. These photopolymerized gels showed excellent *in vivo* biocompatibility during the study period of 6 weeks, without significant degradation or loss of transparency. In contrast to the results of Schramm *et al.*, another study found no toxic effects of similar ADH cross-linked HA hydrogels, both *in vitro* and *in vivo* [129]. In addition to these conventional approaches of using polymeric hydrogels for vitreous replacement, Feng *et al.* [130] recently proposed using a foldable vitreous-shaped capsule to address the unknown long-term compatibility of these materials. The thin capsule was implanted into the vitreous cavity and subsequently filled with a PVA hydrogel; a prolonged *in vivo* stability was observed during the investigation period of 180 days. Moreover, the authors mentioned the possibility of incorporating drug molecules into the system. Although significant improvements have been achieved over the past years, there are up until now no artificial vitreous substitutes that reach the properties of the natural vitreous body. Even *in situ* cross-linkable hydrogels, which are generally favored due to the absence of shear thinning, do not meet all of the requirements to act as long-term vitreous substitute [29,111,113].

2.4.6 Intravitreal drug delivery systems

As mentioned earlier, PDR and AMD are among the leading causes of visual impairment or blindness in industrialized nations [131]. Characteristic for both diseases is an abnormal neovascularization due to increased levels of VEGF [132]. Besides photodynamic therapy and photocoagulation, current therapeutic approaches aim at neutralizing VEGF by intravitreal injections of anti-VEGF antibodies or antibody fragments every 4-6 weeks. These frequent intravitreal injections are associated with high healthcare costs, significant discomfort, and rare complications including endophthalmitis, retinal detachment, and uveitis [10]. Furthermore, it has been shown that VEGF plays an important role in supporting the adult subretinal vasculature, which is important for nurturing the photoreceptors and maintaining central vision [132–134]. Therefore, caution may be required when patients receive long-term treatment with anti-VEGF agents. One promising approach to solve these problems would be the local release

of anti-VEGF agents from controlled release systems over extended time periods. Besides implants, microspheres and nanoparticulate systems, hydrogels may serve as drug delivery systems in the posterior segment of the eye [35–37]. For obvious reasons, *in situ* forming hydrogels that can be injected by minimally invasive techniques are particularly favorable. In contrast to vitreous substitutes, hydrogel-based drug delivery systems usually occupy only a small part of the vitreous cavity, they are not required to be transparent, and degradability is often desired. Achieving high levels of drug loading and preserving the stability of the active ingredients are significant challenges in the development of intravitreal drug delivery systems. Furthermore, the cross-linking density, swelling capacity, and degradation rate of hydrogels need to be fine-tuned to ensure controlled drug release during the period of application. Special care has to be taken that the applied hydrogel does not increase the IOP in order to avoid severe complications, such as glaucoma. For these reasons, the use of temperature-responsive PNIPAAm hydrogels, which were additionally cross-linked with PEG diacrylate, has been suggested [135,136]. At room temperature, the highly swollen gels can be easily injected through small gauge needles. In the body, above the volume phase transition temperature, the hydrogels collapse resulting in an initial burst release of encapsulated drug followed by sustained release over several weeks. The non-degradability of cross-linked PNIPAAm hydrogels and the use of potentially harmful radical initiators are disadvantages of this material. Therefore, poly(ethylene glycol)-poly-(serinol hexamethylene urethane) (ESHU) hydrogels have been developed [137]. In contrast to PNIPAAm gels, the synthesis of ESHU does not require radical initiators; furthermore, ESHU is biodegradable and does not require surgical removal after drug release. ESHU hydrogels could be easily injected through 31-gauge needles. The gels were well tolerated *in vivo*; they did not affect the IOP and there was no evidence of inflammation. ESHU hydrogels sustained the release of incorporated bevacizumab for over 9 weeks; the drug concentration was on average 4.7 times higher than in eyes receiving bolus injections of bevacizumab. Brandl *et al.* [138] suggested using four-armed PEG-succinimidyl propionate that can be cross-linked *in situ* with PEG-amines to yield transparent hydrogels with high water content. The performed *in vitro* tests, including rheological characterization of mechanical properties, cytotoxicity studies and release experiments, suggested the suitability of PEG hydrogels as ophthalmic drug delivery system. In a similar approach, four-armed PEG was cross-linked via Michael-type addition reactions between sulfhydryl and maleimide groups [139]. Incorporated bevacizumab was released

over 14 days; the hydrogels might, therefore, be suitable to treat intraocular neovascularization. And very recently, Yu *et al.* [59,140] reported the preparation of *in situ* chemically cross-linked hydrogels from vinyl sulfone functionalized HA and thiolated dextran. To reduce the covalent binding of proteins, both the concentration and the degree of modification of the thiolated dextran were increased relative to the vinyl sulfone functionalized HA. The incorporated bevacizumab was released over 3 months *in vitro*; the release rate was found to depend on the polymer concentration but not the degree of modification. First *in vivo* studies demonstrated the biocompatibility of the hydrogel; the hydrogel was able to prolong the retention of bevacizumab at therapeutically relevant concentrations for at least 6 months. Hydrogels have also been proposed for the treatment of retinal detachment. Neffe *et al.* [141] have synthesized a cross-linked HA hydrogel that can be applied as a patch to cover retinal breaks. The gel patches could be injected into the vitreous cavity, showed excellent intraocular biocompatibility, and good retinal adherence; the developed patches were slowly degrading and provided controlled release of incorporated triamcinolone.

2.4.7 Cell-based approaches

While intravitreal injections of anti-VEGF drugs are able to delay the progression of PDR and AMD, patients who have already lost vision due to severe ocular diseases or trauma may profit from cell-based therapeutic approaches. For example, it has been shown that the implantation of stem cells may have benefits in the treatment of corneal injuries and certain retinal diseases [142–145]. The cornea consists of three major layers: an outer stratified squamous epithelium, a thick stromal layer, and an inner monolayer of specialized endothelial cells. These endothelial cells play an important role in maintaining corneal clarity by regulating fluid and solute transport between the aqueous humor and the corneal stroma [146]. Tissue-engineered corneal epithelial cell sheets have already been used to treat patients with total limbal stem cell deficiencies [147]. Furthermore, the implantation of endothelial cell sheets has proven to be successful in animal models [148]. Human corneal endothelial cells were cultured on thermoresponsive PNIPAAm surfaces for 3 weeks at 37 °C and harvested as transplantable cell sheets by lowering the temperature to 20 °C. The subsequent transplantation to endothelium-denuded rabbit corneas could restore corneal function and clarity [148,149]. Ozcelik *et al.* [150] developed ultrathin chitosan-PEG hydrogel films for corneal tissue engineering. The films were approximately 50 µm thick, had desirable mechanical and

optical properties, and facilitated the attachment and proliferation of ovine corneal endothelial cells. In addition, attempts to regenerate the corneal stroma have been reported; however, none of these approaches have been deemed clinically feasible. Mimura *et al.* [151] suggested the implantation of fibroblast precursors in combination with gelatin hydrogels as possible strategy for corneal stromal regeneration. When implanted into corneal stromal pockets, the developed gelatin hydrogels remained transparent and promoted the deposition of extracellular matrix. In a similar approach, hydroxypropyl chitosan was cross-linked with gelatin and chondroitin sulfate to synthesize a scaffold that mimics the stromal layer of the cornea; the obtained material was able to support the adhesion and proliferation of keratocytes [152]. While tissue-engineered corneal epithelial cell sheets may enter clinical use in the near future, approaches to regenerate the retina are still in the early stages of development [153]. It has been shown that photoreceptor precursor cells can be successfully transplanted into the adult or degenerating retina. The transplanted cells differentiated into rod photoreceptors, formed synaptic connections and improved visual function [154]. Furthermore, the transplantation of retinal stem cells (RSC) or retinal progenitor cells (RPC) has shown promise for the treatment of retinal degeneration. However, survival of the grafted cells and integration into the host tissue remain major barriers to functional cell replacement [155]. To promote the survival and differentiation of RPC, biodegradable poly(lactic acid)/poly(lactic-co-glycolic acid) substrates have been used [156]. While significant progress has been made, polymer matrices do not match the elastic modulus of the retina and lack the flexibility required for subretinal injection. To overcome these limitations, a temperature-responsive hydrogel composed of HA and MC has been developed; the material supported the survival and proliferation RSC/RPC *in vitro*. After injection into the subretinal space of mice, RSC and RPC delivered in HA/MC gels were evenly distributed; hydrogels may, therefore, help to improve cell integration into the retina [157]. A similar approach has been described by Liu *et al.* [158]; *in situ* cross-linkable HA hydrogels promoted an even distribution of RPC in the subretinal space without causing major disruption to the host retina. After 3 weeks, the hydrogels were completely degraded; the transplanted cells expressed the mature photoreceptor marker recovering. Using biodegradable HA-based hydrogels as a vehicle, intravitreally injected mesenchymal stem cells were successfully transplanted into the retina of rats; the transplanted cells induced Müller cells to produce nerve growth factor and brain-derived neurotrophic factor [159]. To improve the gelation kinetics of HA-based materials,

oxidized glutathione has been proposed as biocompatible cross-linking agent. Thiolated hyaluronan could be cross-linked with oxidized glutathione in less than 5 minutes; the hydrogel was able to support the proliferation of adipose-derived stem cells *in vitro* and showed biocompatibility in preliminary *in vivo* experiments [160]. Temperature-responsive hydrogels were obtained from copolymers of NIPAAm and acrylic acid *N*-hydroxysuccinimide. The copolymers were conjugated with HA and cell adhesive peptides; the hydrogels demonstrated excellent compatibility with retinal pigment epithelial cells [161]. Hertz *et al.* [162] developed a library of hydrogels made from PEG and poly(L-lysine); the synthesized hydrogels exhibited a wide range of chemical and mechanical properties. Hydrogels with a 3:1 or 4:1 ratio of amines to hydroxyls and an elastic modulus between 3.8 kPa and 5.7 kPa were able to support the survival, migration and neurite outgrowth of retinal ganglion cells and amacrine cells. In conclusion, significant advances have been made by using hydrogels for cellular delivery to the degenerating retina. Hydrogels may promote survival, differentiation and integration of the delivered cells; however, further *in vivo* studies are required before potential benefits of stem cell transplantation can be definitely judged.

2.5 Limitations of hydrogel-based drug delivery systems

Although hydrogels have many possible applications in ophthalmology, comparatively few products have been brought on the market. While hydrogel-based SCL and foldable IOL have proven to be extremely successful, the clinical use of hydrogel-based vitreous substitutes or intravitreal drug delivery systems is still not feasible. The reasons for this are manifold: first of all, hydrogels are notoriously difficult to sterilize [163,164]. Most natural and synthetic polymers are degraded during heat sterilization; radiation or chemical sterilization may induce side reactions that affect the gel properties. These problems are exacerbated when proteins or other biopharmaceuticals are incorporated. In addition, the shelf life of preformed hydrogels is generally limited; likewise, the reactivity of *in situ* cross-linkable polymers may decrease during storage. Further limitations arise from the type and quantity of drugs that can be incorporated into hydrogels [44]. While hydrophilic low-molecular-weight drugs are easily loaded into hydrogels by partitioning from concentrated drug solutions, this process is ineffective in case of hydrophobic drugs (e.g., corticosteroids) or macromolecular drugs (e.g., proteins or nucleic acids). Hydrophobic drugs are poorly soluble in the gel matrix; thus, drug loading can be

improved by introducing hydrophobic domains or cyclodextrins. In contrast to that, the uptake of macromolecular drugs is typically limited by restricted diffusion. This can be addressed by *in situ* encapsulation of macromolecular drugs; however, cross-linking of hydrogels in the presence of biopharmaceuticals is still a formidable challenge [13,14,17,44,45,]. While physical cross-linking may preserve the stability of encapsulated biopharmaceuticals, it provides less control over gel degradation and drug release. On the other hand, chemical cross-linking permits the preparation of hydrogels with well-defined properties; however, it may affect the stability and availability of biopharmaceuticals. Furthermore, toxic reagents must be completely removed prior to application, which may also leach part of the drug out of the hydrogel. Another disadvantage is that preformed hydrogels must be implanted, since the high elastic modulus of cross-linked materials generally excludes their extrusion through needles. For that reason, there is considerable interest in hydrogels that are cross-linked *in situ*, i.e., inside the vitreous cavity [13,14,44,45]. However, many cross-linking reactions, such as radical polymerization, may have toxic side effects *in vivo*; this may prevent approval of *in situ* gelling formulations unless extensive biocompatibility studies are done. Alternative cross-linking reactions, such as Michael-type additions, strain-promoted azide-alkyne cycloadditions or DA reactions, might not be fast enough to effectively entrap the drug after injection. Conversely, rapidly gelling formulations may clog the needle and prevent injection of the hydrogel. However, the most important reason why many developments did not get beyond the early stages is the unknown long-term performance of hydrogels. Since only limited drug amounts can be incorporated, it is debatable whether hydrogels will be useful in the treatment of chronic eye diseases such as PDR and AMD. Furthermore, the high water content of hydrogels typically results in rapid drug release unless certain strategies, such as molecular imprinting or covalent bonding, are used [13,14,44]. Increasing the polymer concentration or cross-linking density may not be effective in controlling the diffusion of small molecules. Moreover, both methods can reduce the hydrophilicity and hence the biocompatibility of the hydrogel [14]. Antibodies or antibody fragments, which are more slowly released from hydrogels, may not be stable over several weeks or months [165,166]. Once the drug depot has been formed, the degradation rate of the hydrogel becomes a critical factor. The observed degradation rate may depend on the underlying diseases and vary among patients; consequently, it might be difficult to predict the release rate of the incorporated drug substances. An increased degradation rate may result in rapid drug release or dose

dumping, whereas delayed degradation may cause incomplete drug release and subtherapeutic drug levels. Furthermore, it should be considered that degradation of hydrogels is usually associated with an increasing degree of swelling. The increasing swelling pressure may possibly cause occlusion of the retinal vasculature and raise the IOP [29,167,168].

2.6 Concluding remarks and future perspectives

Hydrogels have many possible applications in ophthalmology. Hydrogel-based SCL, foldable IOL and *in situ* gelling drug formulations are already approved for human use and well established; furthermore, hydrogel-based tissue adhesives, vitreous substitutes and intravitreal drug delivery systems have shown to be promising in preclinical studies. However, more research is needed to improve the treatment of severe, vision-threatening diseases such as PDR or AMD. The intraocular application of hydrogels may lead to significant advances in this field. While a plethora of different materials has been tested in the past, a catalogue of general requirements would promote a more rational design of intraocularly applied hydrogels. For example, intravitreal drug delivery systems should be injectable and permit controlled drug release over several weeks or months. This may be achieved by *in situ* forming hydrogels, which are injected prior to gelation and form a semi-solid drug depot inside the vitreous cavity. After complete drug release, the hydrogel should degrade without significant swelling. Similar requirements are imposed on hydrogel-based vitreous substitutes; however, these materials must be fully transparent and mechanically stable during the entire application period. If hydrogels are used for stem cell transplantation, additional aspects must be taken into account: the scaffold material should promote survival, differentiation and integration of the transplanted cells. Although significant progress has been made, many challenges remain to improve the safety and clinical performance of intraocularly applied hydrogels. First of all, polymers and cross-linking reactions must be identified that have been proven safe for human use. While most studies evaluated the mechanical properties, the *in vitro* drug release and cytotoxicity of the proposed materials, data showing their long-term compatibility and clinical performance are frequently missing. In the light of these facts, it might be more appropriate to fully characterize the existing hydrogels rather than developing new polymers or materials. Special emphasis should be placed on the long-term tolerability of the applied hydrogels, their biodegradability, and possible excretion routes of the

degradation products. The gained results will be extremely helpful in improving the existing hydrogels and may ultimately lead to clinically approved products. And finally, the existing injection devices, such as two-chamber syringes and mixing systems, should be improved to enable easy and safe handling of *in situ* forming hydrogels in clinical settings.

Chapter 3

Investigation of the Diels-Alder Reaction as a Cross-Linking Mechanism for Degradable Poly(ethylene glycol) Based Hydrogels

This chapter was published as: S. Kirchhof, F. P. Brandl, N. Hammer and A. M. Goepferich, *J. Mater. Chem. B* 1 (2013) 4855–4864, doi: 10.1039/C3TB20831A.

Abstract

The DA reaction was investigated as a cross-linking mechanism for PEG based hydrogels. Two complementary macromonomers were synthesized by functionalizing star-shaped PEG with furyl and maleimide groups. Gel formation occurred in water at 37 °C; the gelation time ranged between 171 ± 25 min and 14 ± 1 min depending on the used hydrogel formulation. The complex shear modulus was dependent on the concentration, branching factor and molecular weight of the macromonomers; values between 2821 ± 1479 Pa and 37097 ± 6698 Pa were observed. Hydrogel swelling and degradation were influenced by the same parameters; the degradation time varied between a few days and several weeks. Gel dissolution was found to occur by rDA reaction and subsequent hydrolysis of maleimide groups. Calculations of the network mesh size revealed that the prepared hydrogels would be suitable for the controlled release of therapeutic proteins.

3.1 Introduction

Over the past two decades, polymeric hydrogels received much interest in the scientific community and a great deal of potential applications of these versatile materials has been proposed [169]. Amongst others, hydrogels were investigated as liquid-absorbing wound dressings [170], as injectable drug delivery systems [13,14,44,171], or as three-dimensional scaffolds for cell transplantation [172–174]. In most of these applications, precise control over the cross-linking density, and hence the swelling capacity, mechanical properties and degradability of the hydrogel, is crucial for success or failure of the system [15]. For example, by decreasing the cross-linking density of hydrogels, the release profiles of incorporated drug molecules dramatically change due to the increasing swelling ratio, mesh size and degradation rate [175]. The same physicochemical parameters were shown to influence cell morphology, proliferation and differentiation in tissue engineering applications [176–178]. For example, mesenchymal stem cells were shown to differentiate into neurogenic, myogenic or osteogenic cell lineages depending on the stiffness of their supportive matrix [179].

However, by means of classical chain-growth polymerization techniques, such as the free radical cross-linking of polymers with acrylate or methacrylate groups, it is rarely possible to obtain gel networks of defined architecture [16]. The produced hydrogels often suffer from poor reproducibility and incomplete cross-linking that potentially poses a toxicological risk. Much better control over cross-linking density can be achieved by step-growth polymerization of star-shaped polymers or multifunctional dendrimers that have been functionalized with one or two different types of reactive end-groups. An extremely versatile cross-linking reaction would be the copper(I)-catalyzed azide-alkyne cycloaddition that occurs in aqueous solution at room temperature with extraordinary efficiency and specificity [180,181]. Major drawbacks, however, are the toxicity and protein denaturizing effects of the copper(I) catalyst [182]. Therefore, the catalyst needs to be completely removed before protein loading, cell encapsulation, or any other application of the hydrogels. To circumvent these expensive purification procedures and expand the scope of this reaction, research focused on alternative, copper(I)-free “click” reactions [183–185].

The DA reaction is another chemical reaction that meets the criteria of “click” chemistry outlined by Sharpless [181]. This [4+2] cycloaddition between a conjugated diene and a substituted alkene is highly specific and occurs in water without any catalysts or initiators. Although the DA reaction is widely used in organic chemistry [19,20], its application in

the field of biomaterials is less common and only a few examples of hydrogels have been described in the literature [21,22,186,187,188]. The existing hydrogels were predominantly prepared from linear polymers with pendant functional groups and relatively short bifunctional cross-linkers, which typically results in rather undefined, highly cross-linked networks. Although the DA reaction is reversible at higher temperatures, the described hydrogels were permanent at body temperature due to the low rate of the rDA reaction and the high cross-linking density. In contrast, our concept is based on the step-growth polymerization of star-shaped, PEG-derived macromonomers. This approach provides better control over the network architecture and allows for the synthesis of hydrogels that readily degrade at body temperature. PEG was chosen as raw material due to its high solubility in water, excellent biocompatibility and broad acceptance by regulatory agencies [14,23]. In this paper, we first describe a straightforward way to functionalize PEG with furyl and maleimide groups; the thus obtained macromonomers were then used for gel preparation. The cross-linked hydrogels were characterized by rheological experiments, swelling and degradation studies. The hydrogel network mesh size was calculated and the obtained data was interpreted with regard to potential applications in protein delivery. To the best of our knowledge, this is the first example of hydrogels that readily degrade by rDA reactions at body temperature.

3.2 Experimental Section

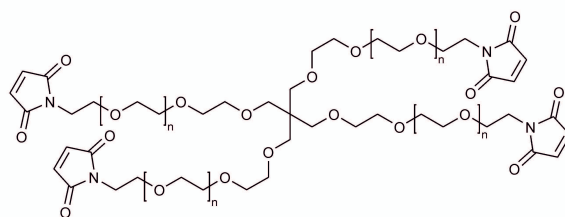
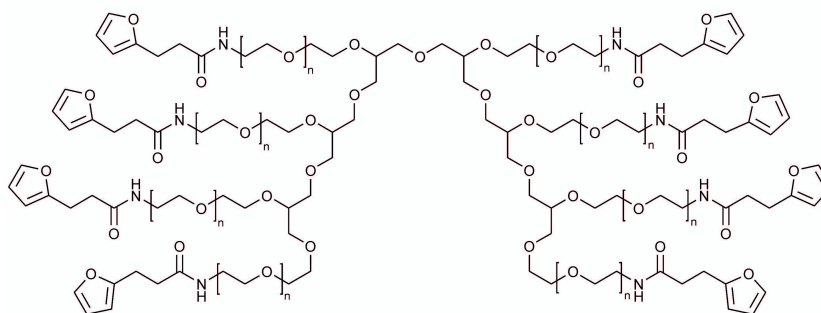
3.2.1 General procedure

¹H-NMR spectra were recorded in CDCl₃ (purchased from Sigma-Aldrich, Taufkirchen, Germany) at room temperature on a Bruker Avance 300 spectrometer (Bruker BioSpin GmbH, Rheinstetten, Germany) unless otherwise stated.

3.2.2 Materials

N,N'-Dicyclohexylcarbodiimide (DCC), diisopropyl azodicarboxylate (DIAD), furan, 3-(2-furyl)propanoic acid, *N*-hydroxysuccinimide (HOSu), maleimide and *N*-methoxycarbonylmaleimide were purchased from Sigma-Aldrich (Taufkirchen, Germany). Dichloromethane (DCM), 1,4-dioxane (anhydrous), sodium bicarbonate, sodium sulfate (anhydrous) and triphenylphosphine were received from Acros Organics (Geel, Belgium). Four-armed poly(ethylene glycol), molecular weight 10 kDa (pentaerythritol

core, 4armPEG10k-OH), eight-armed poly(ethylene glycol), molecular weight 10 kDa (hexaglycerol core, 8armPEG10k-OH) and eight-armed poly(ethylene glycol), molecular weight 20 kDa (hexaglycerol core, 8armPEG20k-OH) were received from JenKem Technology (Allen, TX, USA). Diethyl ether was of technical grade and purchased from CSC Jäcklechemie (Nuremberg, Germany). Water was obtained using a Milli-Q water purification system from Millipore (Schwalbach, Germany). All other chemicals were purchased from Merck KGaA (Darmstadt, Germany).

A**B**

Scheme 3.1. Chemical structures of 4armPEG-maleimide (A) and 8armPEG-furan (B).

3.2.3 Synthesis of branched PEG-amines (4armPEG10k-NH₂, 8armPEG10k-NH₂ and 8armPEG20k-NH₂)

Branched PEG-amines were prepared according to previously established protocols [138].

3.2.4 Synthesis of furyl-substituted four-armed PEG (4armPEG10k-furan)

3-(2-furyl)propanoic acid (1.6 mmol, 224.2 mg), HOSu (1.6 mmol, 184.2 mg) and DCC (1.6 mmol, 330.1 mg) were dissolved in 10 mL of anhydrous 1,4-dioxane. After stirring for 6 h at room temperature, the precipitated dicyclohexylurea byproduct was filtered off. The filtrate was combined with a solution of 4armPEG10k-NH₂ (0.2 mmol, 2.18 g) and NaHCO₃ (1.6 mmol, 134.4 mg) in 10 mL of water and stirred overnight at 50 °C. The

next day, the solvent was evaporated and the residue was taken up in 20 mL of water. The raw product was extracted with DCM (4×20 mL). The combined organic phases were dried over anhydrous Na_2SO_4 , filtered and concentrated to approx. 5 mL. The product was crystallized at 0 °C under vigorous stirring by dropwise addition of 50 mL of diethyl ether. The precipitate was collected by filtration, washed with cold diethyl ether and dried under vacuum to yield 2.01 g (88%) of 4armPEG10k-furan. $^1\text{H-NMR}$ (CDCl_3 , 300 MHz): δ 2.50 ppm (t, 8H, $-\text{NHC}(\text{O})\text{CH}_2\text{CH}_2-$), 2.97 ppm (t, 8H, $-\text{NHC}(\text{O})\text{CH}_2\text{CH}_2-$), 3.39 ppm (s, 8H, $\text{R}_3\text{CCH}_2\text{O}-$), 3.62 ppm (s, $-\text{OCH}_2\text{CH}_2-$), 6.00 ppm (s, 4H, Ar), 6.25 ppm (s, 4H, Ar), 7.27 ppm (s, 4H, Ar). The degree of end-group conversion was about 77% as determined by $^1\text{H-NMR}$ spectroscopy.

3.2.5 Synthesis of furyl-substituted eight-armed PEG, molecular weight 10 kDa (8armPEG10k-furan)

8armPEG10k-furan was synthesized from 8armPEG10k- NH_2 in 78% yield (1.69 g) as described for 4armPEG10k-furan. $^1\text{H-NMR}$ (CDCl_3 , 300 MHz): δ 2.50 ppm (t, 16H, $-\text{NHC}(\text{O})\text{CH}_2\text{CH}_2-$), 2.97 ppm (t, 16H, $-\text{NHC}(\text{O})\text{CH}_2\text{CH}_2-$), 3.62 ppm (s, $-\text{OCH}_2\text{CH}_2-$), 6.00 ppm (s, 8H, Ar), 6.25 ppm (s, 8H, Ar), 7.27 ppm (s, 8H, Ar). The degree of end-group conversion was about 67% as determined by $^1\text{H-NMR}$ spectroscopy.

3.2.6 Synthesis of furyl-substituted eight-armed PEG, molecular weight 20 kDa (8armPEG20k-furan)

8armPEG20k-furan was synthesized from 8armPEG20k- NH_2 in 90% yield (1.91 g) as described for 4armPEG10k-furan. $^1\text{H-NMR}$ (CDCl_3 , 300 MHz): δ 2.50 ppm (t, 16H, $-\text{NHC}(\text{O})\text{CH}_2\text{CH}_2-$), 2.97 ppm (t, 16H, $-\text{NHC}(\text{O})\text{CH}_2\text{CH}_2-$), 3.62 ppm (s, $-\text{OCH}_2\text{CH}_2-$), 6.00 ppm (s, 8H, Ar), 6.25 ppm (s, 8H, Ar), 7.27 ppm (s, 8H, Ar). The degree of end-group conversion was about 79% as determined by $^1\text{H-NMR}$ spectroscopy.

3.2.7 Synthesis of 3,6-epoxy-1,2,3,6-tetrahydrophthalimide (ETPI)

ETPI was synthesized according to previously reported procedures with the following modifications [189,190]. A mixture of maleimide (42 mmol, 4.0 g) and furan (156 mmol, 18.6 mL) in 32 mL of ethyl acetate was stirred for 3 days at room temperature. The white precipitate that formed during the reaction was filtered off, washed with cold diethyl ether

and dried under vacuum to yield 5.78 g (84%) of ETPI. The adduct was a mixture of the endo (61.5%) and the exo (38.5%) form. $^1\text{H-NMR}$ (CDCl_3 , 300 MHz): δ 2.89 ppm (s, 2H, $-\text{C}(\text{O})\text{CHRCCHRC}(\text{O})-$, exo), 3.56 ppm (s, 2H, $-\text{C}(\text{O})\text{CHRCCHRC}(\text{O})-$, endo), 5.30 ppm (s, 2H, $-\text{RCHOCHR}-$), 6.50 ppm (s, 2H, $-\text{CH}=\text{CH}-$).

3.2.8 Synthesis of ETPI-substituted four-armed PEG (4armPEG10k-ETPI)

The protocol was adapted from a previously described procedure [191]. Briefly, 4armPEG10k-OH (0.2 mmol, 2.06 g) was dried under vacuum at 45 °C and dissolved together with ETPI and triphenylphosphine in 15 mL of DCM. Then, a solution of DIAD (in 5 mL of DCM) was added dropwise. After stirring for 48 h at room temperature, the solvent was evaporated under reduced pressure. For purification, the raw product was dissolved in 50 mL of water, filtered and washed two times with 50 mL of diethyl ether. After the water had been evaporated, the raw product was dissolved in 5 mL of DCM and crystallized at 0 °C under vigorous stirring by dropwise addition of 50 mL of diethyl ether. The precipitate was collected by filtration, washed with cold diethyl ether and dried under vacuum to yield 1.85 g (89%). $^1\text{H-NMR}$ (CDCl_3 , 300 MHz): δ 2.84 ppm (s, 4H, $-\text{C}(\text{O})\text{CHRCCHRC}(\text{O})-$, exo), 3.39 ppm (s, 8H, $\text{R}_3\text{CCH}_2\text{O}-$), 3.62 ppm (s, $-\text{OCH}_2\text{CH}_2-$), 5.24 ppm (s, 4H, $-\text{RCHOCHR}-$, endo), 5.29 ppm (s, 4H, $-\text{RCHOCHR}-$, exo), 6.40 ppm (s, 4H, $-\text{CH}=\text{CH}-$, endo), 6.50 ppm (s, 4H, $-\text{CH}=\text{CH}-$, exo). The degree of end-group conversion was about 82% as determined by $^1\text{H-NMR}$ spectroscopy.

3.2.9 Synthesis of 4armPEG10k-maleimide

The protocol for the synthesis of 4armPEG10k-maleimide was adapted from a previously published procedure [192]. In brief, 4armPEG10k-ETPI was dissolved in 25 mL of toluene and the solution was heated to reflux for 2 h under argon atmosphere. The solution was then concentrated under reduced pressure and cooled to room temperature. The raw product was dissolved in 4 mL of DCM and crystallized at 0 °C under vigorous stirring by dropwise addition of 40 mL of diethyl ether. The precipitate was collected by filtration, washed with cold diethyl ether and dried under vacuum to yield 1.76 g (86%) of 4armPEG10k-maleimide. $^1\text{H-NMR}$ (CDCl_3 , 300 MHz): δ 3.39 ppm (s, 8H, $\text{R}_3\text{CCH}_2\text{O}-$), 3.62 ppm (s, $-\text{OCH}_2\text{CH}_2-$), 6.69 ppm (s, 8H, $-\text{C}(\text{O})\text{CH}=\text{CHC}(\text{O})-$). The degree of end-group conversion was about 82% as determined by $^1\text{H-NMR}$ spectroscopy.

3.2.10 Synthesis of 8armPEG10k-maleimide

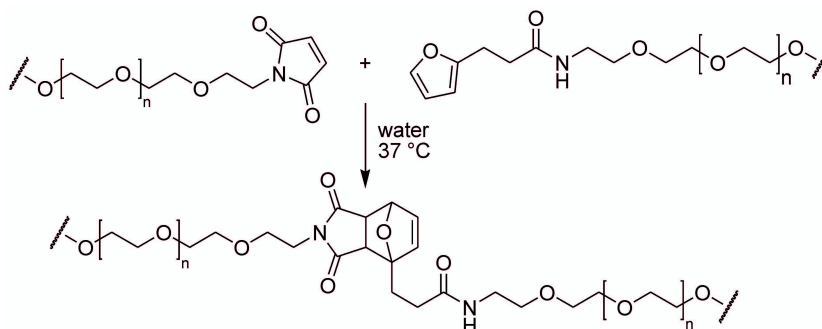
For the synthesis of 8armPEG10k-maleimide, a previously established protocol was modified as follows [193]. 8armPEG10k-NH₂ (0.27 mmol, 2.65 g) was dissolved in a saturated solution of sodium bicarbonate in water (100 mL). The solution was stirred and treated with *N*-methoxycarbonylmaleimide (4.32 mmol, 670 mg) under ice cooling. After 30 min, the ice bath was removed and the solution was allowed to warm up to room temperature. The aqueous solution was extracted with DCM (3 × 115 mL) and the combined organic layers were dried over anhydrous Na₂SO₄. The solvent was evaporated under reduced pressure. The residue was dissolved in 6 mL of DCM and crystallized at 0 °C under vigorous stirring by dropwise addition of 60 mL of diethyl ether. The precipitate was collected by filtration, washed with cold diethyl ether and dried under vacuum to yield 1.66 g (64%). ¹H-NMR (CDCl₃, 300 MHz): δ 3.62 ppm (s, -OCH₂CH₂-), 6.69 ppm (s, 16H, -C(O)CH=CHC(O)-). The degree of end-group conversion was about 68% as determined by ¹H-NMR spectroscopy.

3.2.11 Synthesis of 8armPEG20k-maleimide

8armPEG20k-maleimide was synthesized from 8armPEG20k-NH₂ in 92% (1.92 g) yield as described for 8armPEG10k-maleimide. ¹H-NMR (CDCl₃, 300 MHz): δ 3.62 ppm (s, -OCH₂CH₂), 6.69 ppm (s, 16H, -C(O)CH=CHC(O)-). The degree of end-group conversion was about 70% as determined by ¹H-NMR spectroscopy.

3.2.12 Preparation of Diels-Alder hydrogels

DA hydrogels were prepared by reacting equal molar amounts of furyl and maleimide-substituted PEG of same molecular weight and branching factor in water (Scheme 3.2).



Scheme 3.2. DA reaction of a PEG-maleimide and a furyl-substituted PEG in water at 37 °C. Only one arm of the branched macromonomers is shown for clarity.

The overall polymer concentrations were 5, 10 and 15% (w/v). For example, to prepare 750 μL of a 5% (w/v) 4armPEG10k-hydrogel, 19.1 mg of 4armPEG10k-furan and 18.4 mg of 4armPEG10k-maleimide were separately dissolved in 375 μL of water each. The two liquid precursor solutions were then mixed to initiate gel formation.

3.2.13 Rheological characterization of Diels-Alder hydrogels

To study gelation kinetics and mechanical properties, oscillatory shear experiments were performed on a TA Instruments AR 2000 rheometer (TA Instruments, Eschborn, Germany) with 40 mm parallel plate geometry. Storage (G') and loss moduli (G'') were recorded as a function of time at 37 °C at a constant frequency of 1.0 Hz. Hydrogels with 5, 10 and 15% (w/v) polymer content were prepared as described above. Upon casting the hydrogel precursors (750 μL in total) onto the lower plate of the rheometer, the upper plate was immediately lowered to a gap size of 500 μm and the experiment was started. The cross-over of G' and G'' was regarded as the gel point; the absolute value of the complex shear modulus ($|G^*|$) was determined at the end of the measurement. Water evaporation was minimized by using a solvent trap. All experiments were carried out in triplicate and the results are given as means \pm standard deviations.

3.2.14 Calculation of hydrogel network mesh size

Hydrogels with 5, 10 and 15% (w/v) polymer content were prepared as described above. Directly after mixing, 375 μL of the liquid precursor solutions were cast into cylindrical glass molds (7 mm inner diameter) and allowed to gel for 72 h under standard cell culture conditions (37 °C, 95% relative humidity and 5% CO_2). The gel samples were then weighed in air and hexane before and after swelling for 24 h in 10 mL of pure water using a density determination kit (Mettler-Toledo, Gießen, Germany). The gel cylinders were then freeze-dried to determine the mass of dry PEG in each sample. From these data, the volume of the gel directly after cross-linking (V_{gc}) and after swelling (V_{gs}) was calculated using Archimedes' principle of buoyancy. The volume of the dry polymer, V_p , was determined from the mass of the freeze-dried sample and the density of PEG (taken as 1.12 g/mL). With these parameters, the polymer fraction of the gel after cross-linking, $v_{2c} = V_p/V_{gc}$, and in the swollen state, $v_{2s} = V_p/V_{gs}$, was determined. Using a modified version of the Flory-Rehner equation, the number of moles of elastically active chains in the hydrogel network, ν_e , was calculated [194–196]:

$$v_e = -\frac{V_p}{V_1 v_{2c}} \cdot \frac{[\ln(1 - v_{2s}) + v_{2s} + \chi_1 v_{2s}^2]}{\left[\left(\frac{v_{2s}}{v_{2c}} \right)^{\frac{1}{3}} - \frac{2}{f} \left(\frac{v_{2s}}{v_{2c}} \right) \right]} \quad (3.1)$$

In this equation, χ_1 is the Flory-Huggins interaction parameter for PEG in water (taken as 0.43), V_1 is the molar volume of the swelling agent (18 cm³/mol) and f is the branching factor of the macromonomers (4 in case of 4armPEG and 8 in case of 8armPEG). The average molecular weight between cross-links, \bar{M}_c , was calculated by $\bar{M}_c = m_p / v_e$, where m_p is the total mass of polymer in the hydrogel. The average network mesh size (ξ) was calculated by [197]:

$$\xi = v_{2s}^{-\frac{1}{3}} l \left(\frac{2\bar{M}_c}{M_r} \right)^{\frac{1}{2}} C_n^{\frac{1}{2}} \quad (3.2)$$

where l is the average bond length along the PEG backbone (taken as 0.146 nm), M_r is the molecular mass of the PEG repeating unit (44 g/mol) and C_n is the Flory characteristic ratio (taken as 4 for PEG) [198]. All experiments were carried out in triplicate and the results are given as means \pm standard deviations.

3.2.15 Swelling and degradation of Diels-Alder hydrogels

Hydrogel samples were prepared as described above. The gel cylinders were weighed directly after gelation ($t = 0$ d), immersed in 10 mL of phosphate buffer (50 mmol, pH 7.4) and incubated at 37 °C in a shaking water bath (approximately 10 rpm). To determine hydrogel swelling and degradation, the vials were emptied over 24 mm Netwell™ Inserts (500 μ m mesh size, Corning GmbH, Kaiserslautern, Germany) at periodic time points. The gel cylinders were weighed and incubated again with 10 mL of fresh buffer solution. Gel degradation was assumed to be complete when no macroscopic gel residues could be detected on the Netwell™ Inserts. All experiments were performed in triplicate and the results are presented as means \pm standard deviations.

For ¹H-NMR analysis, 19.1 mg of 4armPEG10k-furan and 18.4 mg of 4armPEG10k-maleimide were separately dissolved in 375 μ L of D₂O each. The two liquid precursor solutions were mixed and transferred into a NMR tube. To follow the cross-linking reaction, ¹H-NMR spectra were recorded on a Bruker Avance 300 spectrometer (Bruker BioSpin GmbH, Rheinstetten, Germany) immediately after mixing ($t = 0$ h) and after 72 h of incubation at 37 °C. To investigate gel degradation, a 5% (w/v) 4armPEG10k-hydrogel was prepared in D₂O as described above and incubated in 10 mL of deuterated phosphate

buffer (50 mmol, pD 7.4) at 37 °C until dissolution. The solution was concentrated using Amicon[®] Ultra centrifugal filters (3 kDa molecular weight cut-off, Millipore, Schwalbach, Germany) and analyzed by ¹H-NMR spectroscopy.

3.3 Results and discussion

3.3.1 Synthesis of furyl- and maleimide-substituted PEG-derivatives

All syntheses were straightforward and the desired products were obtained in high yields. The end-group conversion varied on a high level, as determined by ¹H-NMR. Nevertheless, the end-group conversion was lower for 8armPEG10k-furan (67%) in comparison to 4armPEG10k-furan (77%) and 8armPEG20k-furan (79%). One possible reason therefore could be the divergences in chemical synthesis, such as the use of different PEGs, new batches of solvents and reactants.

Moreover, two different routes were used to synthesize the maleimide-substituted PEG-derivatives. 4armPEG10k-maleimide was obtained after an rDA reaction of 4armPEG10k-ETPI. However, this synthesis was not successful for the modification of the 8armPEGs. Therefore, a second route, the reaction with *N*-methoxycarbonylmaleimide, had to be established.

3.3.2 Rheological characterization of Diels-Alder hydrogels

To study the gelation kinetics and mechanical properties of DA hydrogels, the evolution of loss (G'') and storage modulus (G') was followed at 37 °C. G'' represents the viscous part of the system whereas G' corresponds to the elastic part. A representative rheogram of a 15% (w/v) 4armPEG10k-hydrogel is shown in Figure 3.1. At early time points, G'' was higher than G' ($G'' > G'$), which is characteristic for free-flowing liquids. With beginning cross-linking, both moduli increased with G' increasing faster than G'' . After about 60 min, the cross-over of G' and G'' was observed ($G' = G''$) and the liquid transformed into a gel. During the course of the experiment, G' further increased until a highly elastic hydrogel had formed ($G' \gg G''$). This time-dependent sol-gel transition makes DA hydrogels ideal for biomedical applications in which injection of the biomaterial is required. The material would be injected as a liquid precursor before the cross-over point and then cross-linked *in situ* to form a stable hydrogel.

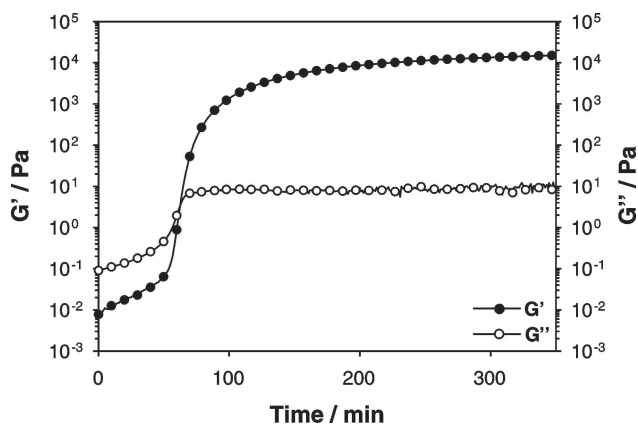


Figure 3.1. Rheogram of a 15% (w/v) 4armPEG10k-hydrogel. The measurement was performed at 37 °C and 1.0 Hz oscillatory frequency using a 40 mm parallel plate geometry with 500 μ m gap size.

The gelation time was controlled by the concentration, branching factor and molecular weight of the macromonomers. As shown in Figure 3.2A, the gelation time could be reduced by increasing the polymer concentration. For example, the gelation times of 4armPEG10k-hydrogels decreased from 171 ± 25 min to 59 ± 5 min by increasing the polymer concentration from 5% (w/v) to 15% (w/v). Using macromonomers of higher branching factor also resulted in lower gelation times. By doubling the branching factor and keeping all other factors unchanged, the gelation times of 10% (w/v) hydrogels decreased from 106 ± 14 min (4armPEG10k-hydrogels) to 24 ± 1 min (8armPEG10k-hydrogels). The molecular weight of the macromonomers also had a distinct influence on gelation kinetics. The gelation times of 8armPEG20k-hydrogels were generally higher than those of 8armPEG10k-hydrogels. For example, the gelation times of 15% (w/v) hydrogels increased from 14 ± 1 min to 34 ± 1 min by doubling the molecular weight of the macromonomers.

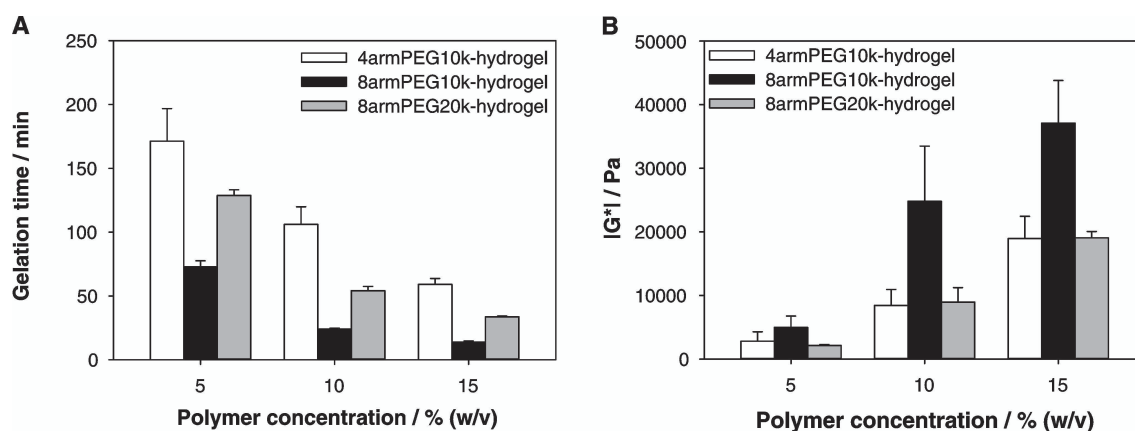


Figure 3.2. Dependence of gelation time (A) and stiffness (B) on concentration, branching factor and molecular weight of the macromonomers. The measurements were performed at 37 °C and 1.0 Hz, and the results are presented as means \pm standard deviations ($n = 3$).

The observed effects are characteristic for step-growth polymerizations and the different gelation times can be explained as follows [199,200]. In theory, gelation kinetics would only depend on the molar concentration of macromonomers and the number of reactive groups per macromonomer. By increasing the macromonomer concentration and keeping all other factors unchanged, the probability that two different macromonomers react with each other and form an elastically active chain is increasing. This was observed for all tested macromonomers (4armPEG10k, 8armPEG10k and 8armPEG20k). Likewise, the probability of forming an elastically active chain increases when increasing the number of reactive groups per macromonomer (increasing the branching factor) and keeping the molar concentration of macromonomers constant. In practice, incomplete functionalization of the macromonomers and loss of functional groups (e.g., due to hydrolysis) will also affect gelation kinetics. Because of the lower branching factor, this effect is more pronounced when using 4armPEG-macromonomers for gel formation. For example, by decreasing the number of functional groups by 50%, 4armPEG-macromonomers can only act as chain extenders and were not active as cross-linking agents while 8armPEG-macromonomers still contribute to cross-linking. This might explain why 4armPEG10k-hydrogels show longer gelation times than 8armPEG20k-hydrogels.

Oscillatory shear experiments were also used to measure the stiffness of the formed hydrogels (Figure 3.2B). As expected, the use of higher macromonomer concentrations led to significantly stiffer hydrogels. By raising the polymer concentration from 5% (w/v) to 15% (w/v), the absolute value of complex shear modulus ($|G^*|$) of 4armPEG10k-hydrogels increased from 2821 ± 1479 Pa to 18950 ± 3511 Pa. The same effect was observed for 8armPEG10k-hydrogels, where $|G^*|$ increased from 4973 ± 1798 Pa to 37097 ± 6698 Pa and for 8armPEG20k-hydrogels, where $|G^*|$ ranged between 2152 ± 144 Pa and 19057 ± 1002 Pa. Similar to the gelation time, the mechanical properties were also influenced by the branching factor of the macromonomers. By using 8armPEG10k instead of 4armPEG10k, $|G^*|$ of 10% (w/v) hydrogels increased from 8447 ± 2492 Pa to 24797 ± 8678 Pa. And by increasing the molecular weight of the used macromonomers from 10 kDa to 20 kDa, the stiffness of the resulting gels decreased likewise. For example, $|G^*|$ of 10% (w/v) 8armPEG10k-hydrogels was determined to be 24797 ± 8678 Pa whereas only 8969 ± 2271 Pa were measured for the corresponding 8armPEG20k-hydrogels, which is comparable to the value of 4armPEG10k-hydrogels (8447 ± 2492 Pa).

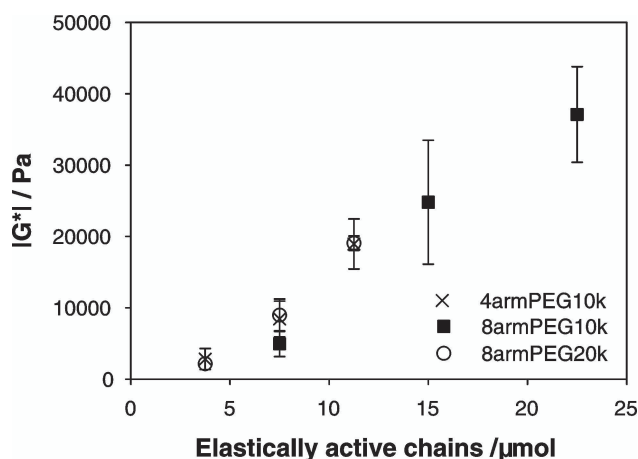


Figure 3.3. Correlation between the theoretical number of moles of elastically active chains (v_e) and the observed stiffness after cross-linking. The value of v_e was calculated according to Elbert *et al.* [186] and Metters *et al.* [189]. Data is presented as means \pm standard deviations.

These findings can be explained by the theory of rubber elasticity which relates the equilibrium modulus to the number of elastically active chains within the network [199,200]. In the case of 8armPEG10k-hydrogels, the number of elastically active chains that can be formed during cross-linking is highest at a given polymer concentrations (Figure 3.3). Consequently, these gels show the highest stiffness of all tested hydrogels. In the case of 4armPEG10k and 8armPEG20k-hydrogels, the number of elastically active chains that can be formed during cross-linking is equal at a given polymer concentrations and half the value of 8armPEG10k-hydrogels (Figure 3.3). As a result, 4armPEG10k and 8armPEG20k-hydrogels both have nearly the same stiffness. The results of the rheological experiments indicated that in some cases, gelation time and mechanical properties could be controlled independently from each other. For example, 8armPEG20k-hydrogels generally showed faster gelation kinetics than the corresponding 4armPEG10k-hydrogels, whereas $|G^*|$ of both gel types was almost the same. The possibility of controlling gelation time and stiffness independently from each other clearly demonstrates the enormous versatility of our approach. The DA reaction is a valuable cross-linking mechanism for many biomedical applications where gel formation and mechanical properties must be precisely controlled.

3.3.3 Calculation of hydrogel network mesh size

Besides mechanical properties, the hydrogel network mesh size is an important parameter that characterizes the network architecture on a sub-microscopic level. Knowing this parameter allows estimating the diffusivity of macromolecules within the gels, which is of significance for the development of hydrogel-based drug delivery systems. To determine the average network mesh size (ξ), the gel samples were swollen in water;

equations (3.1) and (3.2) were then used for calculation. The highest value of ξ (44.0 ± 17.3 nm) was determined for 5% (w/v) 4armPEG10k-hydrogels (Table 3.1). With increasing polymer content and hence increasing cross-linking density, the determined values of ξ decreased accordingly. For example, 10% and 15% (w/v) 4armPEG10k-hydrogels had mesh sizes of 17.8 ± 0.5 nm and 14.8 ± 0.1 nm. Similar trends were observed for all tested hydrogel samples (Table 3.1). Due to the fact that 4armPEG10k- and 8armPEG10k-hydrogels had the same stiffness and the same number of elastically active chains, similar mesh sizes for those hydrogels would be expected. Nevertheless increased values for 4armPEG10k-hydrogels were determined. This became particularly obvious in case of 5% 4armPEG10k- and 8armPEG20k-hydrogels. A mesh size of 16.1 ± 0.1 nm was determined for 5% 8armPEG20k-hydrogels, whereas a dramatically increased value of 44.0 ± 17.3 nm was determined for 5% 4armPEG10k-hydrogels. The reason for this increased values, is the already started degradation of 4armPEG10k-hydrogels, followed by weighing errors, which results in an increased mesh size and a large standard deviation. Besides the concentration and the branching factor of the macromonomers, their molecular weight had a clear influence on the network architecture. The mesh size of 8armPEG20k-hydrogels was nearly twice the mesh size of 8armPEG10k-hydrogels (Table 3.1). For example, 15% (w/v) 8armPEG20k-hydrogels had a mesh size of 11.1 ± 0.1 nm, whereas for 15% (w/v) 8armPEG10k-hydrogels, a mesh size of 5.5 ± 0.0 nm was determined. This is explained by the different molecular weights of the PEG chains originating from each branching point, which are 2500 Da for 8armPEG20k and 1250 Da for 8armPEG10k.

Table 3.1. Calculated network mesh sizes of the prepared hydrogels. The experiments were carried out in triplicate and the results are presented as means \pm standard deviations.

Polymer	Polymer concentration / % (w/v)	Mesh size / nm
4armPEG10k	5	44.0 ± 17.3
	10	17.8 ± 0.5
	15	14.8 ± 0.1
8armPEG10k	5	8.9 ± 0.8
	10	5.5 ± 0.0
	15	5.4 ± 0.4
8armPEG20k	5	16.1 ± 0.1
	10	12.9 ± 0.6
	15	11.1 ± 0.1

The determined mesh sizes can be used to evaluate the size of incorporated therapeutic peptides or proteins that can be released. Smaller peptides, such as insulin (hydrodynamic radius of the hexamer 2.7 nm) [201], are expected to be released from all hydrogels because their mesh sizes are generally above 5.0 ± 0.3 nm. Larger proteins, such as immunoglobulin G (hydrodynamic radius 5.3 nm) [202], are expected to be released from 4armPEG10k-hydrogels (mesh sizes generally above 11.7 ± 0.0 nm) and 8armPEG20k-hydrogels with up to 10% (w/v) polymer content (mesh sizes generally above 11.0 ± 0.5 nm). Based on our calculations, no release from 8armPEG10k-hydrogels is expected because of the small mesh sizes of these hydrogels (generally below 8.9 ± 0.8 nm). However, their mesh sizes will increase during gel degradation and incorporated proteins will eventually be released.

3.3.4 Swelling and degradation of Diels-Alder hydrogels

Swelling and degradation behavior are other important factors that must be considered when developing hydrogels for biomedical applications. For this purpose, gel cylinders were incubated in phosphate buffer pH 7.4 at 37 °C and their masses were determined at predetermined time points.

Surprisingly, all 4armPEG10k-hydrogels completely dissolved within two days of incubation (Figure 3.4A). This was not expected given that the dynamic equilibrium of the DA reaction greatly lies on the side of the cycloaddition products at 37 °C. Increasing the branching factor of the macromonomers could considerably prolong the stability of DA hydrogels. Depending on the used macromonomer concentration, the mass of 8armPEG10k-hydrogels steadily increased before they dissolved after four (5%), seven (10%) and nine (15%) weeks of incubation (Figure 3.4B). By increasing the molecular weight of the macromonomers, the stability of the gel cylinders decreased again (Figure 3.4C). 8armPEG20k-hydrogels were stable for two (5%), three (10%) and four weeks (15%), respectively. Although the rDA reaction has been reported to require temperatures above 60 °C in order to occur at significant rate [203], we still believe that this process is responsible for gel dissolution. To prove this hypothesis, a 5% (w/v) 4armPEG10k-hydrogel was prepared in D₂O, swollen in deuterated phosphate buffer at pD 7.4 until dissolution and analyzed by ¹H-NMR spectroscopy. Directly after mixing the two gel-forming polymers, the ¹H-NMR spectrum showed the characteristic signals of 4armPEG10k-maleimide (signal a in Figure 3.5A) and 4armPEG10k-furan (signals b, c, d, e and f in Figure 3.5A).

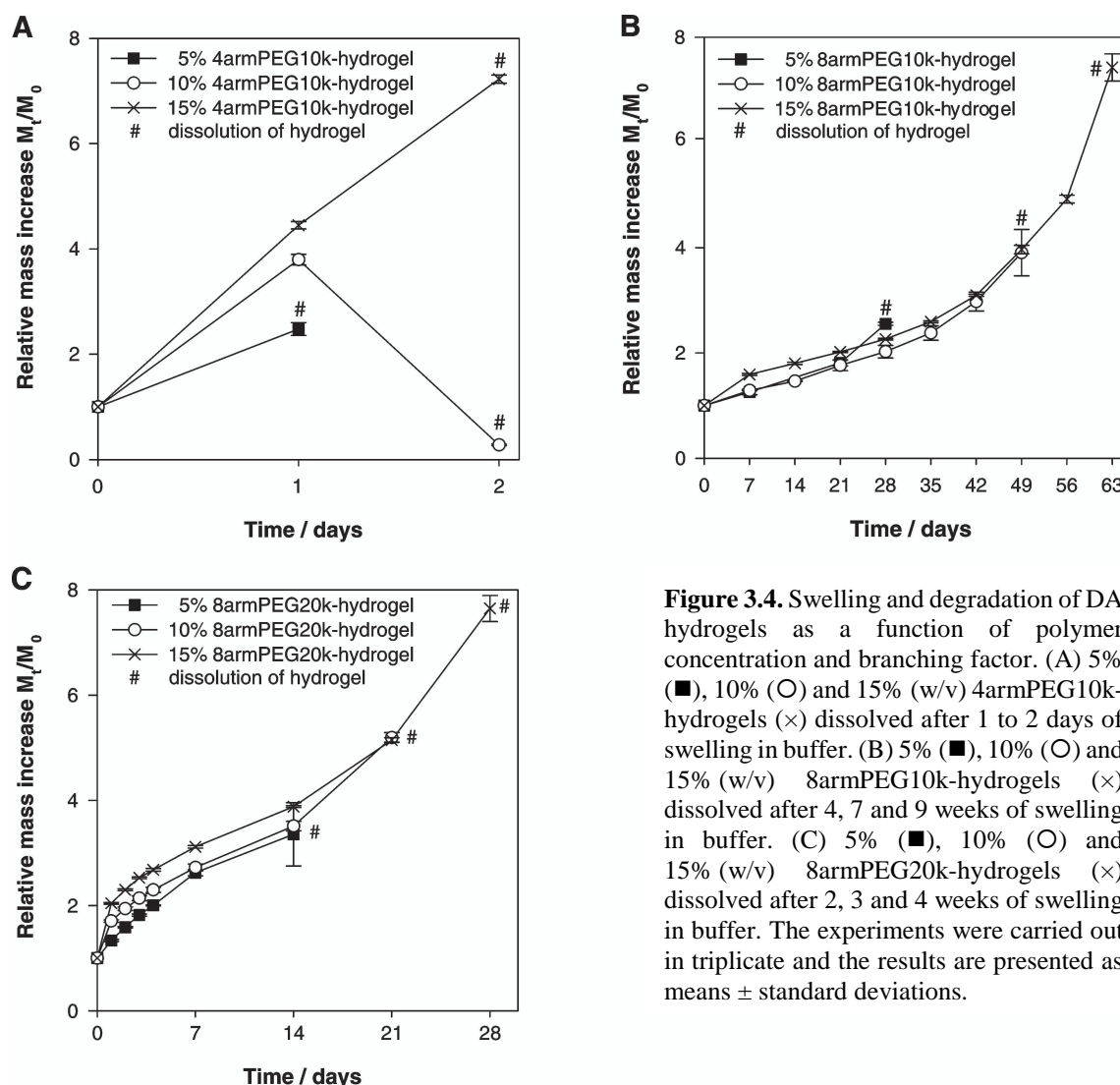


Figure 3.4. Swelling and degradation of DA hydrogels as a function of polymer concentration and branching factor. (A) 5% (■), 10% (○) and 15% (w/v) 4armPEG10k-hydrogels (×) dissolved after 1 to 2 days of swelling in buffer. (B) 5% (■), 10% (○) and 15% (w/v) 8armPEG10k-hydrogels (×) dissolved after 4, 7 and 9 weeks of swelling in buffer. (C) 5% (■), 10% (○) and 15% (w/v) 8armPEG20k-hydrogels (×) dissolved after 2, 3 and 4 weeks of swelling in buffer. The experiments were carried out in triplicate and the results are presented as means \pm standard deviations.

After 72 h of cross-linking, the signals of the educts had decreased and three groups of signals (g, h and i in Figure 3.5B) had appeared that were assigned to the cycloaddition product. In the dissolved gel, these signals were still present, although their integrals had decreased (integrals not shown in Figure 3.5C). Furthermore, we were able to detect the signals of 4armPEG10k-furan in the dissolved hydrogel (signals b, c, d, e and f in Figure 3.5C). Interestingly, no signal of 4armPEG10k-maleimide could be detected. Instead, we observed two new signals (j and k in Figure 3.5C) that were assigned to the hydrolyzed (ring-open) form of 4armPEG10k-maleimide.

These findings explain the degradability of DA hydrogels. Although the dynamic equilibrium of the DA reaction greatly lies on the side of the cycloaddition products at 37 °C, a small amount of the reactants (maleimide and furyl groups) will always be present. The maleimide groups can react with furyl groups in close proximity and form a DA adduct again, or they can be hydrolyzed to maleamic acid derivatives that do not form

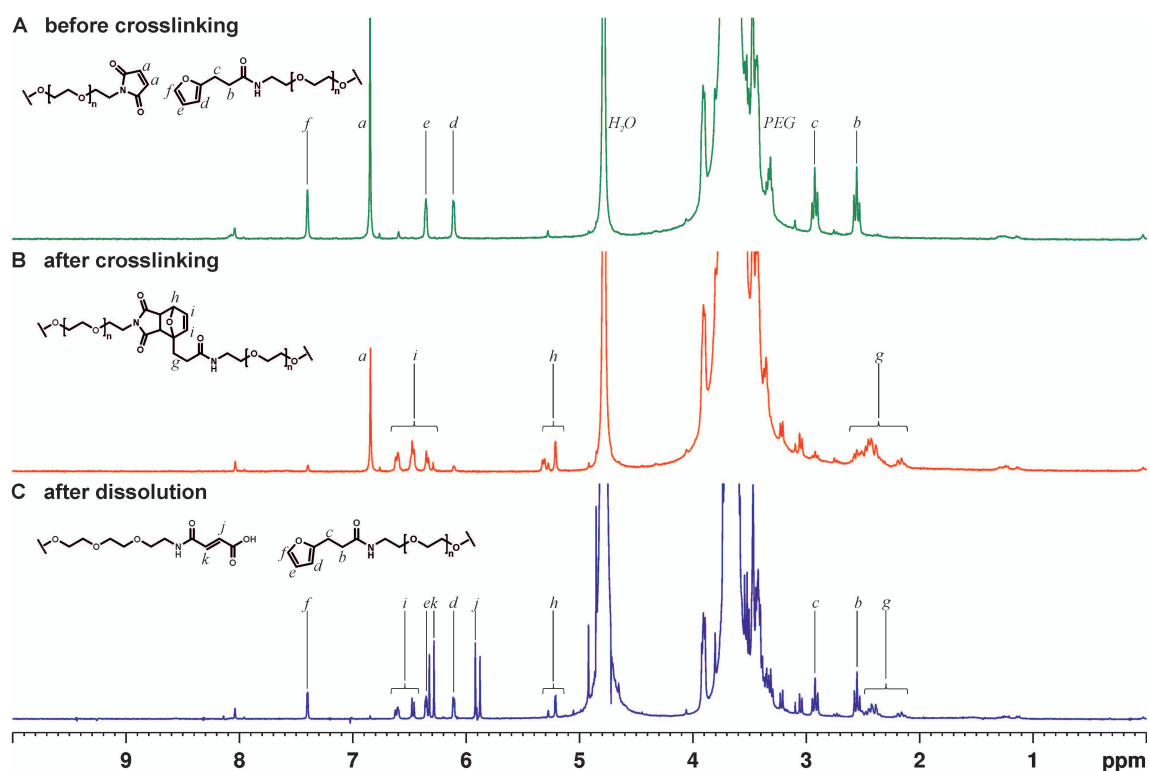


Figure 3.5. ^1H -NMR spectra of 5% (w/v) 4armPEG10k-hydrogels in D_2O . Spectra were recorded directly after mixing the two precursor solutions (A), after 72 h of gelation at 37°C (B), and after dissolution of the hydrogel (C).

cycloaddition products under the experimental conditions (data not shown). Because of hydrolysis to unreactive maleamic acid derivatives, the existing maleimide groups are continuously removed from the dynamic equilibrium and the DA reaction is ultimately reversed. As a consequence, the average network mesh size and swelling capacity of the hydrogels gradually increase until a critical number of elastically active chains have been broken and the gels finally dissolve (Figure 3.4). Once a macromonomer is completely released from the gel network, more starting material is removed from the equilibrium by diffusion into the surrounding medium. This additionally accelerates the rDA reaction independently from the hydrolysis of maleimide groups [204].

With increasing macromonomer concentration, more elastically active chains need to be broken to cause dissolution of the hydrogel network (Figure 3. 6). This explains the longevity of 8armPEG10k-hydrogels, which contain the highest number of elastically active chains of all hydrogels at given polymer concentrations. Furthermore, gel swelling and degradation are also influenced by the branching factor of the gel-forming macromonomers. In case of 4armPEG10k-hydrogels, the probability of releasing macromonomers is increased compared to 8armPEG20k-hydrogels due to the lower concentration of functional groups per branching point. The fast release of macromonomers accelerates the rDA reaction and explains the extremely low stability

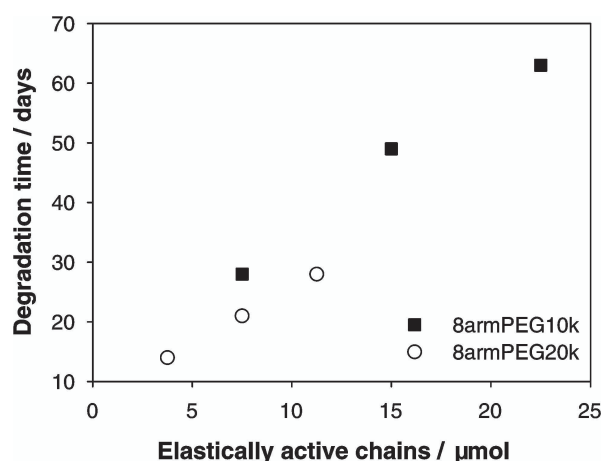


Figure 3.6. Correlation between the theoretical number of moles of elastically active chains (v_e) after cross-linking and the observed degradation time. The value of v_e was calculated according to Elbert *et al.* [186] and Metters *et al.* [189]. 4armPEG10k-hydrogels are not displayed since these gels degraded considerably faster than expected (see text for discussion).

of 4armPEG10k-hydrogels. By combining macromonomers of different branching factor and different molecular weights, it should be possible to tailor the degradation rate and control the release of incorporated proteins.

3.4 Conclusion

We successfully synthesized branched, maleimide and furyl-substituted PEG macromonomers of two different molecular weights that were subsequently used for hydrogel preparation. We demonstrated that the DA cycloaddition is a straightforward and effective reaction for the step-growth polymerization of PEG macromonomers; no catalysts or initiators were required for hydrogel cross-linking. Gelation time and gel stiffness were found to depend on the concentration, branching factor and molecular weight of the used macromonomers. The calculated values of the average network mesh size were in a size range that makes DA hydrogels interesting for applications involving the controlled release of therapeutic peptides or proteins. Unexpectedly, the prepared hydrogels dissolved within days to several weeks with the degradation rate depending on the polymer concentration and the type of the used macromonomers. Hydrogel degradation was found to occur by rDA reaction and subsequent hydrolysis of the formed maleimides to unreactive maleamic acid derivatives. To the best of our knowledge, this is the first report on hydrogels that degrade by rDA reactions at body temperature. The enormous versatility of the DA reaction and the possibility of precisely controlling the properties of the resulting hydrogels make our approach an alternative to conventional cross-linking reactions. Potential applications of DA hydrogels are seen as wound dressings, as injectable drug delivery systems or in the field of tissue engineering. Especially, in case of injectable applications the degradability of the hydrogels has to be

mentioned as a special benefit. Thus, the patient can get rid of the implanted gel in an elegant way after release of the therapeutic agent. The applicability of DA hydrogels for the controlled release of proteins is currently under investigation and will be subject of an upcoming publication. Particularly, 8armPEG10k-hydrogels promise a very interesting slow release mechanism.

Chapter 4

New Insights into the Cross-Linking and Degradation Mechanism of Diels-Alder Hydrogels

This chapter was published as: S. Kirchhof, A. Strasser, H.-J. Wittman, V. Messmann, N. Hammer A. M. Goepferich and F. P. Brandl, *J. Mater. Chem. B* 2 (2015) 449–457, doi: 10.1039/c4tb01680g.

Data which were not obtained or analyzed by S. Kirchhof were highlighted at the appropriate points.

Abstract

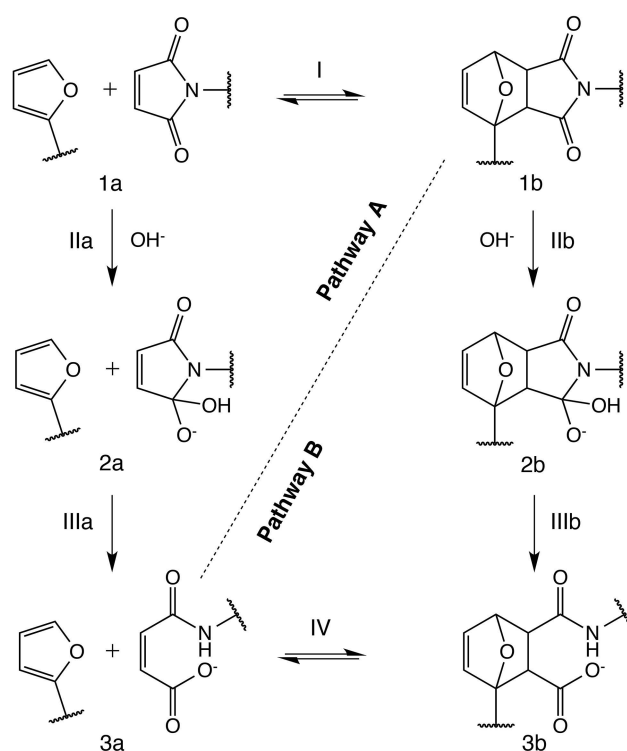
Eight-armed poly(ethylene glycol) was functionalized with furyl and maleimide groups. The two macromonomers were cross-linked by DA reactions and the degradation behavior of the formed hydrogels was investigated. UV spectroscopy showed that maleimide groups were subject to ring-opening hydrolysis above pH 5.5, with the reaction rate depending on the pH and temperature. As a result of this, the gelation kinetics and stiffness of DA hydrogels were dependent on the temperature and the pH of the cross-linking medium, as demonstrated by rheological experiments. The gel time varied between 87.8 min (pH 3.0, 37 °C) and 374.7 min (pH 7.4, 20 °C). Values between 420 Pa (pH 9.0, 37 °C) and 3327 Pa (pH 3.0, 37 °C) were measured for the absolute value of the complex shear modulus. Hydrogel swelling and degradation were influenced by the same parameters. With increasing pH and temperature the degradation time was reduced from 98 days (pH 7.4, 20 °C) to 2 days (pH 7.4, 50 °C); no degradation was observed at pH 3.0 and 5.5. Molecular modeling studies of the DA and rDA moieties revealed that hydrogel degradation occurred by rDA reaction followed by OH⁻-catalyzed ring-opening hydrolysis of maleimide groups to unreactive maleamic acid derivatives.

4.1 Introduction

The concept of click chemistry has, without doubt, revolutionized macromolecular synthesis and materials science [56,205–207]. The reasons for the importance of click reactions are their wide scope, their high efficiency and selectivity, and the ease of purification of the resulting products. Furthermore, it is advantageous that click reactions can be conducted in aqueous media under mild conditions (e.g., at room temperature). Besides azide-alkyne cycloadditions and thiol-ene reactions, DA reactions, which rely on carbon-carbon bond formation between conjugated dienes and substituted alkenes, have been frequently applied in macromolecular synthesis [19,208]. For instance, the DA reaction has been used for the synthesis of block copolymers and dendrimers, the surface modification of nanoparticles [209], and the preparation of hydrogels [21,210–213]. Interestingly, the DA reaction and its counterpart, the rDA reaction, are reversible under certain conditions (e.g., at elevated temperature or in organic solvents). The DA/rDA equilibrium has been exploited, e.g., for the synthesis of recyclable, mendable or self-healing materials [214–216]. Furthermore, the DA/rDA reaction has been used for the protection/deprotection of maleimide groups, which allowed the preparation of methacrylate-based thiol-reactive hydrogels [192,217,218]. The rDA fragmentation has also been explored for the purpose of binding and release drugs from macromolecular carriers [219]. And recently, the DA/rDA system has been proposed as a mechanism to control the release of drug molecules from PEG-based hydrogels [204,220].

Despite the reversibility of the DA/rDA reaction, hydrogels cross-linked by DA reactions did not readily degrade by rDA reactions as the rate of these reactions is too slow at body temperature. In order to achieve degradation, multiple rDA reactions must occur simultaneously at significant rate, which is unlikely in highly cross-linked networks. This limited the scope of the DA/rDA reaction to situations compatible with high temperatures and required the introduction of hydrolytically or enzymatically cleavable sites to render the hydrogels biodegradable. For example, hydrogels with hydrolytically cleavable ester bonds decomposed in acid or basic media, with the degradation rate being controlled by the pH of the solution [210]. In a slightly different approach, furan-modified hyaluronic acid (HA) derivatives were cross-linked with dimaleimide PEG [21,221] or maleimide-functionalized HA [211]. The resulting hydrogels degraded in the presence of hyaluronidase and might be suitable for applications in regenerative medicine.

In our previous work, we investigated the DA reaction as a cross-linking mechanism for PEG-based hydrogels [212]. Two complementary macromonomers were synthesized by functionalizing star-shaped PEG of two different branching factors (four-armed and eight-armed PEG) and two different molecular weights (10 kDa and 20 kDa) with furyl and maleimide groups. Hydrogels were prepared by step-growth polymerization of the synthesized macromonomers and characterized with regard to their mechanical properties, average network mesh size and swelling behavior. Somewhat surprising, the cross-linked hydrogels degraded in phosphate buffer, pH 7.4 at 37 °C, with the degradation time depending on the number of moles of elastically active chains. NMR analysis of the degradation products revealed the presence of furyl groups whereas no maleimide groups could be detected. Instead we observed two new signals that were assigned to newly generated maleamic acid groups. While maleimide is a strong dienophile, maleamic acid (ring-open form of maleimide) is much less reactive in DA reactions [204,222] and no hydrogel formation is observed. Based on these findings, two potential pathways for the degradation of DA hydrogels can be formulated (Scheme 4.1).



Scheme 4.1. Potential degradation pathways of DA hydrogels.

In pathway A, the DA adduct first undergoes rDA reaction (reaction I). In a second step, OH^- is added to the carbonyl moiety of the formed maleimide (reaction IIa), which is then subject to a ring-opening reaction yielding furan and unreactive maleamic acid (reaction IIIa). In pathway B, OH^- is first added to the carbonyl moiety of the DA

adduct (reaction IIb). The formed complex is then subject to ring opening (reaction IIIb) and subsequent rDA reaction yielding furan and unreactive maleamic acid (reaction IV). Herein we present new insights into the cross-linking and degradation mechanism of PEG-based DA hydrogels. In the first experiment, the hydrolytic stability of PEG-maleimide was investigated at different pH-values and temperatures. Next, we studied the influence of pH and temperature on the cross-linking kinetics and stiffness of DA hydrogels. Based on the obtained results, in-depth degradation studies were performed at different pH-values and temperatures. The experiments were supplemented with semi-empirical molecular dynamics (SEMD) simulations of the DA and rDA complexes at basic pH. In the following, we will present the results of these studies and discuss which pathway (Scheme 4.1) hydrogel degradation most likely follows.

4.2 Experimental section

4.2.1 Materials

Eight-armed PEG, molecular weight 10 kDa (hexaglycerol core, 8armPEG10k-OH) was purchased from JenKem Technology (Allen, TX, USA) and functionalized with furyl (8armPEG10k-furan) and maleimide groups (8armPEG10k-maleimide) as previously described [212]. Citric acid and sodium dihydrogen phosphate monohydrate were received from Merck KGaA (Darmstadt, Germany). 2-(*N*-Morpholino)-ethanesulfonic acid (MES) was purchased from Sigma-Aldrich (Taufkirchen, Germany). Water was obtained by using a Milli-Q water purification system from Millipore (Schwalbach, Germany).

4.2.2 Hydrolytic stability of 8armPEG10k-maleimide

The hydrolytic stability of 8armPEG10k-maleimide was determined by UV spectroscopy. For stability testing, 20 mg of 8armPEG10k-maleimide were dissolved in 2 mL of 50 mM citrate buffer (pH 3.0), 50 mM MES buffer (pH 5.5) or 50 mM phosphate buffer (pH 7.4, pH 9.0 and pH 11.0). The samples were placed in a Kontron UVIKON® 941 spectrophotometer (Kontron Instruments S.p.A, Milan, Italy) equipped with a temperature-controlled cell changer; 10 mm quartz cuvettes were used. The decrease in the absorbance at 299 nm (UV maximum of 8armPEG10k-maleimide) was monitored for 1200 min at 37 °C. To determine the temperature dependence of hydrolysis, 20 mg of

8armPEG10k-maleimide were dissolved in 2 mL of 50 mM phosphate buffer (pH 7.4). The decrease in the absorbance was monitored at 20 °C, 30 °C, 40 °C and 50 °C as described above. All measurements were performed in triplicate and the obtained data was normalized. Assuming that the pH of the buffered solutions does not change during hydrolysis (constant OH⁻ concentration), pseudo-first-order kinetic models were least-squares fitted to the experimental data to determine the hydrolysis rate constants (k_{obs}) and half-lives ($t_{1/2}$) of 8armPEG10k-maleimide. The plateau value was shared between all groups and k_{obs} was set greater than zero.

4.2.3 Rheological characterization of DA hydrogels

To study the influence of the pH of the cross-linking medium on gelation kinetics and mechanical properties, oscillatory shear experiments were performed on a TA Instruments AR 2000 rheometer (TA Instruments, Eschborn, Germany) with parallel plate geometry (40 mm in diameter, 500 μm gap size). For the measurements, equal molar amounts of 8armPEG10k-furan (19.0 mg) and 8armPEG10k-maleimide (18.5 mg) were dissolved in 750 μL of 50 mM citrate buffer (pH 3.0), 50 mM MES buffer (pH 5.5) or 50 mM phosphate buffer (pH 7.4, pH 9.0 and pH 11.0). After the hydrogel precursor solution had been cast onto the lower plate of the rheometer, the upper plate was immediately lowered to a gap size of 500 μm and the experiment was started. A solvent trap was used to minimize water evaporation. The time evolution of storage modulus (G') and loss modulus (G'') was recorded at 37 °C and an oscillatory frequency of 1.0 Hz. The crossover of G' and G'' was regarded as the gel point; the absolute value of the complex shear modulus ($|G^*|$) was determined after the maximum value had been reached. To study the influence of the temperature, the rheological measurements were repeated in 50 mM MES buffer (pH 5.5) and 50 mM phosphate buffer (pH 7.4) at 20 °C. All experiments were performed in triplicate and the results are shown as means ± standard deviations.

4.2.4 Swelling and degradation of DA hydrogels

For swelling and degradation studies, equal molar amounts of 8armPEG10k-furan (114.3 mg) and 8armPEG10k-maleimide (110.7 mg) were dissolved in 4500 μL of water. Directly after mixing, 375 μL of the liquid precursor solutions were filled into cylindrical

glass molds (7 mm inner diameter) and allowed to gel for 72 h under standard cell culture conditions (37 °C, 95% relative humidity and 5% CO₂). The gel cylinders were weighed ($t = 0$ days), immersed in 10 mL of 50 mM citrate buffer (pH 3.0), 50 mM MES buffer (pH 5.5) or 50 mM phosphate buffer (pH 7.4, pH 9.0 and pH 11.0) and incubated at 37 °C in a shaking water bath (approximately 10 rpm). To determine the influence of temperature on hydrogel degradation, gel cylinders were prepared as described above, immersed in 10 mL of 50 mM phosphate buffer (pH 7.4) and incubated at 20 °C, 30 °C, 40 °C or 50 °C. The vials were emptied over 24 mm Netwell-Inserts (500 μ m mesh size, Corning GmbH, Kaiserslautern, Germany) at periodic time points, the gel cylinders were weighed, and incubated again with 10 mL of fresh buffer solution. The experiment was continued until no macroscopic gel residues could be detected on the Netwell-Inserts. All experiments were performed in triplicate and the results are presented as means \pm standard deviations.

4.2.5 Molecular modeling studies

To minimize the calculation time, the polymer structures of 8armPEG10k-furan and 8armPEG10k-maleimide were reduced to 2-methylfuran and *N*-methylmaleimide, respectively. All complexes were constructed with SYBYL 7.0 (Tripos Inc., St. Louis, MO) and preminimized using the Tripos force field. Subsequently, the resulting structures were converted into a MOPAC (Stewart Computational Chemistry, Colorado Springs, CO) input file. Using the keyword line “ $t = 1000$ am1 pdb mmok gnrm = 0.1 eps = 78 charge = -1” the complexes were minimized in order to obtain the enthalpy of formation. In setting up the system for the SEMD simulation using the MOPAC 2009 package, the complex of interest was solvated with a water shell consisting of about 60 water molecules and showing the density of water at 25 °C. The relative molar mass of the atoms of the water molecules in the outer hydration shell was set to 9999 in order to avoid expansion of the system. The simulations were performed for > 10 ps in all cases.

4.2.6 Statistical analysis

The results of the rheological characterization were analyzed by means of one-way ANOVA followed by Tukey’s post-hoc test (GraphPad Prism, Version 5.01, GraphPad Software Inc., La Jolla, CA). The differences were considered statistically significant at $p < 0.05$.

4.3 Results and discussion

4.3.1 Hydrolytic stability of 8armPEG10k-maleimide

To investigate the possible degradation pathways, we first studied the hydrolytic stability of 8armPEG10k-maleimide. It is well known from the literature that maleimides and *N*-alkylmaleimides hydrolyze in alkaline solution [223–225]. However, data on the hydrolytic stability of 8armPEG10k-maleimide is still missing. The hydrolytic ring opening of 8armPEG10k-maleimide is a key step in degradation pathway A and can be easily followed by UV spectroscopy (Figure 4.1A). When 8armPEG10k-maleimide was incubated at pH 3.0 or pH 5.5, the absorbance at 299 nm slowly decreased indicating high stability of the maleimide. At pH 7.4, the absorbance decreased more rapidly indicating faster hydrolysis of the maleimide in comparison to pH 3.0 and pH 5.5. When the pH was further increased to pH 9.0, 8armPEG10k-maleimide was subject to fast ring opening as indicated by the rapidly decreasing absorbance. At pH 11, the hydrolytic ring opening of 8armPEG10k-maleimide was extremely fast and reliable measurements could not be made (data not shown). Besides the pH, the stability of 8armPEG10k-maleimide was found to depend on the incubation temperature. When the temperature was increased from 20 °C to 50 °C, the rate of hydrolysis increased likewise (Figure 4.1B).

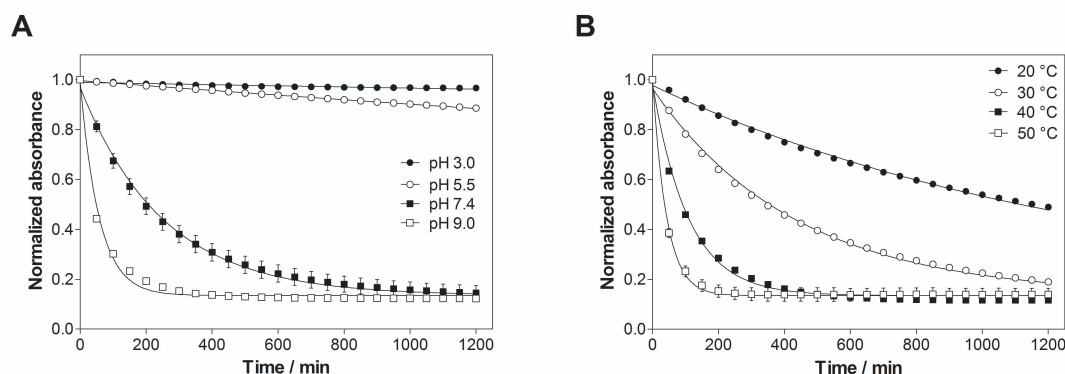


Figure 4.1. Hydrolytic stability of 8armPEG10k-maleimide at 37 °C and different pH-values (A), and at pH 7.4 and different temperatures (B). The experimental data is indicated by symbols; the solid lines represent the least-squares fits of pseudo-first-order kinetic models. The experiments were carried out in triplicate and the results are presented as means \pm standard deviations.

Since the concentrations of OH^- and H_3O^+ are constant during the reaction in buffered solutions, it is reasonable to assume that the hydrolysis of 8armPEG10k-maleimide follows the pseudo-first-order equation (4.1).

$$-\frac{d[\text{8armPEG10k-maleimide}]}{dt} = k_{obs} \cdot [\text{8armPEG10k-maleimide}] \quad (4.1)$$

$$k_{obs} = k \cdot [\text{OH}^-] \quad (4.2)$$

Rate constants (k_{obs}) and half-lives ($t_{1/2}$) were calculated by fitting the integrated form of equation (4.1) to the experimental data (Table 4.1 and 4.2). Our results clearly show that the rate of the ring-opening reaction increases with increasing pH and temperature. Since the reaction rate is not negligible at neutral pH and room temperature, hydrolysis of maleimide groups to unreactive maleamic acid derivatives may play an important role during cross-linking and degradation of DA hydrogels.

Table 4.1. Pseudo-first-order rate constants (k_{obs}) of the ring-opening hydrolysis and half-lives ($t_{1/2}$) of 8armPEG10k-maleimide at 37 °C and different pH-values.

pH	k_{obs} / s^{-1}	$t_{1/2} / \text{min}$	$3 \cdot t_{1/2} / \text{days}$	R^2
3.0	$4.83 \cdot 10^{-7}$	26358	54.9	0.7630
5.5	$1.92 \cdot 10^{-6}$	6020	12.5	0.9989
7.4	$6.55 \cdot 10^{-5}$	177	0.4	0.9813
9.0	$2.60 \cdot 10^{-4}$	44	0.1	0.9764

Table 4.2. Pseudo-first-order rate constants (k_{obs}) of the ring-opening hydrolysis and half-lives ($t_{1/2}$) of 8armPEG10k-maleimide at pH 7.4 and different temperatures.

$T / ^\circ\text{C}$	k_{obs} / s^{-1}	$t_{1/2} / \text{min}$	$3 \cdot t_{1/2} / \text{days}$	R^2
20	$1.24 \cdot 10^{-5}$	929	1.9	0.9969
30	$3.81 \cdot 10^{-5}$	303	0.6	0.9979
40	$1.47 \cdot 10^{-4}$	79	0.2	0.9926
50	$3.85 \cdot 10^{-4}$	30	0.1	0.9652

4.3.2 Rheological characterization of DA hydrogels

The influence of the pH on cross-linking kinetics and stiffness of DA hydrogels was investigated by oscillatory shear experiments at 37 °C. As shown in Figure 4.2A, the gel time was not significantly different at pH 3.0, pH 5.5 and pH 7.4; values between 87.8 ± 8.2 min (pH 3.0) and 97.2 ± 6.5 min (pH 7.4) were observed. The gel time increased to 207.6 ± 21.5 min at pH 9.0, which was significantly longer compared to the three lower pH-values ($p < 0.05$). When the pH was further increased to 11.0, no gel formation was observed within 4 h (data not shown). The stiffness of the cross-linked

hydrogels generally decreased with increasing pH (Figure 4.2B). The absolute value of G^* (3328 ± 373 Pa) was significantly higher at pH 3.0 than in all other experimental groups ($p < 0.05$). When the pH was raised to 5.5, the absolute value of G^* decreased to 2517 ± 176 Pa; however, this value was still significantly higher than at pH 7.4 and pH 9.0 ($p < 0.05$). Further increasing the pH resulted in mechanically weaker hydrogels. The magnitude of G^* decreased to 685 ± 169 Pa at pH 7.4, which was not significantly different from that value at pH 9.0 (420 ± 205 Pa).

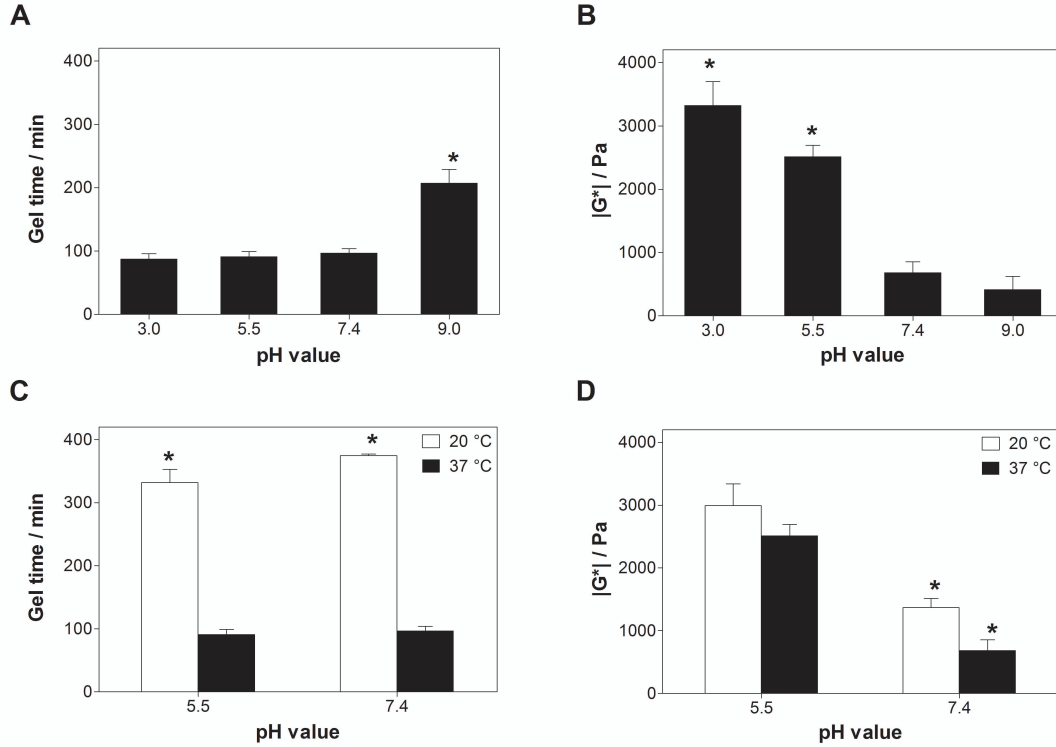


Figure 4.2. Influence of the pH on the gel time (A) and stiffness (B) of DA hydrogels at 37 °C. Influence of the temperature on the gel time (C) and stiffness (D) of DA hydrogels at pH 5.5 and 7.4. The measurements were performed in triplicate and the results are presented as means \pm standard deviations; * indicates statistically significant differences versus all other experimental groups ($p < 0.05$).

For step-growth polymerizations of f -functional species, the conversion of functional groups at the gel point (α) can be calculated according to the Flory-Stockmayer theory [226]:

$$\alpha = \frac{1}{f - 1} \quad (4.3)$$

According to equation (4.3), gelation of DA hydrogels made from eight-armed PEG ($f = 8$) occurs at approximately 15% conversion of both furyl and maleimide groups. The time to reach the gel point, which is approximated by the crossover of G' and G'' , can be used to describe the kinetics of cross-linking. In cross-linked networks, the absolute value

of G^* relates to the number of elastically active chains, which can be calculated from the degree of cross-linking or conversion of functional groups [226]. Oscillatory shear experiments can, therefore, be used to describe the kinetics of cross-linking and to approximate the conversion of functional groups. In our experiments, both the kinetics of cross-linking and the conversion of functional groups were greatly influenced by the pH (Figure 4.2A and B). While Brønsted acid catalysis of DA reactions was reported in both polar and nonpolar organic solvents [227–229], no general Brønsted acid catalysis was observed in water. The rate constants for the DA reaction between cyclopentadiene and dienophiles with basic sites were considerably faster in 0.01 M HCl than in pure water; however, no Brønsted acid catalysis was detected in the DA reaction of cyclopentadiene with non-basic naphthoquinones [230]. Since neither furan nor maleimide contain any basic sites, acid catalysis of the DA reaction between 8armPEG10k-furan and 8armPEG10k-maleimide is unlikely. Furthermore, acid catalysis may explain the faster reaction kinetics at acidic pH but not the higher magnitude of G^* . However, pH-dependent ring opening of maleimide groups and generation of unreactive maleamic acid derivatives can explain the observed results. In the sol state at pH 3.0, pH 5.5 and pH 7.4, the ring-opening reaction is slow compared to the DA reaction and the gel time is basically independent from the pH. However, the cross-linking process considerably slows down after gelation and the competitive reaction becomes increasingly important. As discussed above, the rate of the ring-opening reaction increases with increasing pH; consequently, the degree of cross-linking decreases with increasing pH. At pH 9.0 and pH 11.0, the ring-opening reaction is fast compared to the DA reaction. This results in significantly prolonged gel times and low degrees of cross-linking.

Besides the pH, the temperature is expected to influence the gelation kinetics and the degree of cross-linking of DA hydrogels. The observed gel times (332.5 ± 21.1 min at pH 5.5 and 374.7 ± 2.5 min at pH 7.4) were significantly longer at 20 °C than at 37 °C (Figure 4.2C). In contrast to the gel time, the absolute value of G^* was strongly influenced by the pH; values between 2992 ± 347 Pa (pH 5.5) and 1369 ± 148 Pa (pH 7.4) were measured at 20 °C (Figure 4.2D). Our results clearly demonstrate that increasing the temperature accelerates the DA reaction. Gelation was more than three times faster at 37 °C than at 20 °C. Despite the lower reaction rate at 20 °C, the absolute value of G^* was equally high or higher than at 37 °C. This can be explained by the changed hydrolytic stability of maleimides at different pH-values and temperatures. At pH 5.5, the ring-

opening hydrolysis of maleimides is extremely slow for both tested temperatures (Figure 4.1A). Consequently, the absolute values of G^* and hence the degrees of cross-linking were comparable at 20 °C and 37 °C. At pH 7.4, however, the rate of the ring-opening reaction is strongly influenced by the temperature (Figure 4.1B). The observed rate constants were approximately five times higher at 37 °C than at 20 °C ($6.55 \cdot 10^{-5} \text{ s}^{-1}$ vs. $1.24 \cdot 10^{-5} \text{ s}^{-1}$, Table 4.1 and 4.2). As a result of this, the magnitude of G^* was approximately two times higher at 20 °C than at 37 °C ($1369 \pm 148 \text{ Pa}$ vs. $685 \pm 169 \text{ Pa}$). It can be concluded from our rheological experiments that cross-linking of DA hydrogels is best performed in slightly acidic solutions (e.g., at pH 5.5) to ensure high cross-linking degrees. Furthermore, cross-linking should be performed above room temperature (e.g., at 37 °C) to fasten gel formation.

4.3.3 Swelling and degradation of DA hydrogels

DA hydrogels prepared from star-shaped PEG macromonomers degraded in phosphate buffer, pH 7.4 at 37 °C as reported in our previous publication [212]. This was surprising since the described hydrogels, unlike other degradable DA hydrogels [21,210,211,213], did not contain labile ester bonds or enzymatically degradable substrates. To investigate factors influencing the stability of DA hydrogels, cross-linked gel cylinders were incubated at 37 °C and different pH-values (Figure 4.3A). At pH 3.0 and pH 5.5, the mass of the incubated gel samples remained nearly constant. After approximately 10 months, the mass of hydrogels incubated at pH 5.5 had slightly increased compared to those at pH 3.0. In contrast to that, hydrogels incubated at pH 7.4, pH 9.0 or pH 11.0 showed pH-dependent swelling behavior. The mass of the samples increased exponentially until the gels dissolved after 4 days (pH 11.0), 18 days (pH 9.0) and 25 days (pH 7.4). Our experiment demonstrates that the stability of DA hydrogels strongly depends on the pH of the incubation medium. The equilibrium of the DA/rDA reaction between furan and maleimide is thermally controlled (reaction I); temperatures up to 60 °C favor the forward (DA) reaction and adduct formation (complex 1b), whereas temperatures above 100 °C induce the reverse (rDA) reaction and the regeneration of furan and maleimide moieties (complex 1a) [231–234]. Therefore, hydrogel degradation at 37 °C is most likely not solely driven by an rDA process as the reaction kinetics is too slow at body temperature. Furthermore, a DA/rDA mechanism cannot explain the observed pH dependence of the gel stability. The few studies investigating the pH dependence of the DA/rDA reaction point towards an increased rate of the rDA reaction in the presence of

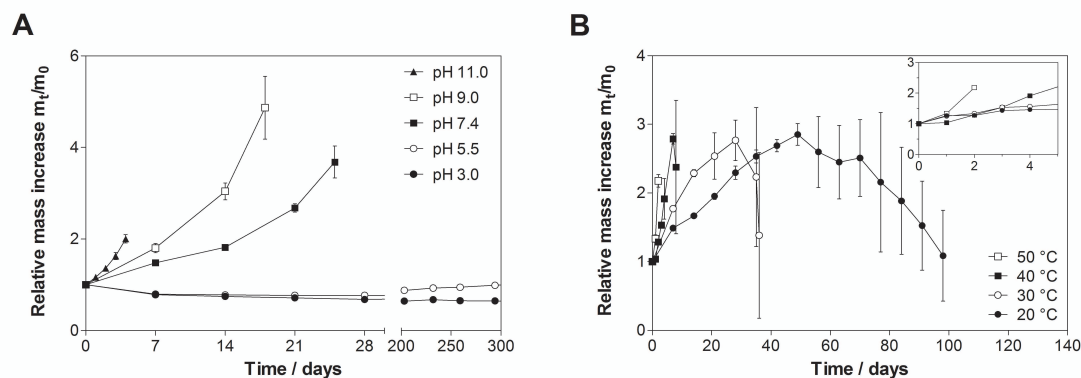


Figure 4.3. Swelling and degradation of 10% (w/v) 8armPEG10k-hydrogels. Hydrogels incubated at 37 °C dissolved after 4 days (pH 11.0), 18 days (pH 9.0) and 25 days (pH 7.4); gels incubated at pH 5.5 and pH 3.3 were stable for more than 300 days (A). Hydrogels incubated at pH 7.4 dissolved after 2 days (50 °C), 8 days (40 °C), 36 days (30 °C) and 98 days (20 °C) (B). The inset shows the relative mass increase during the first 5 days of incubation. The experiments were carried out in triplicate and the results are presented as means \pm standard deviations.

Brønsted acids [234], which contradicts our observations. However, the experimental results could be explained by a DA/rDA mechanism in combination with ring-opening hydrolysis of the generated maleimide groups (Scheme 1, degradation pathway A). Removal of maleimide groups from the DA/rDA equilibrium, e.g., by conversion into unreactive maleamic acid derivatives (reaction IIa and IIIa), causes the DA adduct (complex 1b) to revert to the starting materials (complex 3a). In this way, the rate of the rDA reaction is increased according to Le Châtelier's principle and gel degradation is incited [219]. The higher the pH of the incubation medium gets, the faster the maleimide groups are consumed and the faster the hydrogels dissolve. Another possible mechanism that could explain the experimental results would be the direct addition of OH^- to the carbonyl moiety of the DA adduct (reaction IIb) followed by a ring-opening reaction (reaction IIIb) and rDA reaction (reaction IV, Scheme 1, degradation pathway B).

To verify our hypothesis, cross-linked hydrogels were incubated at pH 7.4 and different temperatures (Figure 4.3B). Although all incubation temperatures were below the temperature usually required for the rDA reaction to proceed at a significant rate [231–233], hydrogel degradation was observed at all conditions. The gel samples dissolved after 2 days (50 °C), 8 days (40 °C), 36 days (30 °C) and 98 days (20 °C). Assuming that hydrogel degradation follows a simple first-order process, the hydrogels should dissolve after 85% of the DA linkages have been broken, i.e., after approximately three half-lives [225]. If the degradation process was actually controlled by ring-opening

hydrolysis of maleimide groups, it should be possible to predict the degradation time from the observed rate constants. However, the observed values were approximately 50 times higher than the predicted values (Figure 4.4). Therefore, the ring-opening reaction is most likely not the rate-determining step in the degradation process; hydrogel degradation is most likely not controlled by the ring-opening reaction. Furthermore, it should be emphasized that hydrogel degradation is most likely not adequately described by a single first-order process; additional factors, such as the cross-linking density and the branching factor of the macromonomers, must be taken into account. For example, it has been shown that the stability of hydrogels made from four-armed PEG (10 kDa molecular weight) and eight-armed PEG (20 kDa molecular weight) differs, even though the number of elastically active chains should be identical in both systems [212]. In hydrogels made from four-armed PEG, the number of functional groups per branching point is lower than in eight-armed PEG gels. Consequently, the cross-linking density of four-armed PEG hydrogels decreases faster during degradation; the gel stability is greatly reduced. The experimental findings would fully support the proposed degradation pathway A. The degradation of DA hydrogels is based on the DA/rDA equilibrium, with the rDA reaction most likely being the rate-determining step. Increasing the temperature catalyzes the ring-opening hydrolysis of maleimide groups; consequently, the rate of the rDA reaction is increased and gel degradation is incited without requiring elevated temperatures.

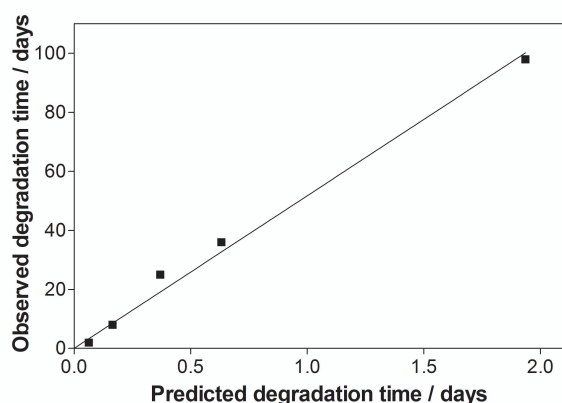


Figure 4.4. Comparison of the predicted ($3 \cdot t_{1/2}$) and observed degradation times at pH 7.4 and different temperatures. The solid line represents a least-squares fit of a linear equation to the data points. The observed values were approximately 50 times higher than the predicted values.

4.3.4 Molecular modeling studies

Modeling the actual degradation process of hydrogels is a great challenge because of the extremely large box size and, consequently, large number of sites that are required to describe the system. Even qualitative results can hardly be achieved, especially if formation and breaking of bonds should be taken into account. Therefore, only the reactive moieties were considered in the SEMD simulations. Further extending the system, e.g., by adding ethylene glycol units, may produce artificial results. In SEMD simulations, side chains next to the reactive center are flexible; oxygen atoms may form hydrogen bonds with water to direct the addition of OH^- to the maleimide portion of the DA adduct. In highly swollen gel networks, however, the polymer chains are stretched and restricted in their movement. Therefore, it is acceptable to reduce the polymer structures of 8armPEG10k-furan and 8armPEG10k-maleimide to 2-methylfuran and *N*-methylmaleimide, respectively, without compromising the validity of the model. Figure 4.5 shows possible reaction pathways connecting different maleimide/furan-complexes in the presence of a water molecule and an OH^- -ion. Furthermore, a corresponding schematic energy diagram based on the semi-empirical calculation of the enthalpy of formation is depicted in the center of Figure 4.5. The calculations predict that the DA adduct 1b is enthalpically favored compared to complex 1a. This is in agreement with the experimental results showing the formation of the DA adduct from maleimide and furan. Addition of OH^- to the carbonyl moiety of the DA adduct would lead to a further enthalpic stabilization (complex 2b), as indicated by semi-empirical calculations. The calculations further indicate that the ring-open complex 3b would be enthalpically favored compared to complex 2b. In addition to the exo adduct, the formation of the endo isomer also has to be considered. However, semi-empirical calculations predicted no significant differences in the standard enthalpy of formation between the corresponding endo and exo isomers. Because of the DA/rDA equilibrium, a second pathway must be considered. Addition of the OH^- to the carbonyl moiety of the maleimide (complex 2a) and the subsequent ring opening would lead to a strong enthalpic stabilization (complex 3a). Since no hydrogel formation was observed between 8armPEG10k-furan and the ring-open form of 8armPEG10k-maleimide (results of the rheological experiments not shown), the formation of complex 3b from complex 3a cannot be suggested.

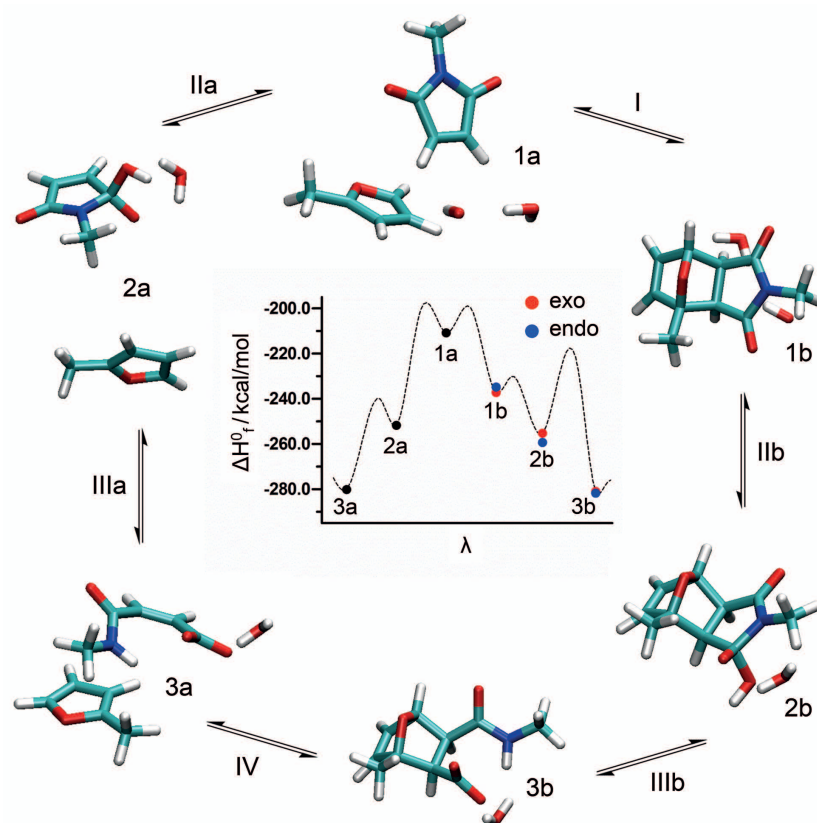


Figure 4.5.* Possible reaction pathways connecting different maleimide/furan-complexes in the presence of a water molecule and an OH^- -ion. The schematic energy diagram in the center is based on the semi-empirical calculation of the enthalpy of formation. The exo isomer is marked by red dots and the endo isomer is marked by blue dots; no significant energetic differences were observed between the two isomers. For reasons of clarity, only the chemical structures of the exo isomers are shown.

* Data were obtained and analyzed by A. Strasser and H.-J. Wittmann, Department of Pharmaceutical and Medicinal Chemistry II, University of Regensburg.

To investigate which pathway hydrogel degradation most likely follows, the OH^- -catalyzed ring-opening hydrolysis of maleimide was simulated (reaction IIIa). Figure 4.6A shows the progress in the ring-opening reaction, based upon the distances of relevant atoms marked by C, H, O and N, as a function of time for the model system *N*-methylmaleimide. At an early state of the reaction, the length of the C–O bond decreases, whereas the distance between the carbon and the nitrogen atom increases, indicating the cleavage of the C–N bond. After a period of about 1750 fs, the hydrogen atom of the OH^- -group approaches the nitrogen atom, resulting in a significant step of the H–N-distance function. Afterwards, the proton transfer from the oxygen atom to the nitrogen atom takes place, yielding the product *N*-methylmaleamic acid anion. In contrast to the semi-empirical MD simulation of *N*-methylmaleimide, ring opening of complex 2b was not observed (Figure 4.6B), although the ring-open complex 3b would

be enthalpically favored compared to complex 2b. Thus, it can be concluded that the formation of the DA adduct 1b from complex 1a may be kinetically controlled. A reason for the resistance of complex 2b towards ring opening may be a large change in the dihedral angle δ . As observed for *N*-methylmaleimide, the dihedral angle δ undergoes a strong change from $\sim 1^\circ$ to $\sim 56^\circ$ (Figure 4.6A). In contrast to that, such a large change in the dihedral angle is not possible for complex 2b because of the rigid ring system. Based on SEMD simulations it can be concluded that hydrogel degradation most likely follows pathway A (Scheme 4.1). Addition of OH^- to the carbonyl moiety of the DA adduct followed by a ring-opening reaction and rDA reaction (Scheme 4.1, degradation pathway B) cannot be suggested.

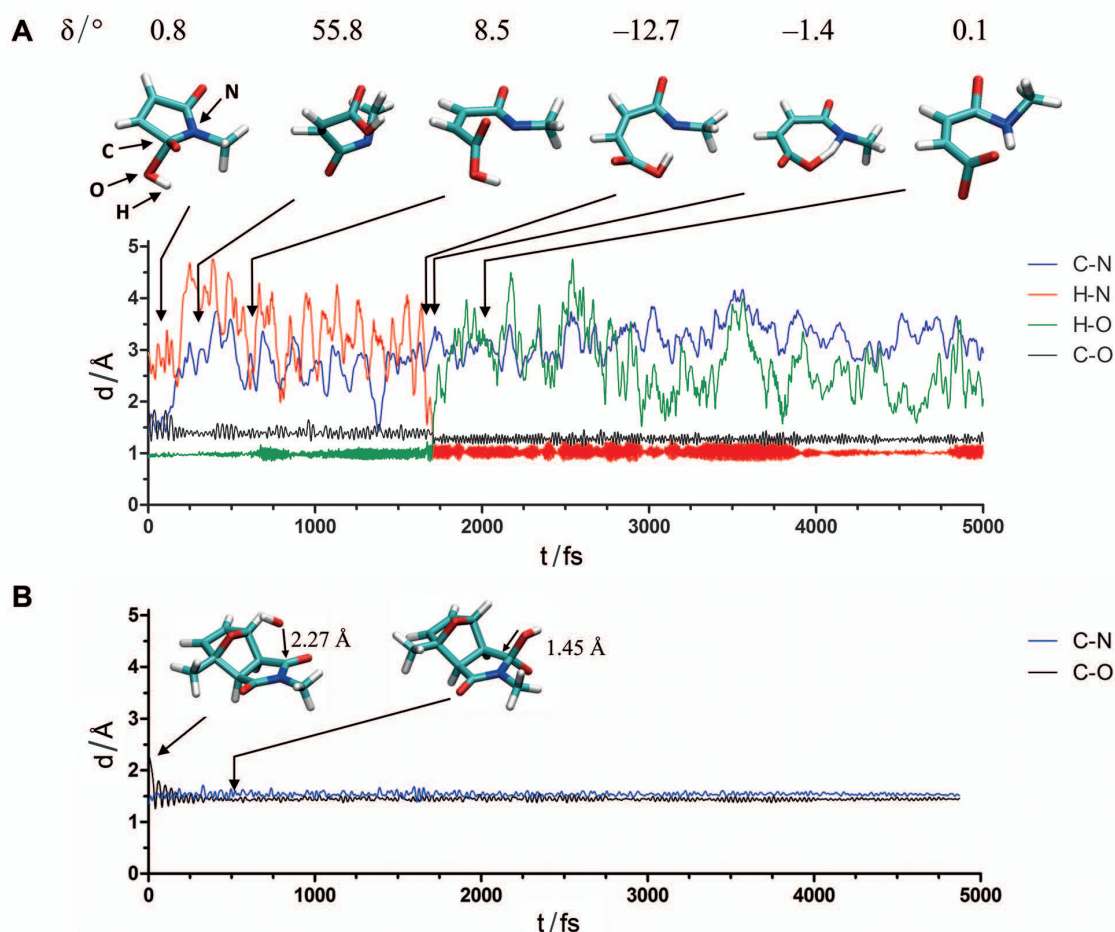


Figure 4.6.* Semi-empirical MD simulations of the ring-opening reaction. The distances of relevant atoms marked by C, H, O and N are shown as a function of time for the model systems *N*-methylmaleimide (A) and complex **2b** (B).

* Data were obtained and analyzed by A. Strasser and H.-J. Wittmann, Department of Pharmaceutical and Medicinal Chemistry II, University of Regensburg.

4.4 Conclusion

In this study we investigated the influence of pH and temperature on the cross-linking and degradation behavior of DA hydrogels. Rheological experiments and swelling studies were supplemented with SEMD simulations. Taken together, the results of our studies show that degradation of DA hydrogels occurs by rDA reaction and subsequent OH⁻-catalyzed ring-opening hydrolysis of the formed maleimides to unreactive maleamic acid derivatives (Scheme 4.1, degradation pathway A). The instability of the involved maleimides directly affects the cross-linking and degradation behavior of DA hydrogels, with pH and temperature being the main influencing factors. These findings have implications for other biomaterials that are cross-linked by DA reactions, especially hydrogels. Cross-linking is best performed in slightly acidic solutions (e.g., at pH 5.5) to ensure high degrees of conversion. Furthermore, cross-linking should be performed above room temperature (e.g., at 37 °C) to fasten the gelation process. When placed into a physiological environment (e.g., in aqueous solution at pH 7.4 and 37 °C), degradability of the cross-linked hydrogels must be considered. Removal of maleimide groups from the DA/rDA equilibrium by ring-opening hydrolysis increases the rate of the rDA reaction according to Le Châtelier's principle. This evades the need for high temperatures to incite the rDA reaction, allowing the synthesis of biomaterials that readily degrade at physiological conditions. We are fully aware that *in vitro* experiments cannot exactly predict the degradation behavior of DA hydrogels in potential applications, e.g. when applied as a biomaterial *in vivo*. Nevertheless, we expect that DA hydrogels will be degraded *in vivo*, with the pH of the tissue having a major influence on the degradation time. Further experiments to investigate the *in vivo* compatibility and degradability of PEG-based DA hydrogels will be run in the near future and presented in an upcoming publication.

Chapter 5

Diels-Alder Hydrogels for Controlled Antibody Release: Correlation between Mesh Size and Release Rate

This chapter was published as: S. Kirchhof, M. Abrami, V. Messmann, N. Hammer, A. M. Goepferich, M. Grassi and F. P. Brandl, *Mol. Pharm.* 12 (2015) 3358-3368, doi: 10.1021/acs.molpharmaceut.5b00375.

Data which were not obtained or analyzed by S. Kirchhof were highlighted at the appropriate points.

Abstract

Eight-armed PEG, molecular mass 10 kDa was functionalized with furyl and maleimide groups, respectively; the obtained macromonomers were cross-linked via DA chemistry. The mesh size (ξ) of the prepared hydrogels was determined by swelling studies, rheology and low field NMR spectroscopy. The *in vitro* release of fluorescein isothiocyanate labeled dextrans (FD) and bevacizumab was investigated. The average mesh size (ξ_{avg}) increased from 5.8 ± 0.1 nm to 56 ± 13 nm during degradation, as determined by swelling studies. The result of the rheological measurements (8.0 nm) matched the initial value of ξ_{avg} very well. Low field NMR spectroscopy enabled the determination of the mesh size distribution; the most abundant mesh size was found to be 9.2 nm. In combination with the hydrodynamic radius of the molecule (R_h), the time-dependent increase of ξ_{avg} was used to predict the release profiles of incorporated FDs applying an obstruction-scaling model. The predicted release profiles matched the experimentally determined release profiles when $R_h < \xi_{avg}$. However, significant deviations from the theoretical predictions were observed when $R_h \geq \xi_{avg}$, most likely due to the statistical distribution of ξ in real polymer networks. The release profile of bevacizumab differed from those of equivalently sized FDs. The delayed release of bevacizumab was most likely a result of the globular structure and rigidity of the protein. The observed correlation between ξ and the release rate could facilitate the design of controlled release systems for antibodies.

5.1 Introduction

Controlled release technology has the potential to improve the safety and efficacy of antibody-based therapies. For example, controlled release systems can improve the local bioavailability of antibodies, maintain effective antibody concentrations over extended periods of time, lower the required antibody dose, and reduce systemic side effects [11]. Compared to other dosage forms, such as implants or microspheres, hydrogels may offer several advantages. For example, the high water content of hydrogels is extremely suitable to accommodate high loads of hydrophilic antibodies. Furthermore, hydrogels are capable of preserving the bioactivity of antibodies, since protein denaturing conditions (i.e., the use of organic solvents and/or high shear forces) are usually avoided during the fabrication process. The mobility of physically entrapped antibodies is limited by the polymer network; the hydrogel forms a reservoir from which the antibody is released in a controlled manner. Depending on the size of the incorporated antibody and the cross-linking density of the hydrogel, the release will be controlled by diffusion, swelling, degradation, or a combination of these mechanisms [13,14].

An important parameter that characterizes the permeability of hydrogels is the mesh size or correlation length, ξ . The mesh size depends on the polymer concentration and is defined as “the average distance between consecutive cross-links” [197]; it indicates the maximum size of solutes that can pass through the gel network. Besides the diffusivity of solutes, the mesh size determines the mechanical strength and degradability of hydrogels. In combination with the size of the entrapped molecule, knowledge of ξ allows to estimate the rate of drug release from hydrogels. Based on Flory’s theory of rubber elasticity, information about the average mesh size of swollen, cross-linked hydrogels can be derived from the elastic modulus or the equilibrium polymer volume fraction [197,235]. While ideal networks are adequately described by the average mesh size, most real hydrogels are characterized by a broad range of mesh sizes that affect the release rate of entrapped drugs. The morphology and network density of hydrogels can be visualized by optical methods such as cryogenic transmission electron microscopy; however, care must be taken during sample preparation to avoid artifacts [236,237]. Other methods that allow the evaluation of the mesh size include confocal laser scanning microscopy [238,239], small angle neutron scattering [240,241], small-angle X-ray scattering [242], and pulsed field gradient NMR spectroscopy [243]. Moreover, the mesh size distribution can be determined by differential scanning calorimetry [244–246] and low field NMR spectroscopy [246,247].

In this manuscript, we focus on the correlation between the mesh size of degradable, PEG based hydrogels and the release rate of macromolecules. In particular, we aim at establishing a theoretical framework that may facilitate the rational design of controlled release systems for antibodies. To this end, eight-armed PEG, molecular weight 10 kDa (8armPEG10k) was functionalized with furyl and maleimide groups, respectively; the obtained macromonomers were cross-linked via DA reaction. As previously reported, the hydrogels degraded under physiological conditions by rDA reaction and subsequent ring-opening hydrolysis of the generated maleimide groups [212,248]. The mesh size of 8armPEG10k-hydrogels was determined using swelling studies, rheology and low field NMR spectroscopy. The calculated values of ξ allowed us to estimate the release rate of fluorescein isothiocyanate-labeled dextran (FD); four different molecular masses (4 kDa, 20 kDa, 150 kDa and 500 kDa) were studied. To verify the validity of the model, the predicted release profiles were compared to the results of *in vitro* release experiments. Finally, the hydrogels were loaded with bevacizumab, which served as a model compound. Bevacizumab is a monoclonal antibody that inhibits angiogenesis by neutralizing VEGF. It is approved for the treatment of various types of cancer; furthermore, it is used off label in the treatment of neovascular AMD [5,249]. Since the bioavailability of antibodies in the posterior segment of the eye is generally low, bevacizumab is administered every four to six weeks by intravitreal injection. However, these injections are associated with significant discomfort and rare but severe complications [10]. To reduce the injection frequency and improve the compliance, the use of controlled release systems for bevacizumab seems obvious. Therefore, the *in vitro* release of bevacizumab from 8armPEG10k-hydrogels was studied and compared with the release profiles of dextran molecules of equivalent size.

5.2 Materials and methods

5.2.1 Materials

Eight-armed PEG (10 kDa molecular mass, hexaglycerol core) was purchased from JenKem Technology (Allen, TX, USA) and functionalized with furyl (8armPEG10k-furan) and maleimide groups (8armPEG10k-maleimide) as previously described [212]. The degree of functionalization with furyl and maleimide groups was 67% and 68%,

respectively, as determined by $^1\text{H-NMR}$ spectroscopy. Fluorescein isothiocyanate-labeled dextrans with molecular masses of 4 kDa, 20 kDa, 150 kDa and 500 kDa (FD4, FD20, FD150 and FD500) were obtained from Sigma-Aldrich (Taufkirchen, Germany). Bevacizumab (Avastin[®], 25 mg mL⁻¹, Roche, Basel, Switzerland) was kindly provided by the hospital pharmacy, University of Regensburg, Germany. Ultrapure water was freshly prepared every day using a Milli-Q water purification system (Merck Millipore, Darmstadt, Germany).

5.2.2 Swelling studies

For the preparation of hydrogels, equal molar amounts of 8armPEG10k-furan (19.0 mg) and 8armPEG10k-maleimide (18.5 mg) were dissolved in 375 μL of water, cast into cylindrical glass molds (7 mm inner diameter), and allowed to gel over night at 37 °C. The gel cylinders were weighed in air and hexane using a density determination kit (Mettler-Toledo, Gießen, Germany), and the gel volume after cross-linking (V_{gc}) was calculated. The volume of the dry polymer (V_p) was calculated from the mass of the polymer in the hydrogel (m_p) and the density of PEG (taken as 1.12 g mL⁻¹) [250]. To study the swelling behavior, the gel cylinders were immersed in 10 mL of 50 mM phosphate buffer, pH 7.4 and incubated at 37 °C. The gel volume in the swollen state (V_{gs}) was determined at regular time points as described above. From these data, the polymer fraction of the gel after cross-linking, $v_{2c} = V_p / V_{gc}$, and after swelling, $v_{2s} = V_p / V_{gs}$, was calculated. The number of moles of elastically effective chains in the hydrogel network, ν_e , was calculated using the Peppas-Merrill equation, which is a modified form of the Flory–Rehner equation for highly swollen hydrogels cross-linked in solution [195,196]:

$$\nu_e = -\frac{V_p}{V_1 v_{2c}} \cdot \frac{[\ln(1 - v_{2s}) + v_{2s} + \chi_1 v_{2s}^2]}{\left[\left(\frac{v_{2s}}{v_{2c}}\right)^{\frac{1}{3}} - \frac{2}{f} \left(\frac{v_{2s}}{v_{2c}}\right)\right]} \quad (5.1)$$

where V_1 is the molar volume of the swelling agent (taken as 18 mL mol⁻¹), and χ_1 is the Flory-Huggins interaction parameter for PEG in water. The value of χ_1 was found to be nearly independent of the polymer fraction (v_2 ranging from 0.04 to 0.2); therefore, the average value (0.43) was used in all calculations [251]. The branching factor of the macromonomers, f , was taken as 8, assuming 100% functionalization with furyl and

maleimide groups, respectively 100% reaction during cross-linking. The average mesh size (ξ_{avg}) was then calculated according to eqn. (5.2) [197]:

$$\xi_{avg} = v_{2s}^{-\frac{1}{3}} l \left(\frac{2m_p}{\nu_e M_r} \right)^{\frac{1}{2}} C_n^{\frac{1}{2}} \quad (5.2)$$

where l is the average bond length along the PEG backbone (taken as 0.146 nm) [198,251], M_r is the molecular mass of the PEG repeating unit (taken as 44 g mol⁻¹), and C_n is the Flory characteristic ratio (taken as 4 for PEG) [198,251].

5.2.3 Rheological characterization

Oscillatory shear experiments were performed on a TA Instruments AR 2000 rheometer (TA Instruments, Eschborn, Germany) with parallel plate geometry (40 mm diameter). For the measurements, equal molar amounts of 8armPEG10k-furan (38.0 mg) and 8armPEG10k-maleimide (37.0 mg) were dissolved in 750 μ L of water, and cast onto the lower plate of the rheometer. The upper plate was immediately lowered to a gap size of 500 μ m, and the sample was allowed to gel over night at 37 °C. A solvent trap was used to minimize the evaporation of water. After full gelation, a stress sweep experiment was run at 1 Hz oscillatory frequency to determine the linear viscoelastic region of the sample. Afterwards, a frequency sweep experiment was run at 1000 μ Nm torque (equivalent to a stress of 79.5 Pa and within the linear viscoelastic region, see results and discussion) following the same procedure.

5.2.4 Low field NMR measurements

Equal molar amounts of 8armPEG10k-furan (51.0 mg) and 8armPEG-maleimide (49.0 mg) were dissolved in 1000 μ L of water and transferred into an NMR tube. Low field NMR measurements were performed at 37 °C using a Bruker Minispec mq20 (Bruker Italy, Milan, Italy). A Carr-Purcell-Meiboom-Gill pulse sequence with a 90°–180° pulse separation time of 0.25 ms was used to measure the transverse relaxation time, T_2 (4 scans, 5 s delay). To determine the discrete distribution of T_2 , the signal intensity, I_s , related to the decay of the transverse component of the magnetization vector was fitted by:

$$I(t) = \sum_{i=1}^m A_i e^{-t/T_{2i}}; \langle 1/T_2 \rangle = \frac{\sum_{i=1}^m A_i / T_{2i}}{\sum_{i=1}^m A_i} \quad (5.3)$$

where t is the time, A_i are the dimensionless pre-exponential factors proportional to the number of protons with the relaxation time T_{2i} , and $\langle 1/T_2 \rangle$ is the average value of the inverse relaxation time. Based on a statistical procedure, m was determined by minimizing the product $\chi^2 \cdot 2m$, where χ^2 is the sum of the squared errors and $2m$ represents the number of fitting parameters of eqn. (5.3). The determined T_{2i} value represents the transverse relaxation time of protons of water molecules entrapped in polymer meshes of size ξ_i . To evaluate the mesh size distribution, the continuous distribution of T_2 was considered. To this end, although another approach can be followed [252,253], eqn. (5.4) was fitted to the decay of the signal (I_s):

$$I(t) = \int_{T_2^{min}}^{T_2^{max}} a(T_2) e^{-t/T_2} dT_2 \quad (5.4)$$

$$\approx \sum_{i=1}^N a_i(T_2^i) e^{-t/T_{2i}} (T_2^{i+1} - T_2^i) = \sum_{i=1}^N A_i(T_2^i) e^{-t/T_{2i}}$$

where $a(T_2)$ is the unknown amplitude of the spectral component at relaxation time T_2 , e^{-t/T_2} represents the decay term, and $T_2^{min} - T_2^{max}$ indicates the range of the T_2 distribution (here $T_2^{min} = 40$ ms, $T_2^{max} = 4000$ ms and $N = 200$). The initial values of all unknowns (A_i) were set to zero and a constrained fitting was performed imposing that $A_i \geq 0$ (negative values would be physically meaningless). The fitting parameters, A_i and $a_i = A_i / (T_{2i+1} - T_{2i})$, were determined by minimizing the smoothed sum of the squared error (χ_s^2):

$$\chi_s^2 = \sum_{i=1}^N \left(\frac{I_s(t_i) - I(t_i)}{\sigma_i} \right)^2 + \mu \sum_{i=1}^{N-2} |A_{i+2} - 2A_{i+1} + A_i|^2 \quad (5.5)$$

where σ_i is the standard deviation of the noise, and μ is the weight of smoothing term [254,255]. The optimal value of μ was determined as described by Wang and Ni (here $\mu = 200$) [255]. The average value of the inverse relaxation time, $\langle 1/T_2 \rangle$, was then calculated by eqn. (5.6):

$$\left\langle \frac{1}{T_2} \right\rangle = \frac{\sum_{i=1}^N A_i / T_{2i}}{\sum_{i=1}^N A_i} \quad (5.6)$$

To study the mobility of water molecules inside the gel network, pulsed gradient spin-echo (PGSE) measurements were performed at 37 °C. A Carr-Purcell-Meiboom-Gill sequence with two equal gradient pulses ($\delta = 1$ ms) occurring at $x_1 = 1$ ms and $x_2 = 1$ ms after the 90° and 180° pulses, respectively, was applied. The interval between the gradient

pulses, indicated by Δ ($\approx \tau - x_1 - \delta + x_2$), is related to the diffusion time of the water molecules (t_d) according to $t_d \approx \Delta - \delta / 3$. The self-diffusion coefficient of the water molecules was determined by fitting eqn. (5.7) to the experimental data:

$$A_t = \sum_{i=1}^p A_{0i} \cdot \exp^{-q^2 t_d D_i}; \quad q = \gamma \cdot g \cdot \delta; \quad A_0 = \sum_{i=1}^p A_{0i} \quad (5.7)$$

where A_t and A_0 are the measured amplitudes of the echo with and without the gradient applied, γ is the gyromagnetic ratio of the protons, g is the known magnetic field gradient, and A_{0i} are the fractions of water molecules characterized by a self-diffusion coefficient D_i . In case of homogenous systems, the summation is limited to the first term ($p = 1$), as all water molecules are characterized by the same self-diffusion coefficient. In case of heterogeneous systems, however, $p > 1$ occurs. In this case, p was determined by minimizing the product $\chi^2 \cdot 2p$, where χ^2 is the sum of the squared errors and $2p$ represents the number of fitting parameters (A_{0i} and D_i) of eqn. (5.7).

5.2.5 In vitro release of fluorescein isothiocyanate-labeled dextran

Hydrogels were loaded with fluorescein isothiocyanate-labeled dextran (FD); different molecular masses (4 kDa, 20 kDa, 150 kDa and 500 kDa) were investigated. For the preparation of hydrogels, equal molar amounts of 8armPEG10k-furan (61.0 mg) and 8armPEG10k-maleimide (59.0 mg) were dissolved in 1080 μL of water; 120 μL of an FD stock solution ($c = 10 \text{ mg mL}^{-1}$) were added. Directly after mixing, 375 μL of the prepared solution were cast into cylindrical glass molds (7 mm inner diameter) and allowed to gel over night at 37 °C. The gel cylinders were carefully removed from the glass molds, immersed in 5 mL of 50 mM phosphate buffer, pH 7.4, and incubated at 37 °C in a shaking water bath. Samples of 1000 μL were withdrawn at regular time points and replaced with fresh buffer. The samples were stored at 4 °C until completion of the release experiment. The amount of released FD ($\lambda_{ex} = 485 \text{ nm}$ and $\lambda_{em} = 510 \text{ nm}$) was determined on a fluorescence microplate reader (BMG LABTECH, Ortenberg, Germany) using standard calibration curves.

5.2.6 In vitro release of bevacizumab

For the preparation of bevacizumab-loaded hydrogels, equal molar amounts of 8armPEG10k-furan (38.0 mg) and 8armPEG10k-maleimide (37.0 mg) were dissolved in 600 μL of water; 150 μL of a bevacizumab stock solution ($c = 25 \text{ mg mL}^{-1}$) were added.

Directly after mixing, 250 μL of the prepared solution were cast into cylindrical glass molds (7 mm inner diameter) and allowed to gel over night at 37 $^{\circ}\text{C}$. The gel cylinders were carefully removed from the glass molds, covered with 5 mL of 50 mM phosphate buffer, pH 7.4, and incubated at 37 $^{\circ}\text{C}$ in a shaking water bath. Samples of 300 μL were withdrawn at regular time points and replaced with fresh buffer. The samples were stored at 4 $^{\circ}\text{C}$ until completion of the release experiment. The amount of released bevacizumab ($\lambda_{ex} = 280 \text{ nm}$ and $\lambda_{em} = 335 \text{ nm}$) was determined on a PerkinElmer LS 55 Fluorescence spectrometer (Perkin Elmer, Wiesbaden, Germany) using a standard calibration curve.

5.3 Results and discussion

5.3.1 Determination of the network mesh size

In order to determine the time-curve of ξ_{avg} , DA hydrogels consisting of 10% (w/v) 8armPEG10k were incubated in 50 mM phosphate buffer, pH 7.4 at 37 $^{\circ}\text{C}$. The volumetric swelling ratio, $Q = V_{gs} / V_p$, was determined at regular time points until complete degradation of the hydrogel (Figure 5.1A); ξ_{avg} was calculated according to eqn. (5.1) and (5.2), and the results are shown in Figure 5.1B.

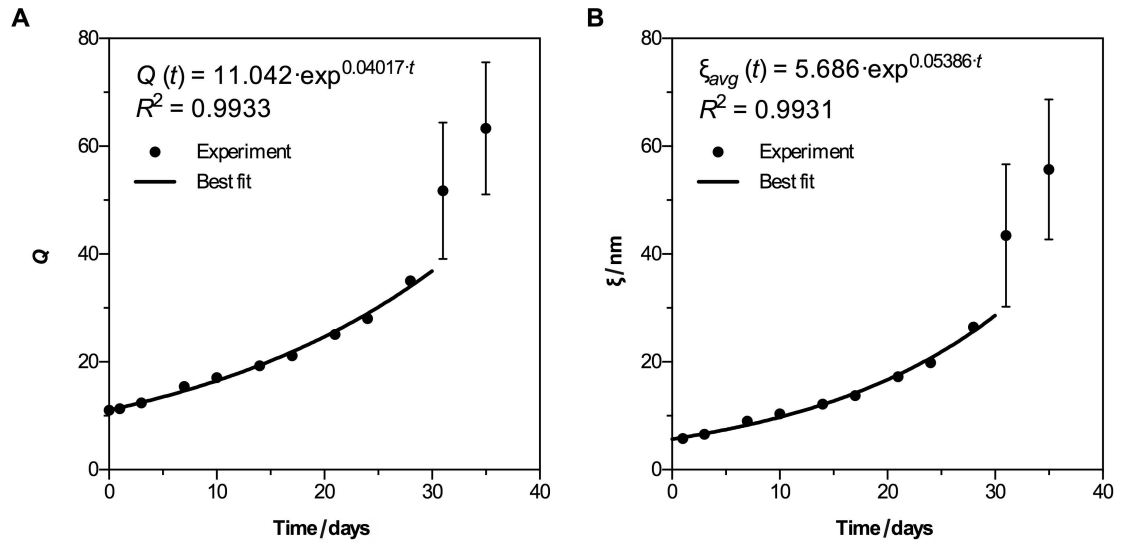


Figure 5.1. Volumetric swelling ratio (A) and average mesh size (B) of 10% (w/v) 8armPEG10k hydrogels in 50 mM phosphate buffer, pH 7.4 at 37 $^{\circ}\text{C}$. The high standard deviations of the last two data points indicate the beginning dissolution of the hydrogel. To describe the increase of Q and ξ over time, exponential equations were fitted to the experimental data by minimizing the sum of the squared errors. Data is expressed as mean \pm standard deviation based on the results of $n = 3$ samples. The error bars are smaller than the symbols, except for the last two data points.

After 1 day of swelling, an initial ξ_{avg} value of 5.8 ± 0.1 nm was determined. During degradation, the number of elastically effective chains in the gel network is decreasing; as a consequence, both Q and ξ_{avg} were increasing during the incubation period. The high standard deviations of the last two data points indicate the beginning dissolution of the hydrogel; the maximum ξ_{avg} value (56 ± 13 nm) was determined at day 35. Since the swelling of DA hydrogels was observed to increase exponentially during the first 30 days, Q can be described by the exponential function:

$$Q(t) = Q_0 \cdot \exp^{k_Q \cdot t} \quad (5.8)$$

where Q_0 is the initial volumetric swelling ratio (here $Q_0 = 11$), and k_Q is the rate constant of the process (here $k_Q = 0.040 \text{ d}^{-1}$). In the same way, ξ_{avg} can be described during the first 30 days by the exponential function:

$$\xi_{avg}(t) = \xi_0 \cdot \exp^{k_\xi \cdot t} \quad (5.9)$$

where ξ_0 is the average mesh size at time $t = 0$ (here $\xi_0 = 5.7$ nm), and k_ξ is the rate constant of the process (here $k_\xi = 0.054 \text{ d}^{-1}$). Thus, Q and ξ_{avg} can be predicted throughout the degradation time.

Rheological experiments were performed to validate the result of the swelling studies. The stress sweep shown in Figure 5.2A indicates a broad linear viscoelastic region of 10% (w/v) 8armPEG10k-hydrogels.

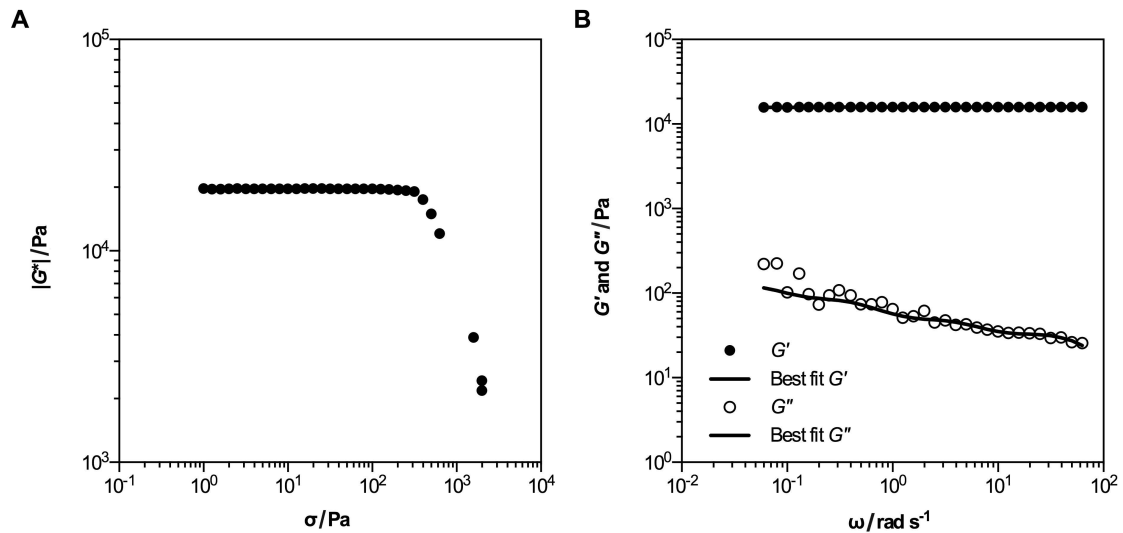


Figure 5.2.* (A) Absolute value of the complex shear modulus vs. oscillatory stress for 10% (w/v) 8armPEG10k hydrogels. (B) Storage and loss modulus vs. oscillatory frequency for 10% (w/v) 8armPEG10k hydrogels. The filled and open symbols represent G' and G'' , respectively; The solid line represents the best fit of eqn. (5.10) and (5.11) to the experimental data. The result of the frequency sweep represents the mean of $n = 3$ samples.

* Data of Figure 5.2 B were fitted by M. Abrami, Department of Life Sciences, University of Trieste and M. Grassi, Department of Engineering and Architecture, University of Trieste

The absolute value of the complex shear modulus ($|G^*|$) was independent from the applied oscillatory stress (σ) between 1 Pa and 200 Pa. The subsequent frequency sweep experiments ($\sigma = 79.5$ Pa) were run within the linear viscoelastic region of the hydrogels. As shown in Figure 5.2B, 10% (w/v) 8armPEG10k-hydrogels are strong, fully elastic hydrogels. The storage modulus (G'), which represents the elastic portion of the hydrogel, was two orders of magnitude higher than the loss modulus (G''), which represents the viscous portion of the hydrogel. Moreover, both G' and G'' were virtually independent from the angular frequency (ω), which is characteristic for covalently cross-linked, permanent hydrogels. To determine ξ_{avg} , the generalized Maxwell model was fitted to the experimental data of G' and G'' [246,247]:

$$G' = G_e + \sum_{i=1}^n G_i \frac{(\lambda_i \omega)^2}{1 + (\lambda_i \omega)^2}; G_i = \eta_i / \lambda_i \quad (5.10)$$

$$G'' = \sum_{i=1}^n G_i \frac{\lambda_i \omega}{1 + (\lambda_i \omega)^2} \quad (5.11)$$

where n is the number of considered Maxwell elements; G_i , η_i and λ_i represent the spring constant, the viscosity of the dashpot component and the relaxation time of the i^{th} Maxwell element, respectively, while G_e is the spring constant of the last Maxwell element, which is supposed to be purely elastic. The simultaneous fitting of eqn. (5.10) and (5.11) to the experimental data of G' and G'' was performed assuming that the relaxation times (λ_i) are scaled by a factor of 10. Hence, the parameters of the model are G_i , G_e and λ_i . Based on a statistical procedure, n was selected in order to minimize the product $\chi^2 \cdot (n + 2)$, where χ^2 is the sum of the squared errors. In this way, the shear modulus (G) can be calculated from the sum of all elastic contributions by $G = G_e + \sum G_i$. According to Flory's theory of rubber elasticity, the cross-link density (defined as the number of moles of cross-links per volume), ρ_x , can be calculated from G :

$$G = \rho_x \cdot RT \quad (5.12)$$

where R is the universal gas constant, and T is the temperature. The "equivalent network" approach allows calculating ξ_{avg} according to eqn. (5.13) [256]:

$$\xi_{avg} = \sqrt[3]{\frac{6}{\pi \cdot \rho_x \cdot N_A}} \quad (5.13)$$

where N_A is the Avogadro constant, and $1 / (\rho_x \cdot N_A)$ is the spherical volume competing with each cross-link. In the case of 10% (w/v) 8armPEG10k-hydrogels, $n = 4$ Maxwell

elements were necessary to describe the mechanical spectrum. On the basis of eqn. (5.10) through (5.12), the values of λ_1 (0.03 s), G (15,988 Pa) and ρ_x ($6.21 \cdot 10^{-6}$ mol cm⁻³) were calculated. Using eqn. (5.13), a ξ_{avg} value of 7.99 nm was calculated, which is in good agreement with the value derived from swelling studies.

To estimate the statistical distribution of ξ , low field NMR measurements were performed. The transverse relaxation time (T_2) of the water protons was measured over 24 h, starting from the time point of gel preparation; however, no significant changes in T_2 were recorded. Thus, it is conceivable that a physical gel is formed initially, which is then reinforced by chemical cross-links. The discrete distribution of T_2 was determined by fitting eqn. (5.3) to the relaxation data. Two different relaxation times were identified, with T_{21} being the longest and most abundant one, and T_{22} being the shortest and least abundant one. The determined T_{2i} values and their relative weights, A_i , are reported in Table 5.1.

Table 5.1.* Transverse relaxation times (T_{2i}) of protons of water molecules entrapped in polymer meshes of size ξ_i ; A_i represent the relative weights of T_{2i} and ξ_i , respectively. The reported T_{2i} values represent the average of all measurements performed during 24 h.

	$i = 1$	$i = 2$
T_{2i} (ms)	2567.6 ± 95.6	603.1 ± 109.3
A_i (%) ^a	90.8 ± 1.6	9.2 ± 1.6
ξ_i (nm)	11.1 ± 2.1	1.0 ± 0.3

^a Calculated by $A_1\% = A_1 \cdot 100\% / (A_1 + A_2)$ and $A_2\% = A_2 \cdot 100\% / (A_1 + A_2)$

* Data were obtained and analyzed by M. Abrami, Department of Life Sciences, University of Trieste and M. Grassi, Department of Engineering and Architecture, University of Trieste.

Since the transverse relaxation time of protons of water molecules near the surface of polymer chains is shorter than the transverse relaxation time of protons of bulk water, T_{2H_2O} , ξ_i can be estimated from T_{2i} [257,258]. The mesh size of an ideal network, ξ_{ideal} , can be calculated on the basis of the Scherer theory by eqn. (5.14) [259,260]:

$$\xi_{ideal} = \sqrt{\frac{3\pi(1 - 0.58\varphi)}{(1 - \varphi)\varphi}} \cdot R_f \quad (5.14)$$

where φ is the polymer volume fraction of the hydrogel (taken as 0.082), and R_f is the radius of the polymer chain (taken as 0.51 nm) [261]. According to the “fiber cell” theory, the average of the inverse relaxation time of the water protons entrapped within the polymer network, $\langle 1/T_2 \rangle$, is given by eqn. (5.15) [258]:

$$\left\langle \frac{1}{T_2} \right\rangle = \frac{1}{T_{2H_2O}} + \frac{2 \langle \mathcal{M} \rangle}{\xi_{ideal} f(\varphi)}; f(\varphi) = \sqrt{\frac{(1 - 0.58\varphi)(1 - \varphi)}{3\pi\varphi}} \quad (5.15)$$

where $\langle \mathcal{M} \rangle$ (length / time) is an empirical parameter (relaxation sink strength) accounting for the effect of the polymer chain surface on proton relaxation. As $\langle 1/T_2 \rangle$, T_{2H_2O} and ξ_{ideal} are known, eqn. (5.15) allows the determination of $\langle \mathcal{M} \rangle$. Furthermore, by knowing T_{2i} and $\langle \mathcal{M} \rangle$, ξ_i can be calculated for each class of network meshes by eqn. (5.16):

$$\frac{1}{T_{2i}} = \frac{1}{T_{H_2O}} + \frac{2\mathcal{M}}{\xi_i f(\varphi)} \quad (5.16)$$

Using this strategy, the ξ_i values of 10% (w/v) 8armPEG10k-hydrogels were estimated. The value of ξ_1 , which represents about 91% of all network meshes, was found to be 11.1 ± 2.1 nm; the value of ξ_2 , which represents the remaining 9% of all network meshes, was 1.0 ± 0.3 nm (Table 5.1). The weighted average mesh size, $\xi_{avg} = 100\% / (A_1\% / \xi_1 + A_2\% / \xi_2)$, was calculated to be 5.4 nm, which is close to the value derived from the swelling experiments (5.8 nm, Table 5.2).

Table 5.2. Mesh size of 10% (w/v) 8armPEG10k hydrogels as determined by swelling studies, rheological experiments and low field NMR measurements.

Type of mesh size	Method	Determined value
Average size (ξ_{avg})	Swelling studies	5.8 ± 0.1 nm ^b
Average size (ξ_{avg})*	Rheological experiments	8.0 nm
Most abundant size (ξ_1)*	Low field NMR (discrete)	11.1 ± 2.1 nm
Least abundant size (ξ_2)*	Low field NMR (discrete)	1.0 ± 0.3 nm
Average size (ξ_{avg})*	Low field NMR (discrete)	5.4 nm ^c
Most abundant size (ξ)*	Low field NMR (continuous)	9.2 nm

^b Determined after 24 h of swelling

^c Calculated by $\xi_{avg} = 100\% / (A_1\% / \xi_1 + A_2\% / \xi_2)$

* Data were obtained by M. Abrami, Department of Life Sciences, University of Trieste and M. Grassi, Department of Engineering and Architecture, University of Trieste.

To evaluate the continuous distribution of the mesh size, the relaxation time distribution, $a(T_2)$, was determined by fitting eqn. (5.4) to the relaxation data. The result reveals the presence of two peaks occurring at relaxation times similar to T_{21} and T_{22} , respectively (Figure 5.3A).

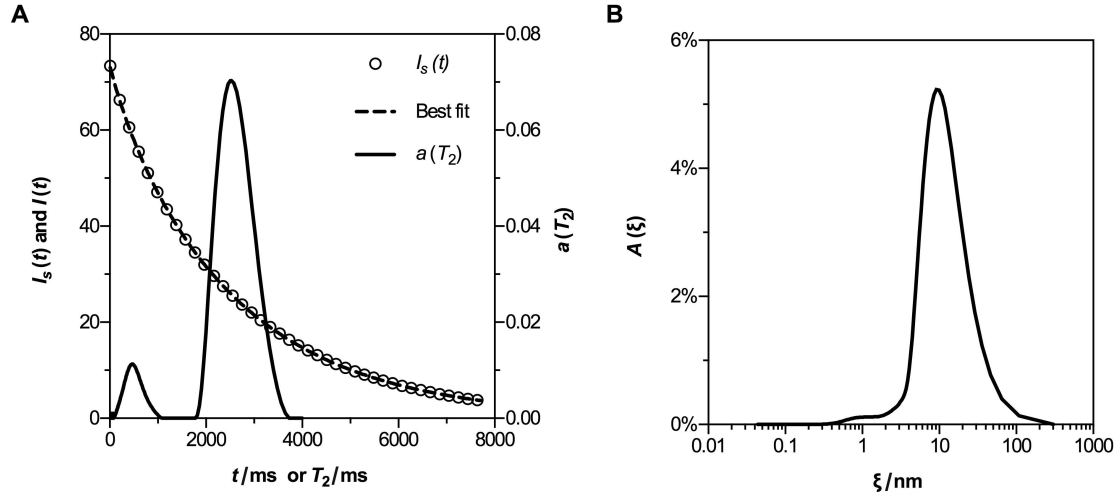


Figure 5.3.* (A) Signal intensity, related to the decay of the transverse component of the magnetization vector, vs. time. The open symbols represent the relaxation data, and the dashed line represents the best fit of eqn. (5.4). The solid line represents the continuous distribution of the relaxation time, $a(T_2)$. (B) Continuous distribution of the mesh size, $A(\xi)$, of 10% (w/v) 8armPEG10k hydrogels. The results represent the average of all measurements performed during 24 h.

* Data were obtained and analyzed by M. Abrami, Department of Life Sciences, University of Trieste and M. Grassi, Department of Engineering and Architecture, University of Trieste.

Once $a(T_2)$ or $A(T_2)$ are known, $\langle \mathcal{M} \rangle$ can be derived from eqn (5.14) and (5.15), with the only difference that $\langle 1/T_2 \rangle$ is calculated according to eqn. (5.6). Using eqn. (5.16), $A(T_2)$ is converted into the mesh size distribution, $A(\xi)$, where $A_i(\xi) = A_i(T_2)$. To allow the comparison of mesh size distributions of different systems, A_i is normalized according to:

$$A_i\%(\xi) = A_i\%(T_2) = \frac{100A_i(T_2)}{\sum_{i=1}^N A_i(T_2)}; \sum_{i=1}^N A_i\% = 100 \quad (5.17)$$

As shown in Figure 5.3B, $A(\xi)$ spanned over three orders of magnitude; meshes as large as 300 nm were observed, even if this probability, A_i , is very low. Two distinct peaks were identified: a small peak at around 1 nm and a larger one at around 10 nm. Interestingly, the proportion between the two peaks matched the result found in the discrete approach (about 9% smaller meshes and 91% larger meshes, Table 5.1); however, the continuous distribution provided more information than the discrete one. The most abundant mesh size ($A_i = 5.2\%$) was found to be 9.2 nm, which is in good agreement with the values derived from the discrete approach (11.1 ± 2.1 nm, Table 5.2). These conclusions are supported by the measurements of the water self-diffusion coefficient. PGSE studies revealed that two exponential terms in eqn. (5.7) are required to properly describe the experimentally

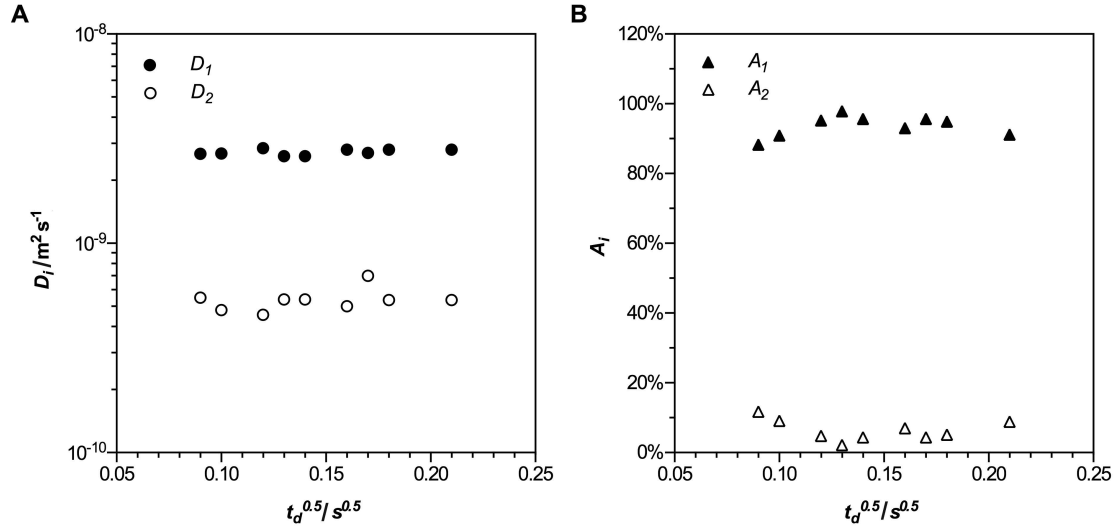


Figure 5.4.* (A) High (D_1) and low (D_2) self-diffusion coefficients of water molecules *versus* the square root of the diffusion time, t_d . The self-diffusion coefficient of free water at 37 °C is $3.04 \cdot 10^{-9} \text{ m}^2 \text{ s}^{-1}$ [262]. (B) $A_1\%$ and $A_2\%$ represent the relative abundance of the fast and slow diffusing species, respectively.

* Data were obtained and analyzed by M. Abrami, Department of Life Sciences, University of Trieste and M. Grassi, Department of Engineering and Architecture, University of Trieste.

determined ratio of A_i / A_0 to q^2 for every t_d considered ($7.6 \text{ ms} < t_d < 44 \text{ ms}$). Figure 5.4 shows the existence of two species of water molecules with different mobility. The fastest species is characterized by a self-diffusion coefficient of $D_1 \approx 2.7 \cdot 10^{-9} \text{ m}^2 \text{ s}^{-1}$, which is close to the self-diffusion coefficient of free water at 37 °C ($3.04 \cdot 10^{-9} \text{ m}^2 \text{ s}^{-1}$) [262], and represents about 94% of all water molecules. The slowest species is characterized by a self-diffusion coefficient of $D_2 \approx 5.4 \cdot 10^{-10} \text{ m}^2 \text{ s}^{-1}$ and represents the remaining 6% of water molecules. While D_1 is connected to the existence of wide network meshes (with respect to the size of the water molecule), D_2 is most likely due to the presence of narrow meshes that significantly hinder the diffusion of water molecules. Interestingly, these findings match the results of the T_2 measurements (about 91% larger meshes and 9% smaller meshes, Table 5.1). Moreover, it is worth mentioning that, as D_1 and D_2 are essentially independent from t_d , both wide and narrow meshes are interconnected [263]. In conclusion, all three methods (*i.e.*, swelling studies, rheological experiments and NMR spectroscopy) give similar estimates of ξ_{avg} . Low field NMR measurements might be the preferred method when the mesh size distribution is important; on the other hand, swelling studied might be most appropriate to determine the mesh size during degradation or drug release.

5.3.2 In vitro release of fluorescein isothiocyanate labeled dextran

To correlate the determined mesh sizes with release profiles, the *in vitro* release of macromolecules from DA hydrogels was investigated. FD was used as model compounds; four different molecular masses (4 kDa, 20 kDa, 150 kDa and 500 kDa) were studied. The hydrodynamic radius (R_h) of FDs can be estimated according to eqn. (5.18) [264]:

$$R_h = 0.0488(M_r)^{0.437}; [R_h] = \text{nm} \quad (5.18)$$

where M_r is the relative molecular mass of the FD. The hydrodynamic radii and the diffusion coefficients in water (D_0), calculated from the Stokes-Einstein equation:

$$D_0 = \frac{kT}{6\pi\eta R_h} \quad (5.19)$$

are listed in Table 5.3. In eqn. (5.19), k is the Boltzmann constant, T is the temperature (310.16 K), and η is the viscosity of water (0.69 mPa s).

Table 5.3: Relative molecular mass (M_r), hydrodynamic radius (R_h) and diffusion coefficient in water (D_0) of the studied fluorescein isothiocyanate-labeled dextrans (FDs). The values of R_h were estimated according to eqn. (5.18); the values of D_0 were calculated from eqn. (5.19).

	M_r (Da)	R_h (nm)	D_0 (cm ² s ⁻¹)
FD4	4,000	1.8	$1.80 \cdot 10^{-6}$
FD20	20,000	3.7	$8.90 \cdot 10^{-7}$
FD150	150,000	8.9	$3.69 \cdot 10^{-7}$
FD500	500,000	15.1	$2.18 \cdot 10^{-7}$

The mobility of solutes in homogenous hydrogels can be described by the obstruction-scaling model developed by Amsden [265]:

$$\frac{D_g}{D_0} = \exp \left[-\frac{\pi}{4} \left(\frac{R_f + R_h}{R_f + 0.5 \xi_{avg}(t)} \right)^2 \right] \quad (5.20)$$

where D_g is the diffusion coefficient of the solute in the hydrogel. Based on the results of the performed swelling studies and eqn. (5.9), eqn. (5.20) can be used to estimate the mobility of FDs within DA hydrogels during the release period (Figure 5.5A).

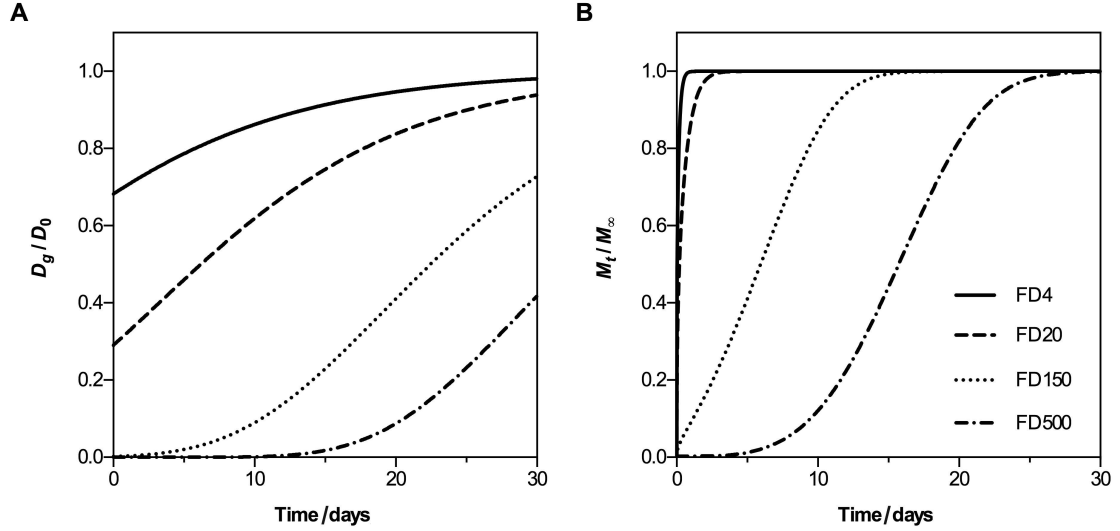


Figure 5.5. (A) Diffusion quotients (D_g/D_0) of fluorescein isothiocyanate-labeled dextrans (FDs) vs. time. The values of D_g/D_0 were calculated from eqn. (5.20). (B) Predicted release of FDs from 10% (w/v) 8armPEG10k hydrogels. The predictions are based on eqn. (5.21).

Since R_h is much smaller than ξ_{avg} , the diffusivity of FD4 should be high in the non-swollen ($t = 0$) and swollen state ($t > 0$). The mobility of FD20 should be restricted in the beginning; however, the diffusivity of entrapped FD20 should increase with increasing degree of swelling. In contrast to this, the R_h values of FD150 and FD500 are much greater than the initial ξ_{avg} value. Thus, both dextrans will not be free to move through the hydrogel network in a spherical conformation. Eqn. (5.20) predicts an extremely low diffusivity at low degrees of swelling; however, the diffusivity of FD150 and FD500 should increase during swelling once a critical ξ_{avg} value is exceeded. Since the D_g values can be calculated from eqn. (5.19) and (5.20), the release of entrapped FDs from hydrogel cylinders can be described according to eqn. (5.21) [266]:

$$\frac{M_t}{M_\infty} = 1 - \frac{32}{\pi^2} \sum_{n=1}^{\infty} \frac{1}{q_n^2} \exp\left(-\frac{q_n^2}{r^2} D_g t\right) \cdot \sum_{p=0}^{\infty} \frac{1}{(2p+1)^2} \exp\left(-\frac{(2p+1)^2 \pi^2}{h^2} D_g t\right) \quad (5.21)$$

where M_t and M_∞ represent the absolute cumulative amounts of FD released at time t and infinity, respectively; q_n are the roots of the Bessel function of the first kind of zero order, and r and h denote the radius and height of the gel cylinder. The increase in r and h due to swelling is taken into account, and the predicted release profiles are shown in Figure 5.5B. As it is expected from the D_g values, the release of FD4 and FD20 from DA hydrogels should be extremely fast; the release should be completed after 1 day and 2 days, respectively. Compared to FD4 or FD20, the release of FD150 should be considerably

slower; the maximum release should be reached after 15 days. In contrast to this, a sigmoidal release profile is predicted for FD500. Since the mobility of FD500 is extremely low during the first 10 days of release, eqn. (5.21) predicts a lag time of approximately 5 days; the release of FD500 should be completed after 25 days. To verify the validity of our model, the release of FDs from DA hydrogels was experimentally determined (Figure 5.6).

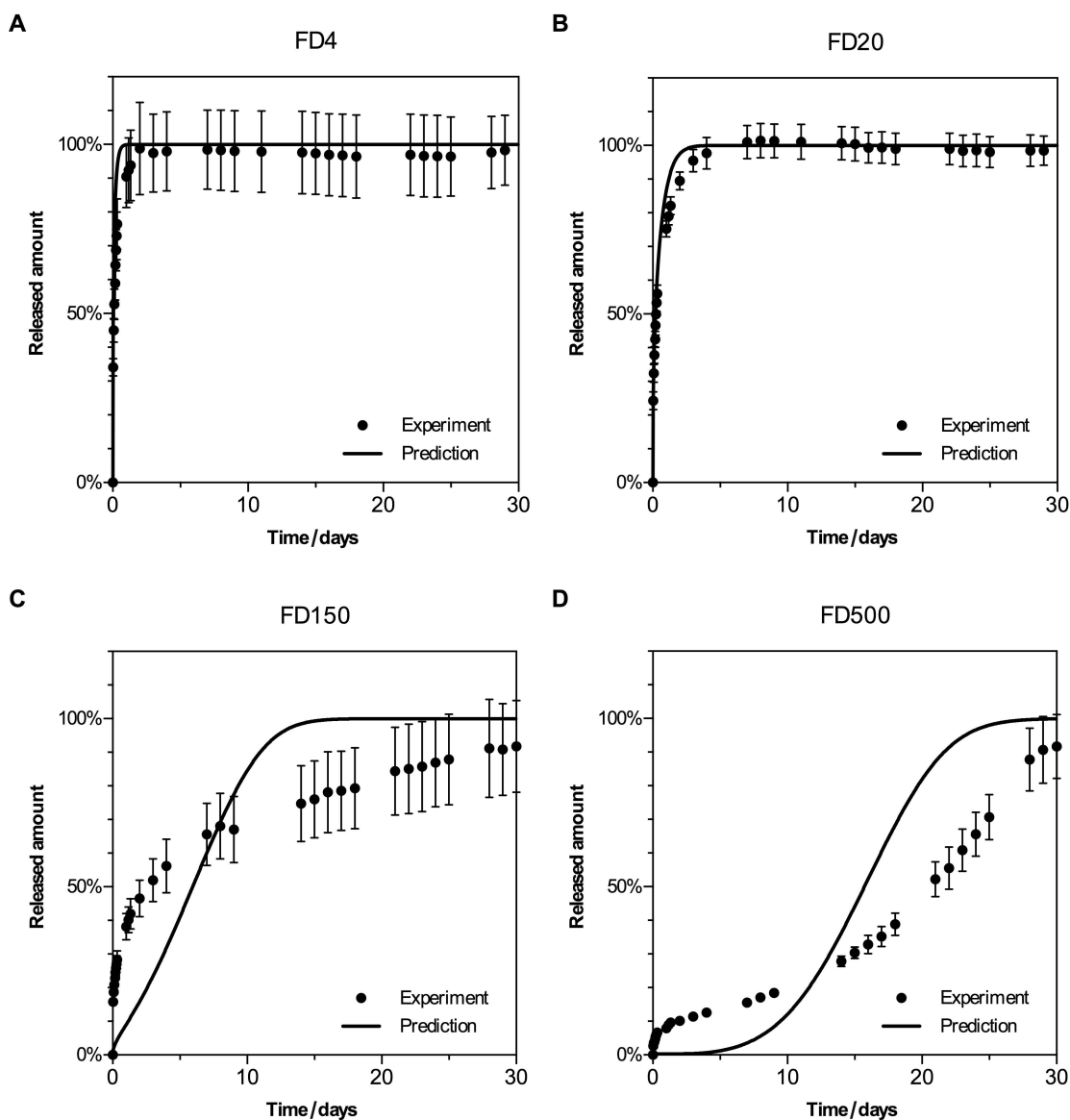


Figure 5.6. Release of fluorescein isothiocyanate-labeled dextrans (FDs) from 10% (w/v) 8armPEG10k hydrogels. The symbols represent the experimental data, and the solid lines represent the predictions based on eqn. (5.21). The theoretical predictions match the release profiles of FD4 (A) and FD20 (B) very well; however, significant differences between the theoretical predictions and the experimental data are observed for FD150 (C) and FD500 (D). Data is expressed as mean \pm standard deviation based on the results of $n = 3$ samples.

The release of FD4 from DA hydrogels was extremely fast; the incorporated dextran was completely released after 2 days (Figure 5.6A). In comparison to FD4, the release of FD20

was slightly slower; the maximum release was reached after 5 days (Figure 5.6B). The release of FD150 from DA hydrogels was considerably slower than the release of FD4 or FD20; 90% of the incorporated dextran was released after 30 days (Figure 5.6C). In contrast to FD4, FD20 and FD150, the release profile of FD500 had a sigmoidal shape. Approximately 10% of the incorporated FD500 was released during the first day; this was followed by a phase of slow release, with approximately 30% of the incorporated dextran being release at day 15. Following this, the release rate considerably increased; 90% of the incorporated FD500 was released after 30 days (Figure 5.6D). The theoretical predictions for the release behavior are shown by the lines in Figure 5.6. In case of FD4 and FD20, the predicted release profiles match the experimentally determined release profiles very well. However, marked differences between the theoretical predictions and the experimental data are observed for FD150 and FD500. On the one hand, the developed model underestimates the initial “burst” release; on the other hand, it overestimates the release rate in the terminal phase of release. These deviations are explained by the statistical distribution of ξ in real polymer networks. As shown in Figure 5.3B, $A(\xi)$ spans over three decades (from 0.3 nm to 300 nm), while eqn. (5.20) only considers ξ_{avg} (5.8 nm at $t = 0$). This simplification may be acceptable when R_h is smaller than ξ_{avg} and the dextran is free to diffuse throughout the gel network; however, deviations from the experimental results occur when R_h is similar to or greater than ξ_{avg} . The existence of larger meshes ($\xi > R_h$) can explain the initial “burst” release, while the continued existence of smaller meshes ($\xi < R_h$) may delay the terminal phase of release. Furthermore, the values of R_h were estimated from the average molecular mass of the FDs, assuming that these molecules were monodisperse. In fact, however, FDs are polydisperse, which may also contribute to the observed deviations. In addition, eqn. (5.20) assumes that the solutes behave as hard spheres; however, dextran is flexible polymer of D-glucopyranose that behaves like a random coil. [264]. When R_h is similar to ξ , the dextran may get “trapped” in the larger meshes, where the molecule can extend and maximize its conformational entropy (“entropic trapping”) [267]. On the other hand, when R_h is greater than ξ , the dextran can migrate through the network in a wormlike fashion (“reptation”) [268]. However, both entropic trapping and reptation are not considered by eqn. (5.20). And last but not least, it is possible that cross-linking in the presence of FD150 or FD500 affects ξ_{avg} , given the large R_h of these molecules. The FD molecules could be physically entangled with the PEG molecules before cross-linking, which would influence the mesh size distribution.

5.3.3 In vitro release of bevacizumab

In the final experiment, the release profiles of bevacizumab and FD were compared. With an hydrodynamic radius of 6.5 nm [269], the release of bevacizumab from 10% (w/v) 8armPEG10k-hydrogels should be comparatively fast; the release profile of bevacizumab should fall between those of FD20 ($R_h = 3.7$ nm) and FD150 ($R_h = 8.9$ nm). However, the experimentally determined release profile differed significantly from those of FD20 and FD150. As shown in Figure 5.7, a sigmoidal release profile was observed for bevacizumab.

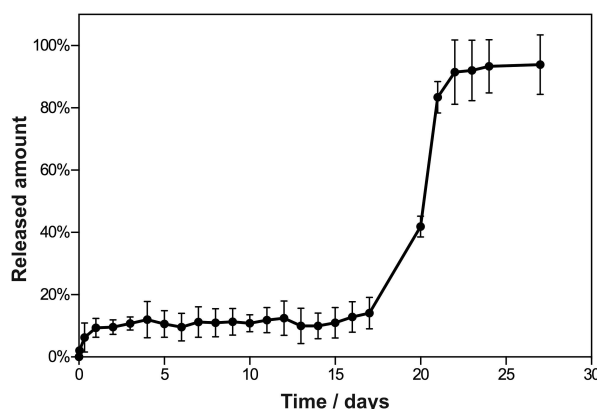


Figure 5.7. Release of bevacizumab from 10% (w/v) 8armPEG10k hydrogels. The amount of drug loading was 1.25 mg of bevacizumab per hydrogel. Data is expressed as mean \pm standard deviation of $n = 3$ samples.

Approximately 10% of the incorporated bevacizumab was released after 24 h; this is attributed to non-entrapped protein molecules located at the surface of the gel cylinders. No bevacizumab release occurred during the following 16 days, indicating that the protein molecules were entrapped within the hydrogel meshes. However, since ξ is increasing during the degradation process, the incorporated bevacizumab was completely released between day 17 and 22 after a critical ξ value had been exceeded. No further release was observed after day 22.

The discrepancy in the release profiles can be explained by the different molecular configuration (i.e., size, charge, shape and deformability) of proteins and dextran molecules. Dextran is a linear, rather flexible polymer of D-glucopyranose; proteins, on the other hand, are globular, rather rigid molecules. As a consequence, dextran molecules are able to pass through pores smaller than the molecule itself. For example, it has been shown that the glomerular sieving coefficient of dextran is approximately sevenfold higher than that of a globular protein of equivalent size [264]. Thus, the delayed release of bevacizumab is the result of the globular structure and rigidity of the protein. Furthermore, it has been shown that 20–30% of the incorporated protein is immobilized

within the hydrogel by Michael-type addition reaction to 8armPEG10k-maleimide [17]. This portion of the protein is not released until the hydrogel dissolves. Depending on the number of PEG molecules remaining attached, the antigen binding activity of these PEGylated antibodies can be slightly decreased or completely lost [270].

Although most controlled release systems for proteins are designed to provide sustained release, the delayed release of bevacizumab from DA hydrogels could prove to be beneficial for the treatment of AMD. There is increasing evidence that chronic blocking of VEGF signaling might have detrimental long-term effects such as the development of geographic atrophy, which is accompanied by a massive loss of photo-receptors [133,134,271]. For that reason, the treatment with VEGF inhibiting antibodies should be intermittent to allow the damaged choriocappilaris to recover during drug-free intervals. DA hydrogels could provide such intermittent drug release. The first dose would be administered together with the hydrogel, while the second dose would be released from the gel four to six weeks after injection.

5.4 Conclusion

Hydrogels were prepared by cross-linking 8armPEG10k-furan and 8armPEG10k-maleimide via DA reaction. The mesh size of the formed hydrogels was determined using swelling studies, rheology and low field NMR spectroscopy. The *in vitro* release of incorporated FDs and bevacizumab was investigated. In principle, all three methods (i.e., swelling studies, rheology and NMR spectroscopy) give similar estimates of ξ_{avg} ; however, low field NMR measurements are the preferred method when the mesh size distribution is important. On the other hand, swelling studies are most appropriate to determine the time-dependent increase of ξ_{avg} during hydrogel degradation or drug release. Combined with the hydrodynamic radius of the drug molecule, the determined values of ξ_{avg} can be used to predict drug release over time. When R_h is smaller than ξ_{avg} , the predicted release profiles match the experimentally determined release profiles very well. However, deviations from the theoretical predictions are observed when R_h is similar to or greater than ξ_{avg} . These deviations are most likely due to the statistical distribution of ξ in real polymer networks. Nevertheless, the model correctly predicts the expected sigmoidal shape of the release profile. Furthermore, the structure and rigidity of the drug molecule must be taken into account. In contrast to globular proteins (e.g., bevacizumab), FDs are able to pass through pores smaller than the molecule itself in a

wormlike fashion (“reptation”). Altogether, we believe that the established correlation between ξ and the release rate may facilitate a more rational design of controlled release systems for antibodies. In the future, the model could be further refined by evaluating the mesh size distribution, $A(\xi)$, instead of ξ_{avg} .

Chapter 6

Diels-Alder Hydrogels with Enhanced Stability: First Steps Toward Controlled Release of Bevacizumab

This chapter was published as: S. Kirchhof, M. Gregoritz, V. Messmann, N. Hammer, A. M. Goepferich, and F. P. Brandl, *Eur. J. Pharm. Biopharm.* 96 (2015) 217-255, doi.org/10.1016/j.ejpb.2015.07.024.

Abstract

Eight-armed PEG was functionalized with furyl and maleimide groups (8armPEG20k-Fur and 8armPEG20k-Mal); degradable hydrogels were obtained by cross-linking via DA chemistry. To increase the stability to degradation, the macromonomers were modified by introducing a hydrophobic Ahx spacer between PEG and the reactive end-groups (8armPEG20k-Ahx-Fur and 8armPEG20k-Ahx-Mal). In an alternative approach, the number of reactive groups per macromonomer was increased by branching the terminal ends of eight-armed PEG with Lys and Ahx residues (8armPEG20k-Lys-Ahx-Fur₂ and 8armPEG20k-Lys-Ahx-Mal₂). The hydrolytic resistance of the synthesized macromonomers was determined by UV spectroscopy; the obtained hydrogels were characterized by rheology and degradation studies. The degradation time of 5% (w/v) 8armPEG20k-Ahx-hydrogels (28 days) was twice as long as the degradation time of 5% (w/v) 8armPEG20k-hydrogels (14 days); this is explained by increased hydrolytic resistance of the maleimide group. Using dendritic 8armPEG20k-Lys-Ahx-macromonomers substantially increased the stability of the resulting hydrogels; degradation of 5% (w/v) 8armPEG20k-Lys-Ahx-hydrogels occurred after 34 weeks. 8armPEG20k-hydrogels had the largest mesh size of all tested hydrogels, while hydrogels made from dendritic 8armPEG20k-Lys-Ahx-macromonomers had the smallest value. To evaluate their potential for the controlled release of therapeutic antibodies, the hydrogels were loaded with bevacizumab. The incorporated bevacizumab was released over 10 days (8armPEG20k) and 42 days (8armPEG20k-Ahx), respectively; release from 8armPEG20k-Lys-Ahx-hydrogels was not completed after 105 days. In summary, we believe that 8armPEG20k-Ahx- or 8armPEG20k-Lys-Ahx-hydrogels could serve as controlled release system for therapeutic antibodies such as bevacizumab.

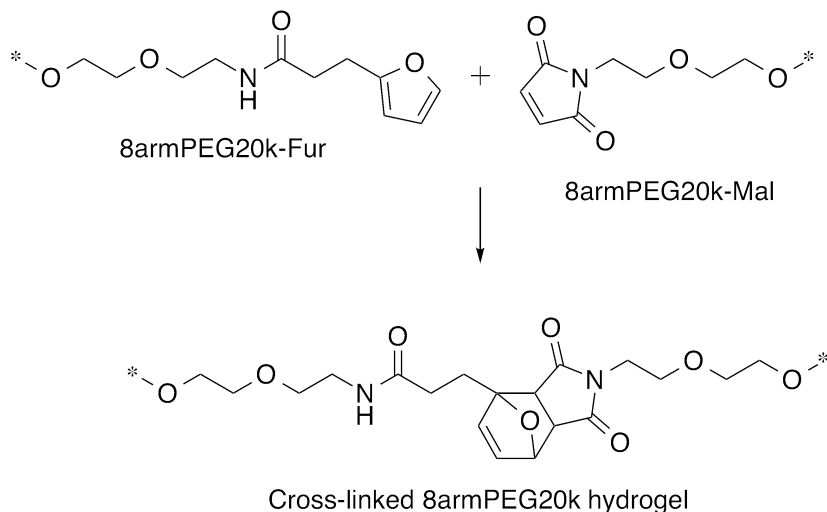
6.1 Introduction

The development of monoclonal antibodies and antibody fragments against VEGF, such as bevacizumab and ranibizumab, represents a milestone in the treatment of AMD and other vision-threatening diseases [5,9]. While antibodies have several desirable characteristics, such as high selectivity and specificity, achieving effective concentrations at the target tissue can be challenging. The bioavailability of systemically or topically administered antibodies in the posterior segment of the eye is generally low; the ocular half-life of antibodies is about 7 to 10 days [11]. To increase the local bioavailability of antibodies and minimize undesired side effects, most anti-VEGF drugs are, therefore, administered every 4 to 6 weeks by intravitreal injection. However, these injections are associated with significant discomfort and rare but severe complications including endophthalmitis, retinal detachment and cataract [10]. Using controlled release systems that prolong the dosing intervals of antibodies may help to improve the patient compliance and reduce the treatment costs.

Compared to other controlled release systems that have been developed for the posterior segment of the eye, such as implants or microspheres, hydrogels may offer several advantages [13,14]. For example, they are deemed biocompatible and capable of preserving the bioactivity of hydrophilic biomolecules. Hydrogels can, furthermore, accommodate high loads of antibodies through *in situ* encapsulation, a method in which drug loading and cross-linking are carried out simultaneously. The mobility of incorporated antibodies is limited by the polymer network; the hydrogel matrix forms a reservoir from which the antibody is slowly released. Depending on the size of the protein and the average mesh size (ξ) of the hydrogel, the release is controlled by diffusion, swelling, degradation, or a combination of these mechanisms. Finally, *in situ* forming hydrogels can be administered by minimally invasive techniques; these hydrogels are injected in liquid form and turn into a viscoelastic drug depot at the site of application. This requires cross-linking reactions that are both effective and non-toxic *in vivo*.

Recently, we described the synthesis of *in situ* forming, biodegradable hydrogels for the controlled release of proteins [212,248]. Eight-armed PEG was functionalized with furyl and maleimide groups (*e.g.*, 8armPEG20k-Fur and 8armPEG20k-Mal), respectively; the obtained macromonomers were cross-linked via DA chemistry (Scheme 1). The DA reaction proceeds in water without any metal catalyst or initiator. This is an advantage over existing controlled release systems for bevacizumab, which are cross-linked by free radical polymerization [135–137]. The reported ξ values would allow the controlled

release of antibodies; however, the relatively fast degradation within 2 to 9 weeks might limit potential applications of DA hydrogels [212]. To effectively prolong the dosing intervals of VEGF-neutralizing antibodies, which are typically administered every 4 to 6 weeks, the hydrogel should be stable for at least 8 to 12 weeks.



Scheme 6.1. Cross-linking of 8armPEG20k-Fur and 8armPEG20k-Mal via DA reaction. The macromonomers were synthesized from eight-armed PEG, molecular mass 20,000 kDa.

Herein, we report on our efforts to increase the stability of DA hydrogels. Since the degradation rate of DA hydrogels is related to the rate of ring-opening hydrolysis of maleimide [248], we aimed at generating hydrogels with increased stability to degradation by improving the hydrolytic stability of the maleimide group. According to the available literature, this can be achieved by introducing a hydrophobic Ahx spacer between PEG and the maleimide end-group [224,272–274]. Moreover, it has been shown that the degradation rate of DA hydrogels depends on the number of reactive groups per macromonomer [212]. To further increase the stability of DA hydrogels we, therefore, synthesized macromonomers with an increased number of reactive groups by branching the terminal ends of star-shaped PEG with Lys and Ahx residues. These dendritic macromonomers should gel more rapidly and yield slow-degrading hydrogels. The hydrolytic stability of the macromonomers and the rate constant of the DA reaction were determined by UV spectroscopy. The hydrogels were characterized by means of rheological, swelling and degradation studies; their ζ values were calculated. Finally, the *in vitro* release of bevacizumab was studied and compared to existing controlled release systems.

6.2 Materials and methods

6.2.1 General procedure

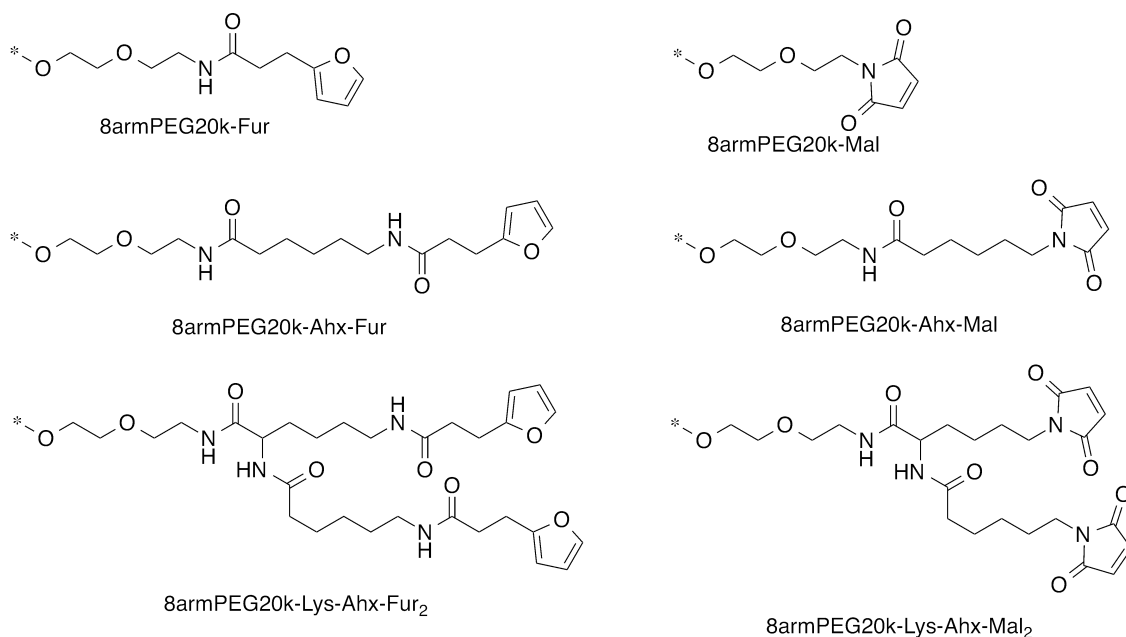
¹H-NMR spectra were recorded in CDCl₃ at room temperature on a Bruker Avance 300 spectrometer (Bruker BioSpin GmbH, Rheinstetten, Germany).

6.2.2 Materials

Acetyl chloride, deuterated chloroform (CDCl₃), *N,N'*-dicyclohexylcarbodiimide (DCC), diisopropyl azodicarboxylate (DIAD), *N,N'*-diisopropylethylamine (DIPEA), anhydrous dimethylformamide (DMF), 3-(2-furyl)propanoic acid, *N*-hydroxysuccinimide (NHS), *N*-methoxycarbonylmaleimide and piperidine were purchased from Sigma-Aldrich (Taufkirchen, Germany). Dichloromethane (DCM), anhydrous 1,4-dioxane, sodium bicarbonate (NaHCO₃), anhydrous sodium sulfate (Na₂SO₄) and triphenylphosphine were received from Acros Organics (Geel, Belgium). Eight-armed poly(ethylene glycol), molecular mass 20,000 (hexaglycerol core) was purchased from JenKem Technology (Allen, TX, USA). Boc-6-aminohexanoic acid and Fmoc-Lys(Boc)-OH were obtained from Bachem (Weil am Rhein, Germany). Diethyl ether was received from CSC Jäcklechemie (Nuremberg, Germany). Water was obtained by using a Milli-Q water purification system from Millipore (Schwalbach, Germany). Bevacizumab (Avastin[®], 25 mg/mL, Roche Ltd., Basel, Switzerland) was kindly provided by the hospital pharmacy, University of Regensburg, Germany. All other chemicals were purchased from Merck KGaA (Darmstadt, Germany).

6.2.3 Synthesis of macromonomers (Scheme 2)

Eight-armed PEG-amine, molecular mass 20 kDa (8armPEG20k-NH₂) was synthesized as previously described [212]. The end-groups of 8armPEG20k-NH₂ were functionalized with furyl (8armPEG20k-Fur) and maleimide groups (8armPEG20k-Mal) as previously described [212]. The synthesis of 8armPEG20k-Ahx-Fur, 8armPEG20k-Ahx-Mal, 8armPEG20k-Lys-Ahx-Fur₂ and 8armPEG20k-Lys-Ahx-Mal₂ is described in the supplement.



Scheme 6.2. Functional end-groups of 8armPEG20k-Ahx-Fur, 8armPEG20k-Ahx-Mal, 8armPEG20k-Lys-Ahx-Fur₂ and 8armPEG20k-Lys-Ahx-Mal₂. The macromonomers were synthesized from eight-armed poly(ethylene glycol), molecular mass 20,000 kDa.

6.2.4 Hydrolytic stability of maleimides

The hydrolytic stability of 8armPEG20k-Mal, 8armPEG20k-Ahx-Mal and 8armPEG20k-Lys-Ahx-Mal₂ was determined by UV spectroscopy as previously described. For this purpose, 20 mg of 8armPEG20k-Mal, 8armPEG20k-Ahx-Mal and 8armPEG20k-Lys-Ahx-Mal₂ were dissolved in 2 mL of water or 50 mM phosphate buffer, pH 7.4. The decrease in the absorbance at 299 nm (UV maximum of the maleimide group) was monitored in 10 mm quartz cuvettes for 1000 min at 37 °C using a Kontron UVIKON[®] 941 spectrophotometer (Kontron Instruments S.p.A., Milan, Italy).

6.2.5 Kinetics of the Diels-Alder reaction

Equal molar amounts of 8armPEG20k-Fur and 8armPEG20k-Mal, 8armPEG20k-Ahx-Fur and 8armPEG20k-Ahx-Mal, or 8armPEG20k-Lys-Ahx-Fur₂ and 8armPEG20k-Lys-Ahx-Mal₂ were dissolved in water. The overall polymer concentrations were 5% (w/v), 10% (w/v) and 15% (w/v). Aliquots of these solutions were pipetted into a 96-well quartz microplate. The decrease in the absorbance at 299 nm (UV maximum of the maleimide group) was monitored at 37 °C using a microplate reader (BMG LABTECH GmbH, Ortenberg, Germany). The absorbance values were converted into maleimide concentrations. A second-order kinetic model was fitted to the experimental data to determine the second-order rate constant (k) of the DA reaction.

6.2.6 Characterization of Diels-Alder hydrogels

For the preparation of hydrogels, equal molar amounts of 8armPEG20k-Fur and 8armPEG20k-Mal, 8armPEG20k-Ahx-Fur and 8armPEG20k-Ahx-Mal, or 8armPEG20k-Lys-Ahx-Fur₂ and 8armPEG20k-Lys-Ahx-Mal₂ were dissolved in water. The overall polymer concentrations were 5% (w/v), 10% (w/v) and 15% (w/v). The hydrogels were characterized by oscillatory shear experiments on a TA Instruments AR 2000 rheometer (TA Instruments, Eschborn, Germany) at 37 °C as previously described. The crossover of storage modulus (G') and loss modulus (G'') was regarded as the gel point; the absolute value of the complex shear modulus (G^*) was determined after the maximum value had been reached. The average mesh size (ζ) of the hydrogels was determined as previously described [212]. For swelling and degradation studies, gel cylinders were immersed in 50 mM phosphate buffer, pH 7.4 and incubated at 37 °C in a shaking water bath. The gel cylinders were weighed at regular times as previously described [212].

6.2.7 In vitro release of bevacizumab

Equal molar amounts of 8armPEG20k-Fur and 8armPEG20k-Mal, 8armPEG20k-Ahx-Fur and 8armPEG20k-Ahx-Mal, or 8armPEG20k-Lys-Ahx-Fur₂ and 8armPEG20k-Lys-Ahx-Mal₂ were dissolved in 600 μ L of water; 150 μ L of a solution of bevacizumab ($c = 25$ mg/mL) were added. The overall polymer concentration was 10% (w/v) in all groups. Directly after mixing, 250 μ L of the solutions were cast into cylindrical glass molds (7 mm inner diameter) and allowed to gel for 72 h under standard cell culture conditions (37 °C, 95% relative humidity and 5% CO₂). The bevacizumab loading was 1.25 mg per gel cylinder. Afterwards, the gel cylinders were removed from the glass molds and incubated in 5 mL of 50 mM phosphate buffer, pH 7.4 at 37 °C in a shaking water bath. Samples of 300 μ L were withdrawn at regular times and replaced by fresh buffer. The samples were stored at 4 °C until completion of the release experiment. The amount of released bevacizumab ($\lambda_{\text{ex}} = 280$ nm and $\lambda_{\text{em}} = 335$ nm) was determined on a PerkinElmer LS 55 Fluorescence spectrometer (Perkin Elmer, Wiesbaden, Germany) using a calibration curve.

6.2.8 Statistical analysis

The results are presented as mean \pm standard deviation based on the results of $n = 3$ samples. The data were analyzed by means of one-way ANOVA followed by Tukey's post-hoc test (GraphPad Prism 5.01, GraphPad Software Inc., La Jolla, CA). The differences were considered statistically significant at $p < 0.05$.

6.3 Results and discussion

6.3.1 Synthesis of macromonomers

Since the DA reaction does not require any metal catalyst or initiator, it is regarded as effective and non-toxic cross-linking method for the preparation of *in situ* forming drug delivery systems [56,21,212]. Moreover, it has been demonstrated that DA hydrogels made from star-shaped PEG degrade under physiological conditions by rDA reaction and subsequent ring-opening hydrolysis of the generated maleimide groups [248]. However, the stability of DA hydrogels might not be sufficient to prolong the dosing intervals of anti-VEGF drugs, such as bevacizumab or ranibizumab, which are typically administered every 4 to 6 weeks. For example, DA hydrogels made from eight-armed PEG were stable for 2 to 9 weeks, with the degradation rate depending on the concentration and molecular mass of the gel-forming macromonomers [212]. Further increasing the polymer concentration can impair the biocompatibility of the hydrogel and affect the stability of encapsulated biomolecules [14]; therefore, alternative ways of increasing the gel stability must be considered. Furthermore, it would be beneficial to decrease the gel time (t_{gel}) of DA hydrogels to ensure the formation of a drug depot in potential applications.

To increase the stability of DA hydrogels, the macromonomers were modified by introducing a hydrophobic Ahx spacer between 8armPEG20k-NH₂ and the reactive end-groups; the alkyl spacer is expected to improve the hydrolytic stability of the maleimide group [224,272–274]. The synthesis proved to be straightforward; the macromonomers 8armPEG20k-Ahx-Fur and 8armPEG20k-Ahx-Mal were obtained in satisfactory yields. The degree of substitution with furyl and maleimide groups was 82% and 65%, respectively; nevertheless, the degree of endgroup functionalization was high enough to enable cross-linking. To further increase the stability and accelerate the gelation of DA

hydrogels, dendritic macromonomers were synthesized by branching the terminal ends of 8armPEG20k-NH₂ with Lys and Ahx residues. In our first approach, 8armPEG20k-NH₂ was reacted with Boc-Lys(Boc)-OH and deprotected; however, the subsequent reaction with *N*-methoxycarbonylmaleimide failed and an insoluble resin was obtained. The reactivity of α - and ϵ -amino groups is apparently different; this could lead to cross-linking via aza-Michael additions. Therefore, we tried an alternative strategy of synthesizing dendritic macromonomers. In the first step, 8armPEG20k-NH₂ was reacted with Fmoc-Lys(Boc)-OH; the Fmoc group was removed, and the intermediate was reacted with Boc-Ahx-OH. After complete deprotection, the macromonomers 8armPEG20k-Lys-Ahx-Fur₂ and 8armPEG20k-Lys-Ahx-Mal₂ could be synthesized in satisfactory yields. The degree of substitution with furyl and maleimide groups was 75% and 86%, respectively, which was sufficiently high to enable cross-linking.

6.3.2 Hydrolytic stability of maleimides

Ring-opening hydrolysis of maleimide to unreactive maleamic acid has been shown to affect both cross-linking and degradation of DA hydrogels [248]. Therefore, the hydrolytic stability of 8armPEG20k-Mal, 8armPEG20k-Ahx-Mal and 8armPEG20k-Lys-Ahx-Mal₂ was investigated in water and 50 mM phosphate buffer, pH 7.4 at 37 °C. When the macromonomers were incubated in water, the absorbance at 299 nm slowly decreased indicating high stability of the maleimide groups (data not shown). In contrast to this, the absorbance measurably decreased in phosphate buffer pH 7.4, which indicates fast ring-opening hydrolysis of maleimide groups (Figure 6.1).

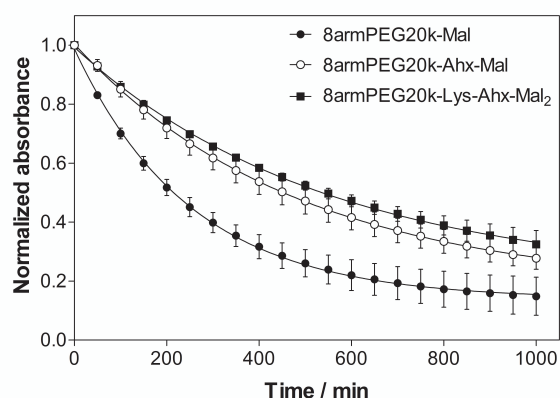


Figure 6.1. Hydrolytic stability 8armPEG20k-Mal, 8armPEG20k-Ahx-Mal and 8armPEG20k-Lys-Ahx-Mal₂ incubated in phosphate buffer, pH 7.4 at 37 °C. The experimental data is indicated by symbols; the solid lines represent the best fits of eqn. (6.1).

Assuming that the hydrolysis of maleimide groups follows a pseudo-first-order process, rate constants (k_{obs}) and half-lives ($t_{1/2}$) can be calculated by fitting the integrated form of equation (6.1) to the experimental data.

$$-\frac{d[\text{maleimide}]}{dt} = k_{obs} \cdot [\text{maleimide}] \quad (6.1)$$

The results listed in Table 6.1 show that 8armPEG20k-Mal, 8armPEG20k-Ahx-Mal and 8armPEG20k-Lys-Ahx-Mal₂ were stable in water; therefore, the cross-linking process was carried out in water. Pure water has a slightly acidic pH due to dissolved carbon dioxide; furthermore, it is conceivable that small amounts of maleamic acid lower the pH of water. The slightly acid pH favors the stability of the maleimide groups; therefore, the cross-linking process was carried out in water. In phosphate buffer pH 7.4, the determined rate constants were almost two orders of magnitude higher than in water; therefore, the cross-linked hydrogels most likely degrade during incubation in phosphate buffer, pH 7.4. Interestingly, the half-lives of 8armPEG20k-Ahx-Mal and 8armPEG20k-Lys-Ahx-Mal₂ were more than twice as long as the half-life of 8armPEG20k-Mal. This was observed in water and in phosphate buffer, pH 7.4. Apparently, the nature of the *N*-substituent of maleimides influences the rate of hydrolysis [224,272–274]. For example, it has been reported that *N*-(2-methoxyethyl)maleimide is subject to rapid hydrolysis at pH 8.0, whereas *N*-butylmaleimide is more stable under the same conditions [273]. As a result of this, 8armPEG20k-Ahx- and 8armPEG20k-Lys-Ahx-hydrogels are most likely more resistant to degradation than 8armPEG20k-hydrogels.

Table 6.1. Calculated rate constants (k_{obs}) of the ring-opening reaction and half-lives ($t_{1/2}$) of 8armPEG20k-Mal, 8armPEG20k-Ahx-Mal and 8armPEG20k-Lys-Ahx-Mal₂ at 37 °C.

Macromonomer	Medium	$k_{obs} / \text{min}^{-1}$	$t_{1/2} / \text{min}$	R^2
8armPEG20k-Mal	water	$6.34 \cdot 10^{-5}$	109410	0.8312
	buffer pH 7.4	$3.92 \cdot 10^{-3}$	177	0.9706
8armPEG20k-Ahx-Mal	water	$3.19 \cdot 10^{-5}$	21759	0.8304
	buffer pH 7.4	$1.87 \cdot 10^{-3}$	372	0.9760
8armPEG20k-Lys-Ahx-Mal ₂	water	$3.13 \cdot 10^{-5}$	22137	0.8592
	buffer pH 7.4	$1.68 \cdot 10^{-3}$	412	0.9893

6.3.3 Gelation kinetics of Diels-Alder hydrogels

The kinetics of the DA reaction between complementary macromonomers was determined by UV spectroscopy. For this purpose, solutions of the macromonomers were

prepared in water and incubated at 37 °C. As shown above, the hydrolysis of maleimide groups is minimal in water; therefore, the kinetics of the DA reaction can be determined by measuring the decrease in the absorbance at 299 nm. Assuming equal starting concentrations of furyl and maleimide groups, the kinetics of the DA reaction can be described by the second-order equation (6.2):

$$\frac{1}{[\text{maleimide}]} = \frac{1}{[\text{maleimide}]_0} + k \cdot t \quad (6.2)$$

where $[\text{maleimide}]$ is the concentration of maleimide groups and $[\text{maleimide}]_0$ the concentration of maleimide groups at time $t = 0$ [233]. The second-order rate constants of the DA reaction (k) were calculated by fitting equation (6.2) to the experimental data (Figure 6.2).

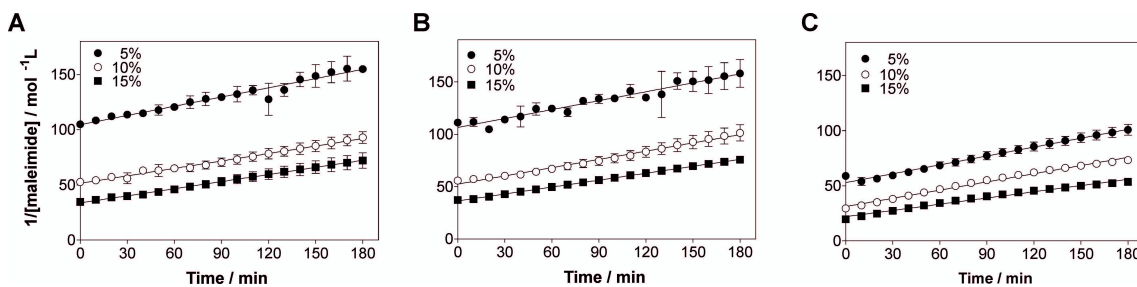


Figure 6.2. Gelation kinetics of 8armPEG20k- (A), 8armPEG20k-Ahx- (B) and 8armPEG20k-Lys-Ahx- hydrogels (C) at 37 °C as a function of the polymer concentration. The experimental data is indicated by symbols; the solid lines represent least-squares fits of second-order kinetic models.

Interestingly, the values of k slightly decreased with increasing polymer concentration (Table 6.2). This trend was observed with all tested macromonomers. Most likely, increasing the polymer concentration from 5% (w/v) to 15% (w/v) increases the viscosity of the system, which consequently results in lower reaction rates. Although statistically significant differences in k were observed between the different macromonomers at given polymer concentrations, no general trends could be derived for the kinetics of the DA reaction. Apparently, introducing Lys and/or Ahx residues between PEG and the reactive end-groups only has a minor influence on the reaction rate. The determined values of k can be used to predict the time to reach the gel point (t_{gel}). The conversion of functional groups at the gel point (α) can be calculated by using the Flory-Stockmayer theory [226]:

$$\alpha = \frac{1}{f - 1} \quad (6.3)$$

According to equation (6.3), gelation of 8armPEG20k- and 8armPEG20k-Ahx-hydrogels ($f = 8$) should occur at approximately 15% conversion of both furyl and maleimide groups; gelation of 8armPEG20k-Lys-Ahx-hydrogels ($f = 16$) should occur at approximately 7% conversion. Assuming that cross-linking follows a second-order process, t_{gel} can be calculated by:

$$t_{gel} = \frac{\alpha}{(1 - \alpha) \cdot [\text{maleimide}]_0 \cdot k} \quad (6.4)$$

The determined values of t_{gel} can be used to describe the kinetics of cross-linking. In general, the predicted values of t_{gel} decreased with increasing polymer concentration (Table 6.2). For example, gelation of 5% (w/v) 8armPEG20k-hydrogels should occur after 69 min, while 15% (w/v) 8armPEG20k-hydrogels should gel after 29 min. Gelation of 8armPEG20k-Ahx-hydrogels should occur at the same rate, with only minor differences being predicted. In contrast to that, our calculations predict that gelation of 8armPEG20k-Lys-Ahx-hydrogels should occur approximately four times faster than gelation of 8armPEG20k- or 8armPEG20k-Ahx-hydrogels. For example, gelation of 5% (w/v) 8armPEG20k-Lys-Ahx-hydrogels should occur after 16 min, while 8armPEG20k- and 8armPEG20k-Ahx-hydrogels should gel after 69 min and 67 min, respectively. The same trends are predicted for the two other polymer concentrations. Obviously, increasing the number of reactive end-groups per macromonomer would be an effective way to accelerate gelation of DA hydrogels.

Table 6.2. Second order rate constants (k) of the DA reaction in 8armPEG20k, 8armPEG20k-Ahx and 8armPEG20k-Lys-Ahx hydrogels. The time to reach the gel point (t_{gel}) was predicted using the determined values of k and compared to the rheological results.

Macromonomers	Conc. / % (w/v)	k /mol ⁻¹ ·L·s ⁻¹	R^2	t_{gel} / min	
				predicted	measured
8armPEG20k-Fur + 8armPEG20k-Mal	5	0.2693 ± 0.004115	0.8879	69	129 ± 4
	10	0.2268 ± 0.002943	0.9165	41	54 ± 3
	15	0.2144 ± 0.002806	0.9152	29	34 ± 1
8armPEG20k-Ahx-Fur + 8armPEG20k-Ahx-Mal	5	0.2963 ± 0.007404	0.7441	67	81 ± 4
	10	0.2654 ± 0.003305	0.9226	37	36 ± 4
	15	0.2206 ± 0.0004153	0.9981	30	23 ± 0
8armPEG20k-Lys-Ahx-Fur ₂ + 8armPEG20k-Lys-Ahx-Mal ₂	5	0.2699 ± 0.002735	0.9477	16	24 ± 0
	10	0.2493 ± 0.001442	0.9822	9	8 ± 1
	15	0.1881 ± 0.001086	0.9823	8	4 ± 1

6.3.4 Rheological characterization of Diels-Alder hydrogels

Oscillatory shear experiments were performed at 37 °C to study the gelation kinetics of DA hydrogels. In these experiments, t_{gel} can be approximated by the crossover of G' and G'' . In general, the measured values showed the same trends as the calculated values (Table 6.2). As shown in Figure 6.3A, the gel time decreased with increasing polymer concentration.

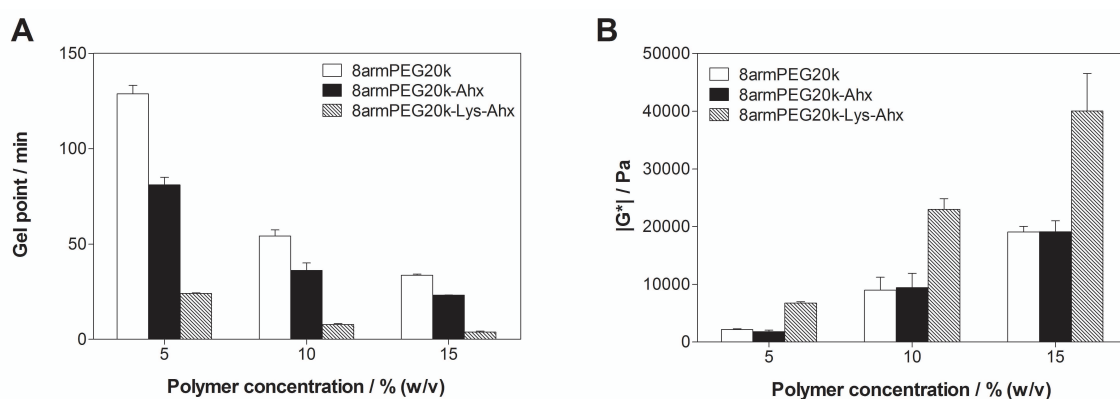


Figure 6.3. Gel time (A) and stiffness (B) of different DA hydrogels. The measurements were performed at 37 °C and 1.0 Hz oscillatory frequency.

For example, t_{gel} of 8armPEG20k-hydrogels decreased from 129 ± 4 min to 34 ± 1 min when the polymer concentration was increased from 5% (w/v) to 15% (w/v). With increasing polymer concentration, the probability of two macromonomers forming an elastically active chain is increasing. Consequently, t_{gel} decreases as predicted by our calculations. Interestingly, the gelation of 8armPEG20k-Ahx-hydrogels was significantly faster than the gelation of 8armPEG20k-hydrogels. This was unexpected since the rate constants of the DA reaction were comparable in both systems. The reason for the faster gelation of 8armPEG20k-Ahx-hydrogels is not totally clear; however, it can be speculated that the introduction of hydrophobic Ahx spacers between PEG and the reactive end-groups favors intermolecular interactions between macromonomers. The association of macromonomers by hydrophobic interactions might facilitate gelation independent of the DA reaction. The gel times of 8armPEG20k-Lys-Ahx-hydrogels were much lower in comparison to 8armPEG20k- and 8armPEG20k-Ahx-hydrogels. This was predicted by our calculations; the faster gelation of 8armPEG20k-Lys-Ahx-hydrogels can be attributed to the higher number of reactive end-groups per macromonomer. Association of macromonomers by hydrophobic interactions might additionally contribute to gelation. Major differences between the calculated and determined values of t_{gel} were only observed in 5% (w/v) 8armPEG20k-hydrogels. Due to the lack of hydrophobic

interactions and the lower concentration of reactive end-groups, this system seems to be more affected by network imperfections, such as dangling ends, than other hydrogels. Furthermore, oscillatory shear experiments can be used to determine the absolute value of G^* , which relates to the number of elastically active chains in cross-linked hydrogels. As shown in Figure 6.3B, the absolute value of G^* increased with increasing polymer concentration. For example, the absolute value of G^* of 8armPEG20k-hydrogels increased from 2152 ± 144 Pa to $19,057 \pm 1002$ Pa when the polymer concentration was increased from 5% (w/v) to 15% (w/v). The same trend was observed for 8armPEG20k-Ahx-hydrogels, where the absolute value of G^* increased from 1797 ± 254 Pa to $19,123 \pm 1877$ Pa, and for 8armPEG20k-Lys-Ahx-hydrogels, where the absolute value of G^* ranged between 6748 ± 230 Pa and $40,027 \pm 6511$ Pa. No significant differences were observed between 8armPEG20k- and 8armPEG20k-Ahx-hydrogels. The absolute value of G^* was similar at all tested polymer concentration; therefore, both types of hydrogel obviously have the same number of elastically active chains. In contrast to that, the absolute value of G^* of 8armPEG20k-Lys-Ahx-hydrogels was 2–3 times higher at all studied polymer concentrations. This is explained by the dendritic structure of the macromonomers. Branching the terminal ends of star-shaped PEG with Lys and Ahx residues increases the number of reactive end-groups per macromonomer and, hence, the number of elastically active chains that can be formed during cross-linking. Furthermore, the cross-linking density of the formed network is increased by adding new branch points to the macromonomers. In summary, gelation of DA hydrogels can be accelerated by introducing hydrophobic Ahx spacers between PEG and the reactive end-groups or by adding new branch points to the macromonomers. While the first method does not affect the mechanical properties of the resulting hydrogels, increasing the number of reactive end-groups per macromonomer always increases the absolute value of G^* . This may have effects on other gel properties, such as the average mesh size and degradation time, which in turn affect the release rate of incorporated drugs.

6.3.5 Determination of the average mesh size

The ζ value is an important parameter of hydrogels that allows estimating the release rate of incorporated drugs [14,13]. Therefore, we calculated the ζ values of different hydrogels after swelling in water as previously described [212]. The results listed in Table 6.3 show that ζ was influenced by the concentration and type of the macromonomers used for hydrogel preparation. 5% (w/v) 8armPEG20k-hydrogels had the largest mesh size with a

ξ value of 16.1 ± 0.1 nm, whereas 15% (w/v) 8armPEG20k-Lys-Ahx-hydrogels had the smallest mesh size with a ξ value of 6.0 ± 0.2 nm. As shown in rheological measurements, increasing macromonomer concentrations resulted in higher cross-linking density; accordingly, the ξ values were decreasing with increasing macromonomer concentrations. 8armPEG20k-hydrogels had the highest ξ values of all tested hydrogels, which is again explained by network imperfections such as dangling ends. As expected from rheological measurements, 8armPEG20k-Lys-Ahx-hydrogels had the smallest ξ values of all hydrogels. This is again explained by the dendritic structure of the macromonomers, which increases the cross-linking density of the resulting networks. The results indicate that all tested hydrogels may allow controlled release of therapeutic proteins. For example, bevacizumab, which served as model protein in our studies, has a hydrodynamic diameter of approximately 13 nm [269]. Depending on the ξ value of the hydrogel, the release of incorporated bevacizumab may be controlled by diffusion of the protein ($\xi \geq 13$ nm) or degradation of the hydrogel ($\xi \ll 13$ nm).

Table 6.3. Average mesh size (ξ) of 8armPEG20k, 8armPEG20k-Ahx and 8armPEG20k-Lys-Ahx hydrogels derived from swelling data.

Macromonomers	Conc. / % (w/v)	ξ / nm
8armPEG20k-Fur	5	16.1 ± 0.1
+	10	12.9 ± 0.9
8armPEG20k-Mal	15	11.1 ± 0.1
8armPEG20k-Ahx-Fur	5	12.3 ± 0.2
+	10	10.3 ± 0.1
8armPEG20k-Ahx-Mal	15	9.8 ± 0.1
8armPEG20k-Lys-Ahx-Fur ₂	5	12.7 ± 0.02
+	10	7.3 ± 0.1
8armPEG20k-Lys-Ahx-Mal ₂	15	6.0 ± 0.2

6.3.6 Swelling and degradation of Diels-Alder hydrogels

To study the swelling and degradation behavior of DA hydrogels, gel cylinders were incubated in 50 mM phosphate buffer, pH 7.4 at 37 °C and weighed at regular times. The polymer concentration was 5% (w/v) in all groups. As shown in Figure 6.4, the mass of 8armPEG20k- and 8armPEG20k-Ahx-hydrogels steadily increased until the gel cylinders were completely degraded after 14 days (8armPEG20k-hydrogels) and 28 days (8armPEG20k-Ahx-hydrogels), respectively. The swelling behavior of 8armPEG20k-Lys-Ahx-hydrogels was slightly different. The mass of these hydrogels slowly increased

over 34 weeks. After a maximum had been reached, the mass steadily decreased until the gel cylinders were completely degraded after 40 weeks.

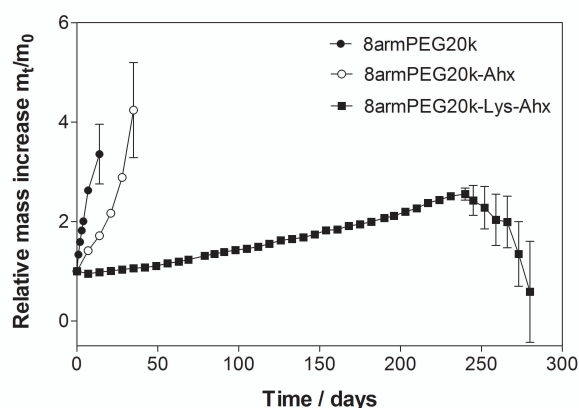


Figure 6.4. Swelling and degradation of 5% (w/v) 8armPEG20k- (●), 8armPEG20k-Ahx- (○) and 8armPEG20k-Lys-Ahx-hydrogels (■). Hydrogels incubated at 37 °C dissolved after 14 days (8armPEG20k), 28 days (8armPEG20k-Ahx) and 280 days (8armPEG20k-Lys-Ahx).

It has been reported that DA hydrogels degrade at pH 7.4 by rDA reaction and subsequent ring-opening hydrolysis of the generated maleimide groups [8]. The hydrolytic step is important as it removes the generated maleimide groups from the DA/rDA equilibrium. This causes the DA adducts to revert to the starting materials and induces hydrogel degradation. Furthermore, it has been shown that gel stability increases with decreasing rate of hydrolysis. Accordingly, the degradation time of 8armPEG20k-Ahx-hydrogels ($t_{1/2}$ of 8armPEG20k-Ahx-Mal = 378 min) was twice as long as the degradation time of 8armPEG20k-hydrogels ($t_{1/2}$ of 8armPEG20k-Mal = 180 min). However, differences in the rate of hydrolysis cannot solely explain the extreme longevity of 8armPEG20k-Lys-Ahx-hydrogels ($t_{1/2}$ of 8armPEG20k-Lys-Ahx-Mal₂ = 419 min). Apparently, the number of reactive end-groups per macromonomer has a pronounced effect on hydrogel degradation. As discussed above, the number of elastically active chains is much higher in 8armPEG20k-Lys-Ahx-hydrogels than in 8armPEG20k- or 8armPEG20k-Ahx-hydrogels. As a consequence, relatively more DA adducts must be broken in 8armPEG20k-Lys-Ahx-hydrogels before degradation becomes obvious (Figure 6.5).

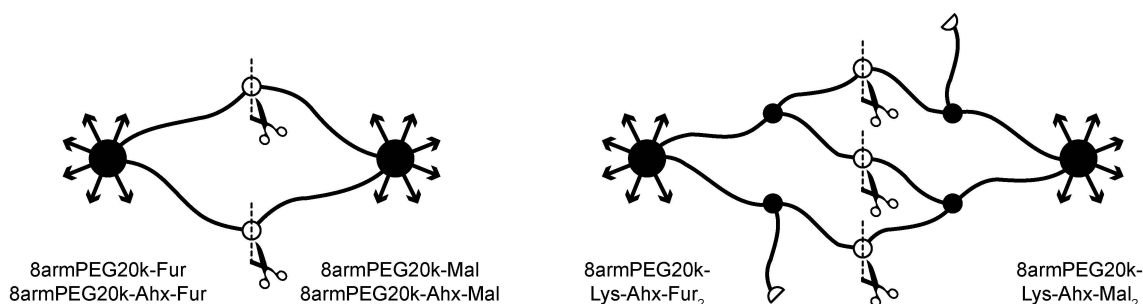


Figure 6.5. Network architecture of different DA hydrogels. In 8armPEG20k- and 8armPEG20k-Ahx-hydrogels (left), less DA adducts must be broken than in 8armPEG20k-Lys-Ahx-hydrogels (right) to cause degradation.

This also explains the lower degree of swelling of 8armPEG20k-Lys-Ahx-hydrogels. Besides hydrolysis, diffusion of macromonomers from the gel network into the swelling medium may also remove furyl and maleimide groups from the DA/rDA equilibrium and accelerate degradation. In 8armPEG20k- and 8armPEG20k-Ahx-hydrogels, the probability of releasing macromonomers from the gel network is much higher than in 8armPEG20k-Lys-Ahx-hydrogels; therefore, these gels degrade faster than 8armPEG20k-Lys-Ahx-hydrogels. Furthermore, it can be speculated that the close proximity of two functional groups in 8armPEG20k-Lys-Ahx-Fur₂ and 8armPEG20k-Lys-Ahx-Mal₂, respectively, may favor the reformation of DA adducts. This would additionally increase the resistance of 8armPEG20k-Lys-Ahx-hydrogels to degradation. Taken together, our experiments demonstrate that the stability of DA hydrogels can be enhanced by introducing hydrophobic Ahx spacers between PEG and the reactive end-groups or by increasing the number of reactive end-groups per macromonomer. While the first method has only moderate effects, using dendritic macromonomers drastically increases the persistence of the resulting hydrogels.

6.3.7 In vitro release of bevacizumab

In the final experiment, we studied the *in vitro* release of bevacizumab from 8armPEG20k-, 8armPEG20k-Ahx- and 8armPEG20k-Lys-Ahx-hydrogels. The polymer concentration was 10% (w/v) in all groups. As shown in Figure 6.6, approximately 20% to 30% of the incorporated bevacizumab was released within the first 24 h. This burst release was observed in all groups; it is most likely caused by non-entrapped protein molecules located at the surface of the gel cylinders. After the first 24 h, the release of bevacizumab was dependent on the hydrogel formulation. All release profiles were sigmoidal; however, their timescales were different. The release of bevacizumab from 8armPEG20k-hydrogels was comparatively fast; the incorporated protein was completely released after 10 days. In comparison to that, protein release from 8armPEG20k-Ahx-hydrogels was considerably slower; the incorporated bevacizumab was completely released after 42 days. The release of bevacizumab from 8armPEG20k-Lys-Ahx-hydrogels initially followed the same kinetics. Approximately 60% of the incorporated protein was released during the first 28 days. This was followed by a second phase of slow protein release; after 105 days, approximately 73% of the incorporated bevacizumab was released.

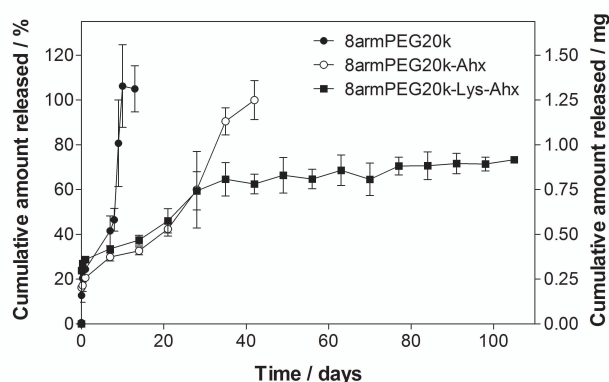


Figure 6.6. Cumulative release of bevacizumab from 10% (w/v) 8armPEG20k- (●), 8armPEG20k-Ahx- (○) and 8armPEG20k-Lys-Ahx-hydrogels (■). Drug release was completed after 10 days (8armPEG20k) and 42 days (8armPEG20k-Ahx), respectively. Release from 8armPEG20k-Lys-Ahx-hydrogels was not completed after 105 days with approximately 73% of the incorporated bevacizumab being released.

As discussed above, the release of bevacizumab is controlled by diffusion of the protein or degradation of the hydrogel. Furthermore, it has been shown that nucleophilic amino acid residues of proteins (mostly Lys residues located on the surface of the protein) can react with maleimides in Michael-type additions [17]. Although the nucleophilicity of these amino acid residues is low in water due to protonation, approximately 20% to 30% of the incorporated protein may react with the gel-forming polymers during cross-linking. This covalently bound fraction is immobile and eventually released during degradation. Depending on the number of PEG molecules remaining attached, the antigen binding activity of these PEGylated antibodies can be slightly decreased or completely lost [270]. The ζ value of 10% (w/v) 8armPEG20k-hydrogels (12.9 ± 0.9 nm) has the same dimension as the hydrodynamic diameter of bevacizumab (approximately 13 nm). Together with the ongoing degradation, this results in fast release of both physically entrapped and covalently bound bevacizumab. In contrast to that, the ζ values of 10% (w/v) 8armPEG20k-Ahx- (10.3 ± 0.1 nm) and 8armPEG20k-Lys-Ahx-hydrogels (7.3 ± 0.1 nm) are below the hydrodynamic diameter of bevacizumab. Therefore, physically entrapped bevacizumab is slowly released from these hydrogels by diffusion. As a result of the starting degradation, protein release from 8armPEG20k-Ahx-hydrogels continues until complete release of both physically entrapped and covalently bound bevacizumab is reached. In contrast to that, the release of bevacizumab from 8armPEG20k-Lys-Ahx-hydrogels levels off after 28 days with approximately 60% of the incorporated protein being released. The remaining 40% are either physically entrapped or covalently bound and not released until gel degradation eventually becomes manifest. Several controlled release systems for bevacizumab have been described in the literature, with *in situ* forming hydrogels being most prominent [59,135–137,139,140,275–281]. For example, hydrogels based on PEG/polyurethane block copolymers could be injected at room temperature and formed a viscoelastic drug depot inside the vitreous cavity [137].

The hydrogels were well tolerated *in vivo* and sustained the release of bevacizumab for 2 months. The duration of release could be further extended by using light-activated hydrogels made from polycaprolactone dimethacrylate and hydroxyethyl methacrylate [279]. The polymer solution was cross-linked for 10 min in the presence of UV light and a photoinitiator. The *in vitro* release of bevacizumab was sustained for 4 months; the drug was retained in the suprachoroidal space of rats up to 60 days. Although 8armPEG20k-Ahx- and 8armPEG20k-Lys-Ahx-hydrogels could not sustain the release of bevacizumab over several months, DA hydrogels offer the advantage of being cross-linked in the absence of metal catalysts or initiators. Photoinitiators generate free radicals during cross-linking, which may induce toxicity and affect the bioactivity of proteins [14,17,18]. Moreover, it should be mentioned that volume (0.25 mL) and drug content (1.25 mg of bevacizumab) of the herein studied hydrogels might not be appropriate for clinical applications. The required bevacizumab dose and the desired release profile (e.g., continuous or intermittent release) must be determined by *in vivo* experiments, which are not subject of the present study. Altogether, this pilot study demonstrates the potential of DA hydrogels for the controlled release of bevacizumab. The release profiles can be further optimized by fine-tuning the mesh size and degradation rate of the hydrogels.

6.4 Conclusion

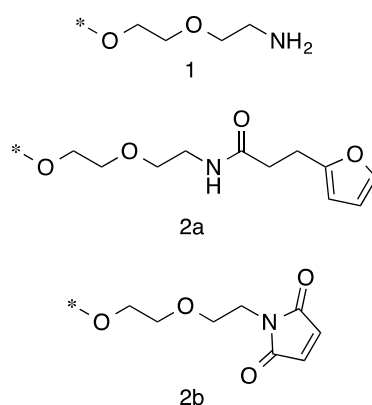
In situ forming hydrogels with potential application as intravitreal delivery system for anti-VEGF drugs, such as bevacizumab or ranibizumab, were developed. To this end, eight-armed PEG was functionalized with furyl and maleimide groups, respectively, and cross-linked via DA chemistry. However, the comparatively fast degradation and the slow cross-linking process may limit the application of plain 8armPEG20k-hydrogels. Introducing hydrophobic Ahx spacers between PEG and the reactive end-groups is effective in decreasing the gel time of DA hydrogels; the degradation of 8armPEG20k-Ahx-hydrogels is significantly prolonged compared to unmodified 8armPEG20k-hydrogels. The gelation of DA hydrogels can be further accelerated by using dendritic 8armPEG20k-Lys-Ahx-macromonomers; the resulting hydrogels are characterized by enhanced mechanical stability and extreme longevity. Both 8armPEG20k-Ahx- and 8armPEG20k-Lys-Ahx-hydrogels may serve as controlled release system for therapeutic antibodies such as bevacizumab. The hydrogels would be injected in liquid form and

rapidly form a viscoelastic drug depot inside the vitreous cavity. Both gel systems are capable of sustaining the *in vitro* release of bevacizumab for at least 6 weeks. The release profiles can be further optimized by fine-tuning the mesh size and degradation rate of DA hydrogels, e.g., by using mixtures of different macromonomers. In summary, especially 8armPEG20k-Lys-Ahx-hydrogels seem promising; the developed hydrogels can possibly reduce the dosing frequency of anti-VEGF drugs and provide intermittent drug release, which would be desirable in anti-VEGF therapy [133,271]. In the next phase, we will evaluate the stability and biological activity of released bevacizumab. Moreover, the safety and effectiveness of DA hydrogels have to be confirmed in animal models of choroidal neovascularization.

6.5 Supplements

6.5.1 Synthesis of 8armPEG20k-NH₂ (**1**), 8armPEG20k-Fur (**2a**) and 8armPEG20k-Mal (**2b**)

Eight-armed PEG-amine, molecular mass 20,000 kDa (8armPEG20k-NH₂, **1**) was synthesized from eight-armed PEG as previously described [212]. 8armPEG20k-Fur (**2a**) and 8armPEG20k-Mal (**2b**) were synthesized from **1** as previously described [212].



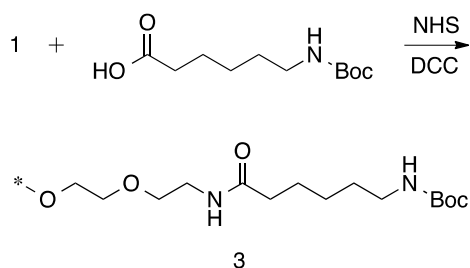
Scheme 6.3. Functional end-groups of **1**, **2a** and **2b**

6.5.2 Synthesis of compound **3**

Boc-6-aminohexanoic acid (5.40 mmol, 1.25 g), NHS (5.40 mmol, 0.62 g) and DCC (5.40 mmol, 1.11 g) were dissolved in 15 mL of anhydrous DMF and stirred for 30 min at 0 °C. Afterwards, the precipitate was filtered off and the filtrate was combined with a

solution of **1** (0.34 mmol, 7.00 g) in 55 mL of anhydrous DCM. The reaction mixture was neutralized with DIPEA and stirred for 1.5 h at room temperature. The precipitate was filtered off and the filtrate was concentrated under reduced pressure. The polymer was precipitated at 0 °C by dropwise addition of diethyl ether. The precipitate was collected by filtration, washed with cold diethyl ether and dried under vacuum to yield 6.79 g (90%) of **3**. The degree of end-group conversion was approximately 82% as determined by ¹H-NMR spectroscopy.

¹H-NMR (CDCl₃, 300 MHz): δ 1.32 ppm (m, 16H, –C(O)CH₂CH₂CH₂CH₂CH₂NH–), 1.42 ppm (s, 72H, –NHC(O)OC(CH₃)₃), 1.63 ppm (m, 16H, –C(O)CH₂CH₂CH₂CH₂CH₂NH–), 2.16 ppm (t, 16H, –C(O)CH₂CH₂CH₂CH₂CH₂NH–), 3.07 ppm (m, 16H, –C(O)CH₂CH₂CH₂CH₂CH₂NH–), 3.62 ppm (s, –OCH₂CH₂–).

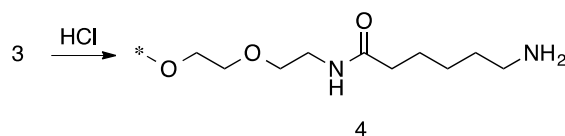


Scheme 6.4. Synthesis of **3** from **1** and Boc-6-aminohexanoic acid

6.5.3 Synthesis of compound 4

Compound **3** (0.30 mmol, 6.79 g) was dissolved in a solution of HCl in methanol (obtained by dropwise addition of 7.0 mL of acetyl chloride to 70 mL of ice-cooled methanol). The reaction mixture was stirred for 30 min at room temperature. The solvent was evaporated under reduced pressure and the residue was dissolved in 35 mL of water. The pH of the solution was adjusted with NaOH to 9–10. The raw product was extracted with DCM (4 × 35 mL). The combined organic phases were dried over anhydrous Na₂SO₄, filtered and concentrated under reduced pressure. The polymer was precipitated at 0 °C by dropwise addition of diethyl ether. The precipitate was collected by filtration, washed with cold diethyl ether and dried under vacuum to yield 6.12 g (93 %) of **4**. ¹H-NMR spectroscopy indicated complete removal of the BOC group.

¹H-NMR (CDCl₃, 300 MHz): δ 1.34 ppm (m, 16H, –C(O)CH₂CH₂CH₂CH₂CH₂NH₂), 1.49 ppm (m, 16H, –C(O)CH₂CH₂CH₂CH₂CH₂NH₂), 1.64 ppm (m, 16H, –C(O)CH₂CH₂CH₂CH₂CH₂NH₂), 2.19 ppm (t, 16H, –C(O)CH₂CH₂CH₂CH₂CH₂NH₂), 2.70 ppm (t, 16H, –C(O)CH₂CH₂CH₂CH₂CH₂NH₂), 3.62 ppm (s, –OCH₂CH₂–).



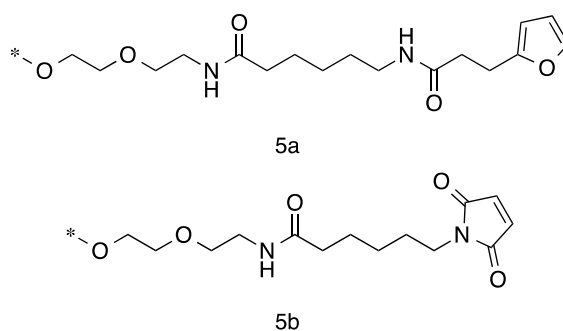
Scheme 6.5. Synthesis of **4** by deprotection of **3**

6.5.4 Synthesis of compound 8armPEG20k-Ahx-Fur (**5a**)

8armPEG20k-Ahx-Fur (**5a**) was synthesized in 94% yield by reacting **4** with a twofold excess of 3-(2-furyl)propanoic acid, NHS and DCC as described for **2a**. The degree of end-group conversion was approximately 82% as determined by $^1\text{H-NMR}$ spectroscopy. $^1\text{H-NMR}$ (CDCl_3 , 300 MHz): δ 1.30 ppm (m, 16H, $-\text{C}(\text{O})\text{CH}_2\text{CH}_2\text{CH}_2\text{CH}_2\text{CH}_2\text{NH}-$), 1.45 ppm (m, 16H, $-\text{C}(\text{O})\text{CH}_2\text{CH}_2\text{CH}_2\text{CH}_2\text{CH}_2\text{NH}-$), 1.61 ppm (m, 16H, $-\text{C}(\text{O})\text{CH}_2\text{CH}_2\text{CH}_2\text{CH}_2\text{CH}_2\text{NH}-$), 2.16 ppm (t, 16H, $-\text{C}(\text{O})\text{CH}_2\text{CH}_2\text{CH}_2\text{CH}_2\text{CH}_2\text{NH}-$), 2.47 ppm (t, 16H, $-\text{C}(\text{O})\text{CH}_2\text{CH}_2\text{Ar}$), 2.95 ppm (t, 16H, $-\text{C}(\text{O})\text{CH}_2\text{CH}_2\text{Ar}$), 3.20 ppm (t, 16H, $-\text{C}(\text{O})\text{CH}_2\text{CH}_2\text{CH}_2\text{CH}_2\text{CH}_2\text{NH}-$), 3.62 ppm (s, $-\text{OCH}_2\text{CH}_2-$), 6.00 ppm (s, 4H, Ar), 6.24 ppm (s, 4H, Ar), 7.26 ppm (s, 4H, Ar).

6.5.5 Synthesis of compound 8armPEG20k-Ahx-Mal (**5b**)

8armPEG20k-Ahx-Mal (**5b**) was synthesized in 96% yield by reacting **4** with a fivefold excess of *N*-methoxycarbonylmaleimide as described for **2b**. The degree of end-group conversion was approximately 65% as determined by $^1\text{H-NMR}$ spectroscopy. $^1\text{H-NMR}$ (CDCl_3 , 300 MHz): δ 1.29 ppm (m, 16H, $-\text{C}(\text{O})\text{CH}_2\text{CH}_2\text{CH}_2\text{CH}_2\text{CH}_2\text{NH}-$), 1.61 ppm (m, 32H, $-\text{C}(\text{O})\text{CH}_2\text{CH}_2\text{CH}_2\text{CH}_2\text{CH}_2\text{NH}-$), 2.14 ppm (t, 16H, $-\text{C}(\text{O})\text{CH}_2\text{CH}_2\text{CH}_2\text{CH}_2\text{CH}_2\text{NH}-$), 3.62 ppm (s, $-\text{OCH}_2\text{CH}_2-$), 6.67 ppm (s, 16H, $-\text{C}(\text{O})\text{CH}=\text{CHC}(\text{O})-$).

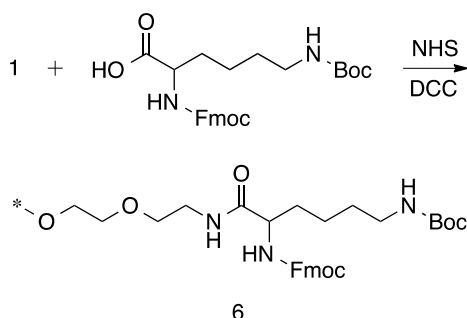


Scheme 6.6. Functional end-groups of **5a** and **5b**

6.5.6 Synthesis of compound 6

Compound **6** was synthesized in 90% yield by reacting **1** with Fmoc-Lys(Boc)-OH as described for **3**. The degree of end-group conversion was approximately 94% as determined by $^1\text{H-NMR}$ spectroscopy.

$^1\text{H-NMR}$ (CDCl_3 , 300 MHz): δ 1.41 ppm (s, 72H, $-\text{NHC(O)OC}(\text{CH}_3)_3$), 3.07 ppm (m, 16H, $-\text{C(O)C}(\text{NHFmoc})\text{HCH}_2\text{CH}_2\text{CH}_2\text{CH}_2\text{NH}-$), 3.63 ppm (s, $-\text{OCH}_2\text{CH}_2-$), 4.19 ppm (m, 16H, $-\text{C(O)C}(\text{NHFmoc})\text{HCH}_2\text{CH}_2\text{CH}_2\text{CH}_2\text{NH}-$ and $-\text{NHC(O)OCH}_2\text{CHR}_2$), 4.37 ppm (m, 16H, $-\text{NHC(O)OCH}_2\text{CHR}_2$), 7.30–7.74 ppm (m, 104H, Ar).

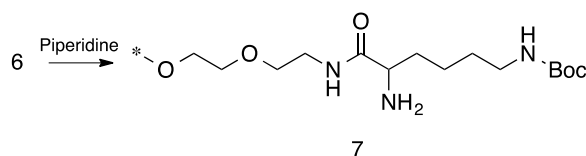


Scheme 6.7. Synthesis of **6** from **1** and Fmoc-Lys(Boc)-OH

6.5.7 Synthesis of compound 7

Compound **6** (0.27 mmol, 6.38 g) was dissolved in 24 mL of DMF; 6 mL of piperidine were added. The reaction mixture was stirred for 30 min at room temperature. The polymer was precipitated at 0 °C by dropwise addition of diethyl ether. The precipitate was collected by filtration, washed with cold diethyl ether and dried under vacuum to yield 5.40 g (92%) of **7**. $^1\text{H-NMR}$ spectroscopy indicated complete removal of the Fmoc group.

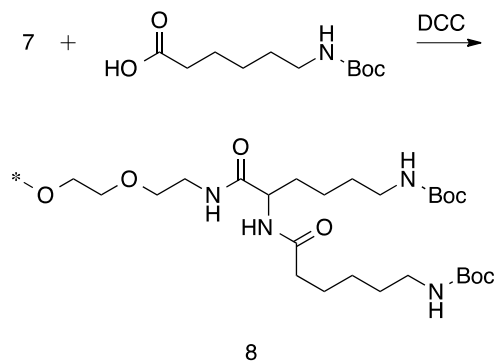
$^1\text{H-NMR}$ (CDCl_3 , 300 MHz): δ 1.41 ppm (s, 72H, $-\text{NHC(O)OC}(\text{CH}_3)_3$), 1.62 ppm (m, 16H, $-\text{C(O)C}(\text{NH}_2)\text{HCH}_2\text{CH}_2\text{CH}_2\text{CH}_2\text{NH}-$), 1.81 ppm (m, 16H, $-\text{C(O)C}(\text{NH}_2)\text{HCH}_2\text{CH}_2\text{CH}_2\text{CH}_2\text{NH}-$), 3.08 ppm (m, 16H, $-\text{C(O)C}(\text{NH}_2)\text{HCH}_2\text{CH}_2\text{CH}_2\text{CH}_2\text{NH}-$), 3.62 ppm (s, $-\text{OCH}_2\text{CH}_2-$).



Scheme 6.8. Synthesis of **7** by deprotection of **6**

6.5.8 Synthesis of compound 8

Boc-6-aminohexanoic acid (7.85 mmol, 1.82 g) and DCC (3.92 mmol, 0.81 g) were dissolved in 10 mL of anhydrous DMF and stirred for 30 min at 0 °C. Afterwards, the precipitate was filtered off and the filtrate was combined with a solution of **7** (0.25 mmol, 5.40 g) in 45 mL of anhydrous DCM. The reaction mixture was neutralized with DIPEA and stirred for 1.5 h at room temperature. The precipitate was filtered off and the filtrate was concentrated under reduced pressure. The polymer was crystallized at 0 °C by dropwise addition of diethyl ether. The precipitate was collected by filtration, washed with cold diethyl ether and dried under vacuum to yield 4.88 g (84%) of **8**. The degree of end-group conversion was approximately 85% as determined by ¹H-NMR spectroscopy. ¹H-NMR (CDCl₃, 300 MHz): δ 1.31 ppm (m, 48H, –C(O)C(NHR)HCH₂CH₂CH₂CH₂NH– and –C(O)CH₂CH₂CH₂CH₂CH₂NH–), 1.41 ppm (s, 144H, –NHC(O)OC(CH₃)₃), 1.62 ppm (m, 32H, –CH₂CH₂CH₂CH₂NH–), 1.81 ppm (m, 16H, –C(O)C(NHR)HCH₂CH₂CH₂CH₂NH–), 2.19 ppm (t, 16H, –C(O)CH₂CH₂CH₂CH₂CH₂NH–), 3.07 ppm (m, 32H, –CH₂CH₂CH₂CH₂NH–), 3.62 ppm (s, –OCH₂CH₂–) 4.37 ppm (m, 8H, –C(O)C(NHR)HCH₂CH₂CH₂CH₂NH–).

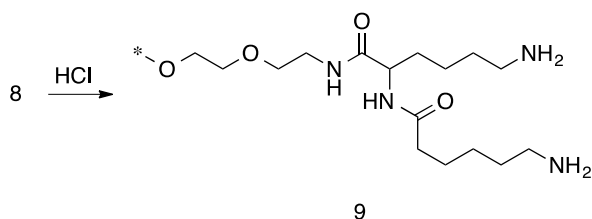


Scheme 6.9. Synthesis of **8** from **7** and Boc-6-aminohexanoic acid

6.5.9 Synthesis of compound 9

Compound **9** was synthesized in 92% yield as described for **4**. ¹H-NMR spectroscopy indicated complete removal of the BOC groups.

¹H-NMR (CDCl₃, 300 MHz): δ 1.31–1.81 ppm (m, 96H, –CH₂CH₂CH₂CH₂NH₂), 2.69 ppm (m, 32H, –CH₂CH₂CH₂CH₂NH₂), 3.62 ppm (s, –OCH₂CH₂–), 4.41 ppm (m, 8H, –C(O)C(NHR)HCH₂CH₂CH₂CH₂NH₂).



Scheme 6.10. Synthesis of **9** by deprotection of **8**

6.5.10 Synthesis of compound 8armPEG20k-Lys-Ahx-Fur₂ (**10a**)

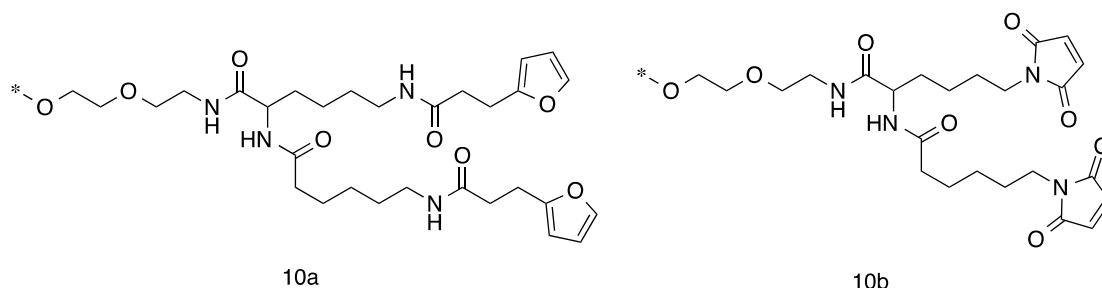
8armPEG20k-Lys-Ahx-Fur₂ (**10a**) was synthesized in 90% yield by reacting **9** with a 1.5-fold excess of 3-(2-furyl)propanoic acid, NHS and DCC as described for **2a**. The degree of end-group conversion was approximately 75% as determined by ¹H-NMR spectroscopy.

¹H-NMR (CDCl₃, 300 MHz): δ 1.30–1.77 ppm (m, 96H, –CH₂CH₂CH₂CH₂NH–), 2.20 ppm (t, 16H, –C(O)CH₂CH₂CH₂CH₂CH₂NH–), 2.48 ppm (t, 16H, –C(O)CH₂CH₂Ar), 2.95 ppm (t, 16H, –C(O)CH₂CH₂Ar), 3.20 ppm (m, 16H, –CH₂CH₂CH₂CH₂NH–), 3.63 ppm (s, –OCH₂CH₂–), 4.35 ppm (m, 8H, –C(O)C(NHR)HCH₂CH₂CH₂CH₂NH–), 6.00 ppm (s, 16H, Ar), 6.25 ppm (s, 16H, Ar), 7.27 ppm (s, 16H, Ar).

6.5.11 Synthesis of compound 8armPEG20k-Lys-Ahx-Mal₂ (**10b**)

8armPEG20k-Lys-Ahx-Mal₂ (**10b**) was synthesized in 89% yield by reacting **9** with a fourfold excess of *N*-methoxycarbonylmaleimide as described for **2b**. The degree of end-group conversion was approximately 86% as determined by ¹H-NMR spectroscopy.

¹H-NMR (CDCl₃, 300 MHz): δ 1.29–2.18 ppm (112 H, aliphatic H), 3.62 ppm (s, –OCH₂CH₂–), 4.35 ppm (m, 8H, –C(O)C(NHR)HCH₂CH₂CH₂CH₂NH–), 6.68 ppm (s, 32H, –C(O)CH=CHC(O)–).



Scheme 6.11. Functional end-groups of **10a** and **10b**

Chapter 7

Summary and Conclusion

7.1 Summary

The aim of this thesis was the development and characterization of hydrogels with potential application as drug delivery systems for the controlled release of antibodies.

As established gelation methods are associated with several disadvantages minimizing the successful use as injectable drug delivery systems, new cross-linking strategies have to be developed. For this purpose, chemical cross-linking is favored because hydrogels with defined mechanical and physicochemical properties are obtained. For these reasons, hydrogels were prepared by step-growth polymerization of star-shaped PEG macromonomers modified with maleimide- and furyl-residues via DA cycloaddition (**Chapter 3**). This reaction can be performed under mild conditions (water, 37 °C) without using any initiator or catalyst and enables the simple loading of sensitive biomolecules, such as antibodies. Rheological experiments indicated a time-dependent sol-gel transition making DA hydrogels ideal for injections. In future applications the hydrogel could be easily injected into the vitreous cavity as a liquid precursor solution, even through small-gauge needles, and form a stable drug depot after application. Gelation time and gel stiffness of the prepared hydrogels could be easily tuned by varying the concentration, branching factor and molecular weight of the used macromonomers. With increasing polymer concentration the gelation time decreased and the gel stiffness increased. The same effects were observed by using macromonomers with higher branching factor and lower molecular weight. The precise control of gel formation and mechanical properties makes the DA cycloaddition a valuable cross-linking mechanism for injectable drug delivery systems for antibodies. Swelling experiments of the covalently cross-linked hydrogels in aqueous solutions (pH 7.4) at 37 °C showed that covalent cross-linked hydrogel degraded within days to several weeks. (Figure 7.1) (**Chapter 3 and 4**).

NMR studies, swelling studies and SEMD simulations indicated an rDA reaction and subsequent OH⁻-catalyzed hydrolysis of the formed maleimides to unreactive maleamic acid derivatives as the reason for the degradation. Since the rDA-rate is increased through the consumption of unreacted maleimide according to Le Châtelier's principle, there is no need for high temperatures to incite the rDA reaction. Thus, DA hydrogels already degraded under physiological conditions and the additional modification with hydrolytically or enzymatically cleavable sites is not necessary to obtain biodegradable hydrogels. Consequently, surgical removal of hydrogel after complete drug release

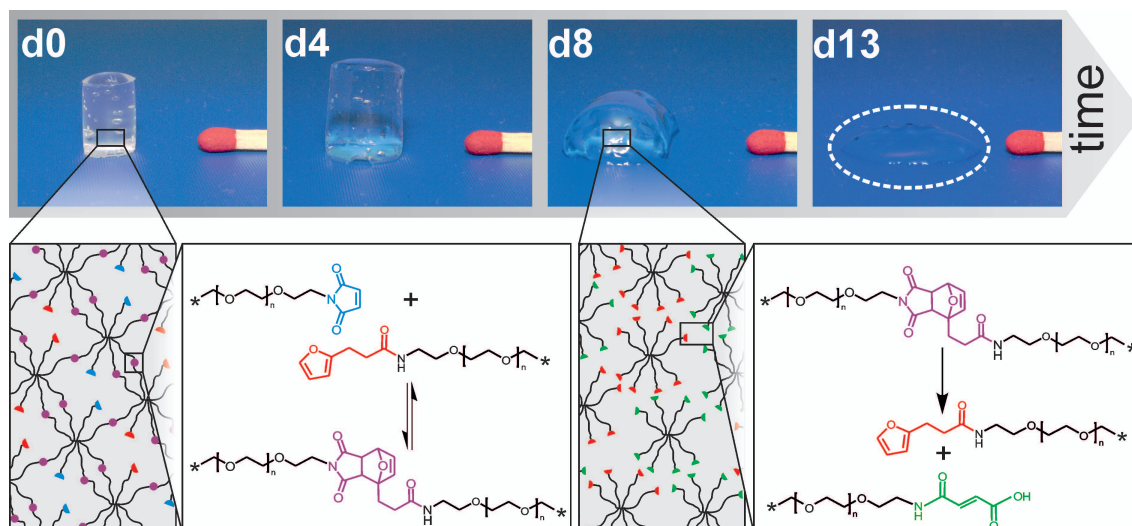


Figure 7.1. DA hydrogels degraded due to rDA reaction and subsequent hydrolysis of maleimide to unreactive maleamic acid.

is not necessary. Temperature and pH-value influenced the described degradation behavior, as well as cross-linking kinetics (**Chapter 4**). To ensure high degrees of conversion slightly acidic solutions (e.g., at pH 5.5) and temperatures above room temperature (e.g., at 37 °C) are preferred.

Besides suitable cross-linking methods, appropriate swelling and degradation behavior, the hydrogel mesh size is an important characteristic to evaluate the suitability of the prepared hydrogels as drug delivery systems. Therefore, swelling studies, rheology and low field NMR spectroscopy were used to determine ξ of the prepared hydrogels (**Chapter 5**). In principle, similar values of ξ_{avg} were determined by all three methods. However, swelling studies were preferred to determine the time-dependent increase of ξ_{avg} during degradation and low field NMR measurements were most appropriate to characterize the mesh size distribution. The calculations of the network mesh size indicated that DA hydrogels are suitable for controlled release of entrapped, therapeutic peptides or proteins. The observed time-dependent increase of ξ_{avg} was used to predict the release profiles of FDs of different R_h . To proof the theoretical prediction, *in vitro* release profiles of FDs of different molecular weight and hence R_h were determined by fluorescence spectroscopy. The observed release profiles matched the prediction when $R_h < \xi_{\text{avg}}$. Moreover, the release profile of entrapped bevacizumab indicated that besides R_h , the globular structure of proteins must be taken into account for theoretical considerations. Bevacizumab showed a different release profile in comparison to equal sized FDs, since its rigid structure inhibits a worm-like diffusion through small network meshes.

The developed hydrogels already fulfilled several requirements for successful intraocular drug delivery, such as injectability, transparency, degradability and sustained release of entrapped macromolecules. However, the slow cross-linking and comparatively fast degradation limited the application of DA hydrogels as *in situ* gelling drug delivery systems due to fast diffusion of entrapped antibodies after injection. To overcome these limitations, the reaction kinetics of the DA cycloaddition had to be increased. As shown in **Chapter 4** the number of reactive groups per macromonomer and the hydrolytic stability of maleimides residues influence the reaction kinetics and the degradation behavior of the prepared gels. Therefore, hydrophobic Ahx acid spacers were introduced between branched PEG and the reactive end-groups to increase the hydrolytic stability of the maleimide function. In addition, the number of reactive groups per macromonomer was doubled by branching eight-armed PEG with Lys and Ahx residues. This modification results in an increased hydrolytic stability of maleimide residues at the same time (**Chapter 6**).

Rheological studies and swelling experiments indicated accelerated gelation kinetics, enhanced mechanical stability and prolonged degradation stability. These effects were observed for both modifications. Nevertheless, doubling the branching factor by introducing Lys and Ahx was more effective than introducing only Ahx as hydrophobic spacer. Their potential for the sustained release of therapeutic antibodies was evaluated by loading bevacizumab into the different hydrogels. The gel systems, prepared from the modified macromonomers, were able to sustain the *in vitro* release of bevacizumab for at least 6 weeks. The modification with Lys and Ahx seems to be most promising to extend the dosing interval of intraocular injection and hence increase the compliance. Moreover, sigmoidal release profiles were observed indicating an intermittent drug release, which is desired in anti-VEGF drug therapy [133,271].

7.2 Conclusion and outlook

In summary, the DA reaction is an ideal cross-linking method for the preparation of PEG-based hydrogels for sustained antibody release after intraocular injection.

The mild reaction conditions of the DA cycloaddition and the high water content of the resulting hydrogel offer a simple and effective loading mechanism, even for highly sensitive drugs, such as proteins and antibodies. Since rheological studies indicated a time-dependent sol-gel transition after mixing the hydrogel precursor solutions, the

hydrogel can be easily injected into the vitreous body using small-gauged needles. When the PEG macromonomers are branched with Lys and Ahx, a rapid formation of a viscoelastic drug depot inside the vitreous cavity is expected. Moreover, the precise control of the resulting mesh size guarantees a sustained antibody release over several weeks. Finally, the cross-linked hydrogels degrade under physiological conditions resulting in a complete drug release.

In the future, the release profiles of entrapped drugs can be optimized by using mixtures of different macromonomers, such as 8armPEG10k and 8armPEG20k, to fine-tune the mesh size and degradation rate of the resulting hydrogels.

However, further experiments are necessary to evaluate the DA hydrogels in more detail. As possible reactions or interactions of PEG with entrapped antibodies may influence the pharmacological effects of the proteins due to conformational changes, the samples have to be analyzed by methods giving more information on protein structure. For instance, the percentage of free antibody and PEGylated protein as well as degradation products of instable antibodies can be detected by high performance liquid chromatography. Moreover, the activity of the released antibodies has to be evaluated to ensure pharmacological effects after intraocular injection. Enzyme linked immunosorbent assays can be used for the quantitative determination of biologically active forms of bevacizumab.

Although, further investigations are necessary, these first reported experiments demonstrate that PEG-based DA hydrogels show great promise as injectable drug delivery systems not only for intraocular application.

References

- [1] M.C. Catley, J. Coote, M. Bari, K.L. Tomlinson, Monoclonal antibodies for the treatment of asthma, *Pharmacol. Ther.* 132 (2011) 333–351.
- [2] C.H. Evans, V.B. Kraus, L.A. Setton, Progress in intra-articular therapy, *Nat. Rev. Rheumatol.* 10 (2014) 11–22.
- [3] V.K. Denmark, L. Mayer, Current status of monoclonal antibody therapy for the treatment of inflammatory bowel disease: an update, *Expert. Rev. Clin. Immunol.* 9 (2013) 77–92.
- [4] A.M. Scott, J.D. Wolchok, L.J. Old, Antibody therapy of cancer, *Nat. Rev. Cancer* 12 (2012) 278–287.
- [5] M.S. Ip, I.U. Scott, G.C. Brown, M.M. Brown, A.C. Ho, S.S. Huang, F.M. Recchia, Anti-vascular endothelial growth factor pharmacotherapy for age-related macular degeneration: a report by the American Academy of Ophthalmology, *Ophthalmology* 115 (2008) 1837–1846.
- [6] N. Butoescu, O. Jordan, E. Doelker, Intra-articular drug delivery systems for the treatment of rheumatic diseases: a review of the factors influencing their performance, *Eur. J. Pharm. Biopharm.* 73 (2009) 205–218.
- [7] M.F. Fransen, T.C. van der Sluis, F. Ossendorp, R. Arens, C.J.M. Melief, Controlled local delivery of CTLA-4 blocking antibody induces CD8⁺ T-cell-dependent tumor eradication and decreases risk of toxic side effects, *Clin. Cancer Res.* 19 (2013) 5381–5389.

- [8] P. Calias, W.A. Banks, D. Begley, M. Scarpa, P. Dickson, Intrathecal delivery of protein therapeutics to the brain: a critical reassessment, *Pharmacol. Ther.* 144 (2014) 114–122.
- [9] A.C. Ho, I.U. Scott, S.J. Kim, G.C. Brown, M.M. Brown, M.S. Ip, F.M. Recchia, Anti-vascular endothelial growth factor pharmacotherapy for diabetic macular edema: a report by the American Academy of Ophthalmology, *Ophthalmology* 119 (2012) 2179–2188.
- [10] K.M. Sampat, S.J. Garg, Complications of intravitreal injections, *Curr. Opin. Ophthalmol.* 21 (2010) 178–183.
- [11] D. Schweizer, T. Serno, A.M. Goepferich, Controlled release of therapeutic antibody formats, *Eur. J. Pharm. Biopharm.* 88 (2014) 291–309.
- [12] A. Bot, T. Tarara, D. Smith, S. Bot, C. Woods, J. Weers, Novel Lipid-Based Hollow-Porous Microparticles as a Platform for Immunoglobulin Delivery to the Respiratory Tract, *Pharm. Res.* 17 (2000) 275–283.
- [13] T. Vermonden, R. Censi, W.E. Hennink, Hydrogels for protein delivery, *Chem. Rev.* 112 (2012) 2853–2888.
- [14] C.-C. Lin, K.S. Anseth, PEG hydrogels for the controlled release of biomolecules in regenerative medicine, *Pharm. Res.* 26 (2009) 631–643.
- [15] N. Huebsch, P.R. Arany, A.S. Mao, D. Shvartsman, O.A. Ali, S.A. Bencherif, et al., Harnessing traction-mediated manipulation of the cell/matrix interface to control stem-cell fate, *Nat. Mater.* 9 (2010) 518–526.
- [16] A.M. Kloxin, C.J. Kloxin, C.N. Bowman, K.S. Anseth, Mechanical properties of cellularly responsive hydrogels and their experimental determination, *Adv. Mater.* 22 (2010) 3484–3494.
- [17] N. Hammer, F.P. Brandl, S. Kirchhof, A.M. Goepferich, Protein Compatibility of Selected Cross-linking Reactions for Hydrogels, *Macromol. Biosci.* 15 (2015) 405–413.
- [18] J. Qu, D. Wang, C.L. Grosskreutz, Mechanisms of retinal ganglion cell injury and defense in glaucoma, *Exp. Eye Res.* 91 (2010) 48–53.

-
- [19] A. Gandini, The furan/maleimide Diels–Alder reaction: a versatile click–unclick tool in macromolecular synthesis, *Prog. Polym. Sci.* 38 (2013) 1–29.
- [20] K.C. Nicolaou, S.A. Snyder, T. Montagnon, G. Vassilikogiannakis, The Diels–Alder reaction in total synthesis, *Angew. Chem. Int. Ed.* 41 (2002) 1668–1698.
- [21] C.M. Nimmo, S.C. Owen, M.S. Shoichet, Diels–Alder click cross-linked hyaluronic acid hydrogels for tissue engineering, *Biomacromolecules* 12 (2011) 824–830.
- [22] H. Tan, J.P. Rubin, K.G. Marra, Direct synthesis of biodegradable polysaccharide derivative hydrogels through aqueous Diels–Alder chemistry, *Macromol. Rapid Commun.* 32 (2011) 905–911.
- [23] A. Kozlowski, J.M. Harris, Improvements in protein PEGylation: pegylated interferons for treatment of hepatitis C, *J. Control. Release* 72 (2001) 217–224.
- [24] H.A. Quigley, The number of people with glaucoma worldwide in 2010 and 2020, *Br. J. Ophthalmol.* 90 (2006) 262–267.
- [25] J.W.Y. Yau, S.L. Rogers, R. Kawasaki, E.L. Lamoureux, J.W. Kowalski, T. Bek, et al., Global Prevalence and Major Risk Factors of Diabetic Retinopathy, *Diabetes Care* 35 (2012) 556–564.
- [26] D.B. Rein, J.S. Wittenborn, X. Zhang, A.A. Honeycutt, S.B. Lesesne, J. Saaddine, Forecasting age-related macular degeneration through the year 2050, *Arch. Ophthalmol.* 127 (2009) 533–540.
- [27] L.S. Lim, P. Mitchell, J.M. Seddon, F.G. Holz, T.Y. Wong, Age-related macular degeneration, *Lancet* 379 (2012) 1728–1738.
- [28] A.W. Lloyd, R.G. Faragher, S.P. Denyer, Ocular biomaterials and implants, *Biomaterials* 22 (2001) 769–785.
- [29] K.E. Swindle, N. Ravi, Recent advances in polymeric vitreous substitutes, *Expert Rev. Ophthalmol.* 2 (2007) 255–265.
- [30] F. Baino, Towards an ideal biomaterial for vitreous replacement: Historical overview and future trends, *Acta Biomater.* 7 (2011) 921–935.

- [31] R. Kholdebarin, R.J. Campbell, Y.-P. Jin, Y.M. Buys, Multicenter study of compliance and drop administration in glaucoma, *Can. J. Ophthalmol.* 43 (2008) 454–461.
- [32] T.F. Patton, J.R. Robinson, Quantitative precorneal disposition of topically applied pilocarpine nitrate in rabbit eyes, *J. Pharm. Sci.* 65 (1976) 1295–1301.
- [33] V.H. Lee, J.R. Robinson, Mechanistic and quantitative evaluation of precorneal pilocarpine disposition in albino rabbits, *J. Pharm. Sci.* 68 (1979) 673–684.
- [34] K. Järvinen, T. Järvinen, A. Urtti, Ocular absorption following topical delivery, *Adv. Drug Deliv. Rev.* 16 (1995) 3–19.
- [35] D.H. Geroski, H.F. Edelhauser, Drug delivery for posterior segment eye disease, *Invest. Ophthalmol. Vis. Sci.* 41 (2000) 961–964.
- [36] E.M. Del Amo, A. Urtti, Current and future ophthalmic drug delivery systems: a shift to the posterior segment, *Drug Discov. Today* 13 (2008) 135–143.
- [37] S.S. Lee, P.M. Hughes, M.R. Robinson, Recent advances in drug delivery systems for treating ocular complications of systemic diseases, *Curr. Opin. Ophthalmol.* 20 (2009) 511–519.
- [38] R. Gaudana, J. Jwala, S.H.S. Boddu, A.K. Mitra, Recent perspectives in ocular drug delivery, *Pharm. Res.* 26 (2009) 1197–1216.
- [39] J.-H. Chang, N.K. Garg, E. Lunde, K.-Y. Han, S. Jain, D.T. Azar, Corneal neovascularization: an anti-VEGF therapy review, *Surv. Ophthalmol.* 57 (2012) 415–429.
- [40] T.F. Vandamme, Microemulsions as ocular drug delivery systems: recent developments and future challenges, *Prog. Retin. Eye Res.* 21 (2002) 15–34.
- [41] K. Pollinger, R. Hennig, A. Ohlmann, R. Fuchshofer, R. Wenzel, M. Breunig, et al., Ligand-functionalized nanoparticles target endothelial cells in retinal capillaries after systemic application, *PNAS* 110 (2013) 6115–6120.

-
- [42] C. Luschmann, J. Tessmar, S. Schoeberl, O. Strauss, C. Framme, K. Luschmann, A.M. Goepferich, Developing an in situ nanosuspension: a novel approach towards the efficient administration of poorly soluble drugs at the anterior eye, *Eur. J. Pharm. Sci.* 50 (2013) 385–392.
- [43] S.S. Lee, P. Hughes, A.D. Ross, M.R. Robinson, Biodegradable implants for sustained drug release in the eye, *Pharm. Res.* 27 (2010) 2043–2053.
- [44] T.R. Hoare, D.S. Kohane, Hydrogels in drug delivery: Progress and challenges, *Polymer* 49 (2008) 1993–2007.
- [45] S.R. van Tomme, G. Storm, W.E. Hennink, In situ gelling hydrogels for pharmaceutical and biomedical applications, *Int. J. Pharm.* 355 (2008) 1–18.
- [46] P.C. Nicolson, J. Vogt, Soft contact lens polymers: an evolution, *Biomaterials* 22 (2001) 3273–3283.
- [47] L. Werner, N. Mamalis, Foldable Intraocular Lenses, in: T. Kohnen, D. Koch (Eds.), *Cataract and Refractive Surgery*, Springer Berlin Heidelberg (2005).
- [48] O. Findl, C. Leydolt, Meta-analysis of accommodating intraocular lenses, *J. Cataract Refract. Surg.* 33 (2007) 522–527.
- [49] M. Zignani, C. Tabatabay, R. Gurny, Topical semi-solid drug delivery: kinetics and tolerance of ophthalmic hydrogels, *Adv. Drug Deliv. Rev.* 16 (1995) 51–60.
- [50] A.K. Agrawal, M. Das, S. Jain, In situ gel systems as 'smart' carriers for sustained ocular drug delivery, *Expert. Opin. Drug Deliv.* 9 (2012) 383–402.
- [51] A.M. Oelker, M.W. Grinstaff, Ophthalmic adhesives: a materials chemistry perspective, *J. Mater. Chem.* 18 (2008) 2521–2536.
- [52] S. Slomkowski, J.V. Alemán, R.G. Gilbert, M. Hess, K. Horie, R.G. Jones, et al., Terminology of polymers and polymerization processes in dispersed systems (IUPAC Recommendations 2011), *Pure Appl. Chem.* 83 (2011).
- [53] K.Y. Lee, D.J. Mooney, Hydrogels for tissue engineering, *Chem. Rev.* 101 (2001) 1869–1880.

- [54] A.S. Hoffman, Hydrogels for biomedical applications, *Adv. Drug Deliv. Rev.* 54 (2002) 3–12.
- [55] J.L. Drury, D.J. Mooney, Hydrogels for tissue engineering: scaffold design variables and applications, *Biomaterials* 24 (2003) 4337–4351.
- [56] C.M. Nimmo, M.S. Shoichet, Regenerative biomaterials that “click”: simple, aqueous-based protocols for hydrogel synthesis, surface immobilization, and 3D patterning, *Bioconjug. Chem.* 22 (2011) 2199–2209.
- [57] N. Hammer, F.P. Brandl, S. Kirchhof, A.M. Goepferich, Cleavable carbamate linkers for controlled protein delivery from hydrogels, *J. Control. Release* 183 (2014) 67–76.
- [58] D. Schweizer, K. Schönhammer, M. Jahn, A.M. Goepferich, Protein–polyanion interactions for the controlled release of monoclonal antibodies, *Biomacromolecules* 14 (2012) 75–83.
- [59] Y. Yu, Y. Chau, Formulation of in situ chemically cross-linked hydrogel depots for protein release: from the blob model perspective, *Biomacromolecules* 16 (2015) 56–65.
- [60] D.M. Maurice, S. Mishima, Ocular Pharmacokinetics, in: M. Sears (Ed.), *Pharmacology of the Eye*, Springer Berlin Heidelberg (1984).
- [61] C. Koelwel, S. Rothschenk, B. Fuchs-Koelwel, B. Gabler, C. Lohmann, A.M. Goepferich, Alginate inserts loaded with epidermal growth factor for the treatment of keratoconjunctivitis sicca, *Pharm. Dev. Technol.* 13 (2008) 221–231.
- [62] R. Gurny, Preliminary study of prolonged acting drug delivery system for the treatment of glaucoma, *Pharm. Acta. Helv.* 56 (1981) 130–132.
- [63] R. Gurny, T. Boye, H. Ibrahim, Ocular therapy with nanoparticulate systems for controlled drug delivery, *J. Control. Release* 2 (1985) 353–361.
- [64] R. Gurny, H. Ibrahim, A. Aebi, P. Buri, C. Wilson, N. Washington, et al., Design and evaluation of controlled release systems for the eye, *J. Control. Release* 6 (1987) 367–373.

-
- [65] N.M. Davies, S.J. Fair, J. Hadgraft, I.W. Kellaway, Evaluation of mucoadhesive polymers in ocular drug delivery. I. Viscous solutions, *Pharm. Res.* 8 (1991) 1039–1043.
- [66] B. Srividya, R.M. Cardoza, P. Amin, Sustained ophthalmic delivery of ofloxacin from a pH triggered in situ gelling system, *J. Control. Release* 73 (2001) 205–211.
- [67] C. Wu, H. Qi, W. Chen, C. Huang, C. Su, W. Li, S. Hou, Preparation and evaluation of a Carbopol[®]/HPMC-based in situ gelling ophthalmic system for puerarin, *Yakugaku Zasshi* 127 (2007) 183–191.
- [68] S.C. Miller, M.D. Donovan, Effect of poloxamer 407 gel on the miotic activity of pilocarpine nitrate in rabbits, *Int. J. Pharm.* 12 (1982) 147–152.
- [69] S.D. Desai, J. Blanchard, In vitro evaluation of Pluronic F127-based controlled-release ocular delivery systems for pilocarpine, *J. Pharm. Sci.* 87 (1998) 226–230.
- [70] A. El-Kamel, In vitro and in vivo evaluation of Pluronic F127-based ocular delivery system for timolol maleate, *Int. J. Pharm.* 241 (2002) 47–55.
- [71] H.-R. Lin, K. Sung, Carbopol/Pluronic phase change solutions for ophthalmic drug delivery, *J. Control. Release* 69 (2000) 379–388.
- [72] H. Qi, W. Chen, C. Huang, L. Li, C. Chen, W. Li, C. Wu, Development of a poloxamer analogs/carbopol-based in situ gelling and mucoadhesive ophthalmic delivery system for puerarin, *Int. J. Pharm.* 337 (2007) 178–187.
- [73] W.-D. Ma, H. Xu, C. Wang, S.-F. Nie, W.-S. Pan, Pluronic F127-g-poly(acrylic acid) copolymers as in situ gelling vehicle for ophthalmic drug delivery system, *Int. J. Pharm.* 350 (2008) 247–256.
- [74] G.-H. Hsiue, S.-h. Hsu, C.-C. Yang, S.-H. Lee, I.-K. Yang, Preparation of controlled release ophthalmic drops, for glaucoma therapy using thermosensitive poly-*N*-isopropylacrylamide, *Biomaterials* 23 (2002) 457–462.

- [75] Y. Cao, C. Zhang, W. Shen, Z. Cheng, L. Yu, Q. Ping, Poly(*N*-isopropylacrylamide)–chitosan as thermosensitive in situ gel-forming system for ocular drug delivery, *J. Control. Release* 120 (2007) 186–194.
- [76] S. Miyazaki, S. Suzuki, N. Kawasaki, K. Endo, A. Takahashi, D. Attwood, In situ gelling xyloglucan formulations for sustained release ocular delivery of pilocarpine hydrochloride, *Int. J. Pharm.* 229 (2001) 29–36.
- [77] P.-E. Jansson, B. Lindberg, P.A. Sandford, Structural studies of gellan gum, an extracellular polysaccharide elaborated by *Pseudomonas elodea*, *Carbohydr. Res.* 124 (1983) 135–139.
- [78] A. Rozier, C. Mazuel, J. Grove, B. Plazonnet, Gelrite®: a novel, ion-activated, in-situ gelling polymer for ophthalmic vehicles. Effect on bioavailability of timolol, *Int. J. Pharm.* 57 (1989) 163–168.
- [79] Y.D. Sanzgiri, S. Maschi, V. Crescenzi, L. Callegaro, E.M. Topp, V.J. Stella, Gellan-based systems for ophthalmic sustained delivery of methylprednisolone, *J. Control. Release* 26 (1993) 195–201.
- [80] J. Balasubramaniam, J.K. Pandit, Ion-activated in situ gelling systems for sustained ophthalmic delivery of ciprofloxacin hydrochloride, *Drug Deliv.* 10 (2003) 185–191.
- [81] Y. Sultana, M. Aqil, A. Ali, Ion-activated, Gelrite®-based in situ ophthalmic gels of pefloxacin mesylate: comparison with conventional eye drops, *Drug Deliv.* 13 (2006) 215–219.
- [82] S. Mandal, G.L. Prabhushankar, M. Thimmasetty, M.S. Geetha, Formulation and evaluation of an in situ gel-forming ophthalmic formulation of moxifloxacin hydrochloride, *Int. J. Pharm. Investig.* 2 (2012) 78–82.
- [83] Z. Liu, J. Li, S. Nie, H. Liu, P. Ding, W. Pan, Study of an alginate/HPMC-based in situ gelling ophthalmic delivery system for gatifloxacin, *Int. J. Pharm.* 315 (2006) 12–17.

-
- [84] Y. Liu, J. Liu, X. Zhang, R. Zhang, Y. Huang, C. Wu, In situ gelling Gelrite/alginate formulations as vehicles for ophthalmic drug delivery, *AAPS PharmSciTech* 11 (2010) 610–620.
- [85] H.-R. Lin, K.C. Sung, W.-J. Vong, In situ gelling of alginate/Pluronic solutions for ophthalmic delivery of pilocarpine, *Biomacromolecules* 5 (2004) 2358–2365.
- [86] O. Wichterle, D. Lím, Hydrophilic gels for biological use, *Nature* 185 (1960) 117–118.
- [87] L. Alvord, J. Court, T. Davis, C.F. Morgan, K. Schindelhelm, J. Vogt, L. Winterton, Oxygen permeability of a new type of high Dk soft contact lens material, *Optom. Vis. Sci.* 75 (1998) 30–36.
- [88] R.C. Peterson, J.S. Wolffsohn, J. Nick, L. Winterton, J. Lally, Clinical performance of daily disposable soft contact lenses using sustained release technology, *Cont. Lens Anterior Eye* 29 (2006) 127–134.
- [89] T. Goda, K. Ishihara, Soft contact lens biomaterials from bioinspired phospholipid polymers, *Expert Rev. Med. Devices* 3 (2006) 167–174.
- [90] C. Alvarez-Lorenzo, H. Hiratani, A. Concheiro, Contact lenses for drug delivery, *Am. J. Drug Deliv.* 4 (2006) 131–151.
- [91] L. Xinming, C. Yingde, A.W. Lloyd, S.V. Mikhalovsky, S.R. Sandeman, C.A. Howel, L. Liewen, Polymeric hydrogels for novel contact lens-based ophthalmic drug delivery systems: A review, *Cont. Lens Anterior Eye* 31 (2008) 57–64.
- [92] L.C. Bengani, K.-H. Hsu, S. Gause, A. Chauhan, Contact lenses as a platform for ocular drug delivery, *Expert. Opin. Drug Deliv.* 10 (2013) 1483–1496.
- [93] I.M. Carvalho, C.S. Marques, R.S. Oliveira, P.B. Coelho, P.C. Costa, D.C. Ferreira, Sustained drug release by contact lenses for glaucoma treatment-a review, *J. Control. Release* 202 (2015) 76–82.
- [94] S.M. Chan, H. Boisjoly, Advances in the use of adhesives in ophthalmology, *Curr. Opin. Ophthalmol.* 15 (2004) 305–310.

- [95] A. Ribeiro, F. Veiga, D. Santos, J.J. Torres-Labandeira, A. Concheiro, C. Alvarez-Lorenzo, Bioinspired imprinted pHEMA-hydrogels for ocular delivery of carbonic anhydrase inhibitor drugs, *Biomacromolecules* 12 (2011) 701–709.
- [96] S.S. Bhatia, Ocular surface sealants and adhesives, *Ocul. Surf.* 4 (2006) 146–154.
- [97] H.T. Peng, P.N. Shek, Novel wound sealants: biomaterials and applications, *Expert Rev. Med. Devices* 7 (2010) 639–659.
- [98] E. Margalit, G.Y. Fujii, J.C. Lai, P. Gupta, S.J. Chen, J.S. Shyu, et al., Bioadhesives for intraocular use, *Retina* 20 (2000) 469–477.
- [99] T. Chen, R. Janjua, M.K. McDermott, S.L. Bernstein, S.M. Steidl, G.F. Payne, Gelatin-based biomimetic tissue adhesive. Potential for retinal reattachment, *J. Biomed. Mater. Res. B Appl. Biomater.* 77 (2006) 416–422.
- [100] J. Sueda, T. Fukuchi, N. Usumoto, T. Okuno, M. Arai, T. Hirose, Intraocular use of hydrogel tissue adhesive in rabbit eyes, *Jpn. J. Ophthalmol.* 51 (2007) 89–95.
- [101] S.S. Anumolu, A.S. DeSantis, A.R. Menjoge, R.A. Hahn, J.A. Beloni, M.K. Gordon, P.J. Sinko, Doxycycline loaded poly(ethylene glycol) hydrogels for healing vesicant-induced ocular wounds, *Biomaterials* 31 (2010) 964–974.
- [102] M.K. Gordon, A. DeSantis, M. Deshmukh, C.J. Lacey, R.A. Hahn, J. Beloni, et al., Doxycycline hydrogels as a potential therapy for ocular vesicant injury, *J. Ocul. Pharmacol. Ther.* 26 (2010) 407–419.
- [103] H. Sheardown, H. Clark, C. Wedge, R. Apel, D. Rootman, Y.-L. Cheng, A semi-solid drug delivery system for epidermal growth factor in corneal epithelial wound healing, *Curr. Eye Res.* 16 (1997) 183–190.
- [104] K. Hori, C. Sotozono, J. Hamuro, K. Yamasaki, Y. Kimura, M. Ozeki, et al., Controlled-release of epidermal growth factor from cationized gelatin hydrogel enhances corneal epithelial wound healing, *J. Control. Release* 118 (2007) 169–176.

-
- [105] M. Tetz, M.R. Jorgensen, New hydrophobic IOL materials and understanding the science of glistenings, *Curr. Eye Res.* (2015) 1–13.
- [106] G. Helary, P. Yammine, V. Migonney, Surface modification of hydrogel intraocular lenses to prevent cell proliferation, *J. Appl. Biomater. Biomech.* 2 (2004) 183–190.
- [107] D. Bozukova, C. Pagnouille, M.-C. de Pauw-Gillet, S. Desbief, R. Lazzaroni, N. Ruth, et al., Improved performances of intraocular lenses by poly(ethylene glycol) chemical coatings, *Biomacromolecules* 8 (2007) 2379–2387.
- [108] C. Brady, S.E.J. Bell, C. Parsons, S.P. Gorman, D.S. Jones, C.P. McCoy, Novel porphyrin-incorporated hydrogels for photoactive intraocular lens biomaterials, *J. Phys. Chem. B* 111 (2007) 527–534.
- [109] C. González-Chomón, A. Concheiro, C. Alvarez-Lorenzo, Drug-Eluting Intraocular Lenses, *Materials* 4 (2011) 1927–1940.
- [110] Y.-C. Liu, T.T. Wong, J.S. Mehta, Intraocular lens as a drug delivery reservoir, *Curr. Opin. Ophthalmol.* 24 (2013) 53–59.
- [111] T.V. Chirila, Y. Hong, P.D. Dalton, I.J. Constable, M.F. Refojo, The use of hydrophilic polymers as artificial vitreous, *Prog. Polym. Sci.* 23 (1998) 475–508.
- [112] M.J. Colthurst, R.L. Williams, P.S. Hiscott, I. Grierson, Biomaterials used in the posterior segment of the eye, *Biomaterials* 21 (2000) 649–665.
- [113] N. Soman, R. Banerjee, Artificial vitreous replacements, *Biomed. Mater. Eng.* 13 (2003) 59–74.
- [114] T.T. Kleinberg, R.T. Tzekov, L. Stein, N. Ravi, S. Kaushal, Vitreous substitutes: a comprehensive review, *Surv. Ophthalmol.* 56 (2011) 300–323.
- [115] J. Fernandez-Vigo, M.F. Refojo, T. Verstraeten, Evaluation of a viscoelastic solution of hydroxypropyl methylcellulose as a potential vitreous substitute, *Retina* 10 (1990) 148–152.

- [116] C. de Jong, E. Bali, J. Libert, L. Caspers-Velu, ADCON-L hydrogel as a vitreous substitute: preliminary results, *Bull. Soc. Belge Ophthalmol.* 278 (2000) 71–75.
- [117] S. Suri, R. Banerjee, In vitro evaluation of in situ gels as short term vitreous substitutes, *J. Biomed. Mater. Res. A* 79 (2006) 650–664.
- [118] M.F. Refojo, Polymers in ophthalmic surgery, *J. Biomed. Mater. Res. A* 5 (1971) 113–119.
- [119] T.E. Hogen-Esch, K.R. Shah, C.R. Fitzgerald, Development of injectable poly(glyceryl methacrylate) hydrogels for vitreous prosthesis, *J. Biomed. Mater. Res. A* 10 (1976) 975–976.
- [120] F.H. Davidorf, R.B. Chambers, O.W. Kwon, W. Doyle, P. Gresak, S.G. Frank, Ocular toxicity of vitreal pluronic polyol F-127, *Retina* 10 (1990) 297–300.
- [121] G.A. Peyman, M.D. Conway, M. Karaçorlu, K.F. Soike, N. Bhatt, L.C. Clark, R.E. Hoffmann, Evaluation of silicone gel as a long-term vitreous substitute in non-human primates, *Ophthalmic Surg.* 23 (1992) 811–817.
- [122] A. Yamauchi, Synthetic Vitreous Body of PVA Hydrogel, in: D. DeRossi, K. Kajiwarra, Y. Osada, A. Yamauchi (Eds.), *Polymer Gels*, Springer US (1991).
- [123] Y. Hong, T.V. Chirila, S. Vijayasekaran, P.D. Dalton, S.G. Tahija, M.J. Cuypers, I.J. Constable, Crosslinked poly(1-vinyl-2-pyrrolidinone) as a vitreous substitute, *J. Biomed. Mater. Res. A* 30 (1996) 441–448.
- [124] G. Leone, M. Consumi, M. Aggravi, A. Donati, S. Lamponi, A. Magnani, PVA/STMP based hydrogels as potential substitutes of human vitreous, *J. Mater. Sci.* 21 (2010) 2491–2500.
- [125] K.E. Swindle-Reilly, M. Shah, P.D. Hamilton, T.A. Eskin, S. Kaushal, N. Ravi, Rabbit study of an in situ forming hydrogel vitreous substitute, *Invest. Ophthalmol. Vis. Sci.* 50 (2009) 4840–4846.
- [126] Y. Tao, X. Tong, Y. Zhang, J. Lai, Y. Huang, Y.-R. Jiang, B.-H. Guo, Evaluation of an in situ chemically crosslinked hydrogel as a long-term vitreous substitute material, *Acta Biomater.* 9 (2013) 5022–5030.

-
- [127] E.A. Balazs, Fine structure and function of ocular tissues. The vitreous, *Int. Ophthalmol. Clin.* 13 (1973) 169–187.
- [128] C. Schramm, M.S. Spitzer, S. Henke-Fahle, G. Steinmetz, K. Januschowski, P. Heiduschka, et al., The cross-linked biopolymer hyaluronic acid as an artificial vitreous substitute, *Invest. Ophthalmol. Vis. Sci.* 53 (2012) 613–621.
- [129] W.-Y. Su, K.-H. Chen, Y.-C. Chen, Y.-H. Lee, C.-L. Tseng, F.-H. Lin, An injectable oxidated hyaluronic acid/adipic acid dihydrazide hydrogel as a vitreous substitute, *J. Biomater. Sci. Polymer Edn.* 22 (2011) 1777–1797.
- [130] S. Feng, H. Chen, Y. Liu, Z. Huang, X. Sun, L. Zhou, et al., A novel vitreous substitute of using a foldable capsular vitreous body injected with polyvinylalcohol hydrogel, *Sci. Rep.* 3 (2013) 1838.
- [131] D. Pascolini, S.P. Mariotti, Global estimates of visual impairment: 2010, *Br. J. Ophthalmol.* 96 (2012) 614–618.
- [132] J.S. Penn, A. Madan, R.B. Caldwell, M. Bartoli, R.W. Caldwell, M.E. Hartnett, Vascular endothelial growth factor in eye disease, *Prog. Retin. Eye Res.* 27 (2008) 331–371.
- [133] S.E. Quaggin, Turning a blind eye to anti-VEGF toxicities, *J. Clin. Invest.* 122 (2012) 3849–3851.
- [134] J.E. Grunwald, E. Daniel, J. Huang, G.-S. Ying, M.G. Maguire, C.A. Toth, et al., Risk of geographic atrophy in the comparison of age-related macular degeneration treatments trials, *Ophthalmology* 121 (2014) 150–161.
- [135] J.J. Kang Derwent, W.F. Mieler, Thermoresponsive hydrogels as a new ocular drug delivery platform to the posterior segment of the eye, *Trans. Am. Ophthalmol. Soc.* 106 (2008) 206–214.
- [136] S.B. Turturro, M.J. Guthrie, A.A. Appel, P.W. Drapala, E.M. Brey, V.H. Pérez-Luna, et al., The effects of cross-linked thermo-responsive PNIPAAm-based hydrogel injection on retinal function, *Biomaterials* (2011).

- [137] B.M. Rauck, T.R. Friberg, C.A. Medina Mendez, D. Park, V. Shah, R.A. Bilonick, Y. Wang, Biocompatible reverse thermal gel sustains the release of intravitreal bevacizumab in vivo, *Invest. Ophthalmol. Vis. Sci.* 55 (2014) 469–476.
- [138] F.P. Brandl, M. Henke, S. Rothschenk, R. Gschwind, M. Breunig, T. Blunk, et al., Poly(ethylene glycol) based hydrogels for intraocular applications, *Adv. Eng. Mater.* 9 (2007) 1141–1149.
- [139] J. Yu, X. Xu, F. Yao, Z. Luo, L. Jin, B. Xie, et al., In situ covalently cross-linked PEG hydrogel for ocular drug delivery applications, *Int. J. Pharm.* 470 (2014) 151–157.
- [140] Y. Yu, L.C.M. Lau, A.C.-Y. Lo, Y. Chau, Injectable chemically crosslinked hydrogel for the controlled release of bevacizumab in vitreous: a 6-Month in vivo study, *Transl. Vis. Sci. Technol.* 4 (2015) 5.
- [141] A.T. Neffe, K.A. Kobuch, M. Maier, N. Feucht, C.P. Lohmann, A. Wolfstein, et al., In vitro and in vivo evaluation of a multifunctional hyaluronic acid based hydrogel system for local application on the retina, *Macromol. Symp.* 309-310 (2011) 229–235.
- [142] F. Sommer, F.P. Brandl, A.M. Goepferich, Ocular Tissue Engineering, in: J.P. Fisher (Ed.), *Tissue Engineering*, Springer US (2007).
- [143] K. Canola, B. Angénieux, M. Tekaya, A. Quiambao, M.I. Naash, F.L. Munier, et al., Retinal stem cells transplanted into models of late stages of retinitis pigmentosa preferentially adopt a glial or a retinal ganglion cell fate, *Invest. Ophthalmol. Vis. Sci.* 48 (2007) 446–454.
- [144] F. Arnalich-Montiel, S. Pastor, A. Blazquez-Martinez, J. Fernandez-Delgado, M. Nistal, J.L. Alio, M.P. de Miguel, Adipose-derived stem cells are a source for cell therapy of the corneal stroma, *Stem Cells* 26 (2008) 570–579.
- [145] P. Rama, S. Matuska, G. Paganoni, A. Spinelli, M. de Luca, G. Pellegrini, Limbal Stem-Cell Therapy and Long-Term Corneal Regeneration, *N. Engl. J. Med.* 363 (2010) 147–155.

-
- [146] K. Engelmann, J. Bednarz, M. Valtink, Prospects for endothelial transplantation, *Exp. Eye Res.* 78 (2004) 573–578.
- [147] K. Nishida, M. Yamato, Y. Hayashida, K. Watanabe, K. Yamamoto, E. Adachi, et al., Corneal reconstruction with tissue-engineered cell sheets composed of autologous oral mucosal epithelium, *N. Engl. J. Med.* 351 (2004) 1187–1196.
- [148] J.-Y. Lai, K.-H. Chen, G.-H. Hsiue, Tissue-engineered human corneal endothelial cell sheet transplantation in a rabbit model using functional biomaterials, *Transplantation* 84 (2007) 1222–1232.
- [149] J.-Y. Lai, Bioengineered human corneal endothelium for transplantation, *Arch. Ophthalmol.* 124 (2006) 1441–1448.
- [150] B. Ozcelik, K.D. Brown, A. Blencowe, M. Daniell, G.W. Stevens, G.G. Qiao, Ultrathin chitosan–poly(ethylene glycol) hydrogel films for corneal tissue engineering, *Acta Biomater.* 9 (2013) 6594–6605.
- [151] T. Mimura, S. Amano, S. Yokoo, S. Uchida, S. Yamagami, T. Usui, et al., Tissue engineering of corneal stroma with rabbit fibroblast precursors and gelatin hydrogels, *Mol. Vis.* 14 (2008) 1819–1828.
- [152] S. Wang, W. Liu, B. Han, L. Yang, Study on a hydroxypropyl chitosan–gelatin based scaffold for corneal stroma tissue engineering, *Appl. Surf. Sci.* 255 (2009) 8701–8705.
- [153] J.-Y. Lai, Y.-T. Li, Evaluation of cross-linked gelatin membranes as delivery carriers for retinal sheets, *Mater. Sci. Eng. C Mater. Biol. Appl.* 30 (2010) 677–685.
- [154] R.E. MacLaren, R.A. Pearson, A. MacNeil, R.H. Douglas, T.E. Salt, M. Akimoto, et al., Retinal repair by transplantation of photoreceptor precursors, *Nature* 444 (2006) 203–207.
- [155] H. Klassen, D.S. Sakaguchi, M.J. Young, Stem cells and retinal repair, *Prog. Retin. Eye Res.* 23 (2004) 149–181.

- [156] M. Tomita, E. Lavik, H. Klassen, T. Zahir, R. Langer, M.J. Young, Biodegradable polymer composite grafts promote the survival and differentiation of retinal progenitor cells, *Stem Cells* 23 (2005) 1579–1588.
- [157] B.G. Ballios, M.J. Cooke, D. van der Kooy, M.S. Shoichet, A hydrogel-based stem cell delivery system to treat retinal degenerative diseases, *Biomaterials* 31 (2010) 2555–2564.
- [158] Y. Liu, R. Wang, T.I. Zarembinski, N. Doty, C. Jiang, C. Regatieri, et al., The application of hyaluronic acid hydrogels to retinal progenitor cell transplantation, *Tissue Eng. Part A* 19 (2013) 135–142.
- [159] J.-Y. Lee, J.-M. Shin, C.E. Yeum, G.T. Chae, M.-H. Chun, S.-J. Oh, Intravitreal delivery of mesenchymal stem cells loaded onto hydrogel affects the regulatory expression of endogenous NGF and BDNF in ischemic rat retina, *Tissue Eng. Regen. Med.* 9 (2012) 249–258.
- [160] T.I. Zarembinski, N.J. Doty, I.E. Erickson, R. Srinivas, B.M. Wirostko, W.P. Tew, Thiolated hyaluronan-based hydrogels crosslinked using oxidized glutathione: An injectable matrix designed for ophthalmic applications, *Acta Biomater.* 10 (2014) 94–103.
- [161] M.A.J. Mazumder, S.D. Fitzpatrick, B. Muirhead, H. Sheardown, Cell-adhesive thermogelling PNIPAAm/hyaluronic acid cell delivery hydrogels for potential application as minimally invasive retinal therapeutics, *J. Biomed. Mater. Res. A* 100 (2012) 1877–1887.
- [162] J. Hertz, R. Robinson, D.A. Valenzuela, E.B. Lavik, J.L. Goldberg, A tunable synthetic hydrogel system for culture of retinal ganglion cells and amacrine cells, *Acta Biomater.* 9 (2013) 7622–7629.
- [163] D. Kanjickal, S. Lopina, M.M. Evanco-Chapman, S. Schmidt, D. Donovan, Effects of sterilization on poly(ethylene glycol) hydrogels, *J. Biomed. Mater. Res. A* 87 (2008) 608–617.
- [164] S.S. Karajanagi, R. Yoganathan, R. Mammucari, H. Park, J. Cox, S.M. Zeitels, et al., Application of a dense gas technique for sterilizing soft biomaterials, *Biotechnol. Bioeng.* 108 (2011) 1716–1725.

-
- [165] E.Y. Chi, S. Krishnan, T.W. Randolph, J.F. Carpenter, Physical stability of proteins in aqueous solution: Mechanism and driving forces in nonnative protein aggregation, *Pharm. Res.* 20 (2003) 1325–1336.
- [166] W. Wang, S. Singh, D.L. Zeng, K. King, S. Nema, Antibody structure, instability, and formulation, *J. Pharm. Sci.* 96 (2007) 1–26.
- [167] W.J. Foster, Internal osmotic pressure as a mechanism of retinal attachment in a vitreous substitute, *J. Bioact. Compat. Polym.* 21 (2006) 221–235.
- [168] J.-Y. Lai, Biocompatibility of chemically cross-linked gelatin hydrogels for ophthalmic use, *J. Mater. Sci.* 21 (2010) 1899–1911.
- [169] B.V. Slaughter, S.S. Khurshid, O.Z. Fisher, A. Khademhosseini, N.A. Peppas, Hydrogels in regenerative medicine, *Adv. Mater.* 21 (2009) 3307–3329.
- [170] J.S. Boateng, K.H. Matthews, H.N. Stevens, G.M. Eccleston, Wound healing dressings and drug delivery systems: A review, *J. Pharm. Sci.* 97 (2008) 2892–2923.
- [171] Y. Qiu, K. Park, Environment-sensitive hydrogels for drug delivery, *Adv. Drug Deliv. Rev.* 53 (2001) 321–339.
- [172] K. Deligkaris, T.S. Tadele, W. Olthuis, A. van den Berg, Hydrogel-based devices for biomedical applications, *Sens. Actuators B Chem.* 147 (2010) 765–774.
- [173] J. Yeom, S.H. Bhang, B.-S. Kim, M.S. Seo, E.J. Hwang, I.H. Cho, et al., Effect of cross-linking reagents for hyaluronic acid hydrogel dermal fillers on tissue augmentation and regeneration, *Bioconjug. Chem.* 21 (2010) 240–247.
- [174] J.K. Tessmar, A.M. Goepferich, Customized PEG-derived copolymers for tissue-engineering applications, *Macromol. Biosci.* 7 (2007) 23–39.
- [175] K.S. Anseth, A.T. Metters, S.J. Bryant, P.J. Martens, J.H. Elisseeff, C.N. Bowman, In situ forming degradable networks and their application in tissue engineering and drug delivery, *J. Control. Release* 78 (2002) 199–209.

- [176] F.P. Brandl, F. Sommer, A.M. Goepferich, Rational design of hydrogels for tissue engineering: Impact of physical factors on cell behavior, *Biomaterials* 28 (2007) 134–146.
- [177] P.M. Gilbert, K.L. Havenstrite, K.E.G. Magnusson, A. Sacco, N.A. Leonardi, P. Kraft, et al., Substrate elasticity regulates skeletal muscle stem cell self-renewal in culture, *Science* 329 (2010) 1078–1081.
- [178] C. Mann, D. Leckband, Measuring traction forces in long-term cell cultures, *Cel. Mol. Bioeng.* 3 (2010) 40–49.
- [179] A.J. Engler, S. Sen, H.L. Sweeney, D.E. Discher, Matrix elasticity directs stem cell lineage specification, *Cell* 126 (2006) 677–689.
- [180] R. Huisgen, Kinetics and reaction mechanisms: selected examples from the experience of forty years, *Pure Appl. Chem.* 61 (1989) 613–628.
- [181] H.C. Kolb, M.G. Finn, K.B. Sharpless, Click chemistry: diverse chemical function from a few good reactions, *Angew. Chem. Int. Ed.* 40 (2001) 2004–2021.
- [182] L. Gaetke, Copper toxicity, oxidative stress, and antioxidant nutrients, *Toxicology* 189 (2003) 147–163.
- [183] S. Yigit, R. Sanyal, A. Sanyal, Fabrication and functionalization of hydrogels through “click” chemistry, *Chem. Asian J.* 6 (2011) 2648–2659.
- [184] T. Yang, H. Long, M. Malkoch, E. Kristofer Gamstedt, L. Berglund, A. Hult, Characterization of well-defined poly(ethylene glycol) hydrogels prepared by thiol-ene chemistry, *J. Polym. Sci. A Polym. Chem.* 49 (2011) 4044–4054.
- [185] J. Zheng, L.A. Smith Callahan, J. Hao, K. Guo, C. Wesdemiotis, R.A. Weiss, M.L. Becker, Strain-promoted cross-linking of PEG-based hydrogels via copper-free cycloaddition, *ACS Macro Lett.* 1 (2012) 1071–1073.
- [186] M. Marref, N. Mignard, C. Jegat, M. Taha, M. Belbachir, R. Meghabar, Epoxy-amine based thermoresponsive networks designed by Diels-Alder reactions, *Polym. Int.* 62 (2013) 87–98.

-
- [187] H.-L. Wei, Z. Yang, L.-M. Zheng, Y.-M. Shen, Thermosensitive hydrogels synthesized by fast Diels-Alder reaction in water, *Polymer* 50 (2009) 2836–2840.
- [188] H. Wei, J. Yang, H. Chu, Z. Yang, C. Ma, K. Yao, Diels–Alder reaction in water for the straightforward preparation of thermoresponsive hydrogels, *J. Appl. Polym. Sci.* 120 (2011) 974–980.
- [189] C. Kim, K.L. Marshall, J.U. Wallace, J.J. Ou, S.H. Chen, Novel cholesteric glassy liquid crystals comprising benzene functionalized with hybrid chiral-nematic mesogens, *Chem. Mater.* 20 (2008) 5859–5868.
- [190] L. Rulišek, P. Šebek, Z. Havlas, R. Hrabal, P. Čapek, A. Svatoš, An experimental and theoretical study of stereoselectivity of furan–maleic anhydride and furan–maleimide Diels–Alder reactions, *J. Org. Chem.* 70 (2005) 6295–6302.
- [191] N.B. Sankaran, A.Z. Rys, R. Nassif, M.K. Nayak, K. Metera, B. Chen, et al., Ring-opening metathesis polymers for biodetection and signal amplification: synthesis and self-assembly, *Macromolecules* 43 (2010) 5530–5537.
- [192] G. Mantovani, F. Lecolley, L. Tao, D.M. Haddleton, J. Clerx, J.J.L.M. Cornelissen, K. Velonia, Design and synthesis of *N*-maleimido-functionalized hydrophilic polymers via copper-mediated living radical polymerization: a suitable alternative to PEGylation chemistry, *J. Am. Chem. Soc.* 127 (2005) 2966–2973.
- [193] K.A. Keller, J. Guo, S. Punna, M. Finn, A thermally-cleavable linker for solid-phase synthesis, *Tetrahedron Lett.* 46 (2005) 1181–1184.
- [194] P.J. Flory, Principles of polymer chemistry, 10. print. ed., Cornell Univ. Pr., Ithaca, (1953).
- [195] J.C. Bray, E.W. Merrill, Poly(vinyl alcohol) hydrogels. Formation by electron beam irradiation of aqueous solutions and subsequent crystallization, *J. Appl. Polym. Sci.* 17 (1973) 3779–3794.

- [196] D.L. Elbert, A.B. Pratt, M.P. Lutolf, S. Halstenberg, J.A. Hubbell, Protein delivery from materials formed by self-selective conjugate addition reactions, *J. Control. Release* 76 (2001) 11–25.
- [197] T. Canal, N.A. Peppas, Correlation between mesh size and equilibrium degree of swelling of polymeric networks, *J. Biomed. Mater. Res. A* 23 (1989) 1183–1193.
- [198] G.P. Raeber, M.P. Lutolf, J.A. Hubbell, Molecularly engineered PEG hydrogels: a novel model system for proteolytically mediated cell migration, *Biophys. J.* 89 (2005) 1374–1388.
- [199] A. Metters, J. Hubbell, Network formation and degradation behavior of hydrogels formed by Michael-type addition reactions, *Biomacromolecules* 6 (2005) 290–301.
- [200] M.P. Lutolf, J.A. Hubbell, Synthesis and physicochemical characterization of end-linked poly(ethylene glycol)-co-peptide hydrogels formed by Michael-type addition, *Biomacromolecules* 4 (2003) 713–722.
- [201] A. Oliva, J. Fariña, M. Llabrés, Development of two high-performance liquid chromatographic methods for the analysis and characterization of insulin and its degradation products in pharmaceutical preparations, *J. Chromatogr. B Biomed. Sci. Appl.* 749 (2000) 25–34.
- [202] J. Armstrong, R. Wenby, H. Meiselman, T. Fisher, The hydrodynamic radii of macromolecules and their effect on red blood cell aggregation, *Biophys. J.* 87 (2004) 4259–4270.
- [203] J.R. McElhanon, T. Zifer, S.R. Kline, D.R. Wheeler, D.A. Loy, G.M. Jamison, et al., Thermally cleavable surfactants based on furan–maleimide Diels–Alder adducts, *Langmuir* 21 (2005) 3259–3266.
- [204] K.C. Koehler, K.S. Anseth, C.N. Bowman, Diels–Alder mediated controlled release from a poly(ethylene glycol) based hydrogel, *Biomacromolecules* 14 (2013) 538–547.

-
- [205] B.S. Sumerlin, A.P. Vogt, Macromolecular engineering through click chemistry and other efficient transformations, *Macromolecules* 43 (2010) 1–13.
- [206] P.L. Golas, K. Matyjaszewski, Marrying click chemistry with polymerization: expanding the scope of polymeric materials, *Chem. Soc. Rev.* 39 (2010) 1338–1354.
- [207] W. Xi, T.F. Scott, C.J. Kloxin, C.N. Bowman, Click chemistry in materials science, *Adv. Funct. Mater.* 24 (2014) 2572–2590.
- [208] M.A. Tasdelen, Diels–Alder “click” reactions: recent applications in polymer and material science, *Polym. Chem.* 2 (2011) 2133–2145.
- [209] M. Shi, J.H. Wosnick, K. Ho, A. Keating, M.S. Shoichet, Immuno-polymeric nanoparticles by Diels–Alder chemistry, *Angew. Chem. Int. Ed.* 46 (2007) 6126–6131.
- [210] H.-L. Wei, K. Yao, H.-J. Chu, Z.-C. Li, J. Zhu, Y.-M. Shen, et al., Click synthesis of the thermo- and pH-sensitive hydrogels containing β -cyclodextrins, *J. Mater. Sci.* 47 (2012) 332–340.
- [211] S.-H. Hyon, W.-I. Cha, Y. Ikada, M. Kita, Y. Ogura, Y. Honda, Poly(vinyl alcohol) hydrogels as soft contact lens material, *J. Biomater. Sci. Polymer Edn.* 5 (1994) 397–406.
- [212] S. Kirchhof, F.P. Brandl, N. Hammer, A.M. Goepferich, Investigation of the Diels–Alder reaction as a cross-linking mechanism for degradable poly(ethylene glycol) based hydrogels, *J. Mater. Chem. B* 1 (2013) 4855–4864.
- [213] F. Yu, X. Cao, L. Zeng, Q. Zhang, X. Chen, An interpenetrating HA/G/CS biomimic hydrogel via Diels–Alder click chemistry for cartilage tissue engineering, *Carbohydr. Polym.* 97 (2013) 188–195.
- [214] S.D. Bergman, F. Wudl, Mendable polymers, *J. Mater. Chem.* 18 (2007) 41–62.
- [215] S. Burattini, B.W. Greenland, D. Chappell, H.M. Colquhoun, W. Hayes, Healable polymeric materials: a tutorial review, *Chem. Soc. Rev.* 39 (2010) 1973–1985.

- [216] Y.-L. Liu, T.-W. Chuo, Self-healing polymers based on thermally reversible Diels–Alder chemistry, *Polym. Chem.* 4 (2013) 2194–2205.
- [217] T. Dispinar, R. Sanyal, A. Sanyal, A Diels-Alder/retro Diels-Alder strategy to synthesize polymers bearing maleimide side chains, *J. Polym. Sci. A Polym. Chem.* 45 (2007) 4545–4551.
- [218] I. Kosif, E.-J. Park, R. Sanyal, A. Sanyal, Fabrication of maleimide containing thiol reactive hydrogels via Diels–Alder/retro-Diels–Alder strategy, *Macromolecules* 43 (2010) 4140–4148.
- [219] A.A. Kislukhin, C.J. Higginson, V.P. Hong, M.G. Finn, Degradable conjugates from oxanorbornadiene reagents, *J. Am. Chem. Soc.* 134 (2012) 6491–6497.
- [220] K.C. Koehler, D.L. Alge, K.S. Anseth, C.N. Bowman, A Diels–Alder modulated approach to control and sustain the release of dexamethasone and induce osteogenic differentiation of human mesenchymal stem cells, *Biomaterials* 34 (2013) 4150–4158.
- [221] F. Yu, X. Cao, Y. Li, L. Zeng, B. Yuan, X. Chen, An injectable hyaluronic acid/PEG hydrogel for cartilage tissue engineering formed by integrating enzymatic crosslinking and Diels-Alder "click chemistry", *Polym. Chem.* 5 (2014) 1082–1090.
- [222] S.-Y. Tang, J. Shi, Q.-X. Guo, Accurate prediction of rate constants of Diels–Alder reactions and application to design of Diels–Alder ligation, *Org. Biomol. Chem.* 10 (2012) 2673–2682.
- [223] R.G. Barradas, S. Fletcher, J.D. Porter, The hydrolysis of maleimide in alkaline solution, *Can. J. Chem.* 54 (1976) 1400–1404.
- [224] S. Matsui, H. Aida, Hydrolysis of some *N*-alkylmaleimides, *J. Chem. Soc., Perkin Trans. 2* (1978) 1277–1280.
- [225] M.N. Khan, Kinetics and mechanism of the alkaline hydrolysis of maleimide, *J. Pharm. Sci.* 73 (1984) 1767–1771.
- [226] G.M. Kavanagh, S.B. Ross-Murphy, Rheological characterisation of polymer gels, *Prog. Polym. Sci.* 23 (1998) 533–562.

-
- [227] A. Wassermann, 129. Homogeneous catalysis and solvent effects in a diene synthesis, *J. Chem. Soc.* (1942) 623.
- [228] A. Wassermann, Notes, *J. Chem. Soc.* (1946) 1089–1090.
- [229] W. Rubin, H. Steiner, A. Wassermann, Catalysis of Diels–Alder diene associations. Part V. Proton- and electron-transfer processes, *J. Chem. Soc.* (1949) 3046–3057.
- [230] E.B. Mubofu, J.B.F.N. Engberts, Specific acid catalysis and Lewis acid catalysis of Diels–Alder reactions in aqueous media, *J. Phys. Org. Chem.* 17 (2004) 180–186.
- [231] J.R. McElhanon, D.R. Wheeler, Thermally responsive dendrons and dendrimers based on reversible furan–maleimide Diels–Alder adducts, *Org. Lett.* 3 (2001) 2681–2683.
- [232] A. Gandini, D. Coelho, A.J. Silvestre, Reversible click chemistry at the service of macromolecular materials. Part 1: Kinetics of the Diels–Alder reaction applied to furan–maleimide model compounds and linear polymerizations, *Eur. Polym. J.* 44 (2008) 4029–4036.
- [233] X. Liu, P. Du, L. Liu, Z. Zheng, X. Wang, T. Joncheray, Y. Zhang, Kinetic study of Diels–Alder reaction involving in maleimide–furan compounds and linear polyurethane, *Polym. Bull.* 70 (2013) 2319–2335.
- [234] A. Maggiani, A. Tubul, P. Brun, 7-Oxabicyclo[2.2.1]heptadiene derivatives: reactivity towards Brønsted acids, *Chem. Commun.* (1999) 2495–2496.
- [235] J.P. Queslel, J.E. Mark, Molecular interpretation of the moduli of elastomeric polymer networks of known structure, in: *Analysis/Networks/Peptides*, Springer Berlin Heidelberg (1984).
- [236] J.D. Hartgerink, E. Beniash, S.I. Stupp, Self-assembly and mineralization of peptide–amphiphile nanofibers, *Science* 294 (2001) 1684–1688.
- [237] L.A. Estroff, L. Leiserowitz, L. Addadi, S. Weiner, A.D. Hamilton, Characterization of an organic hydrogel: a cryo-transmission electron microscopy and X-ray diffraction study, *Adv. Mater.* 15 (2003) 38–42.

- [238] A.W. Watkins, K.S. Anseth, Investigation of molecular transport and distributions in poly(ethylene glycol) hydrogels with confocal laser scanning microscopy, *Macromolecules* 38 (2005) 1326–1334.
- [239] H. Liao, D. Munoz-Pinto, X. Qu, Y. Hou, M.A. Grunlan, M.S. Hahn, Influence of hydrogel mechanical properties and mesh size on vocal fold fibroblast extracellular matrix production and phenotype, *Acta Biomater.* 4 (2008) 1161–1171.
- [240] B. Hammouda, D. Ho, S. Kline, SANS from poly(ethylene oxide)/water systems, *Macromolecules* 35 (2002) 8578–8585.
- [241] T. Matsunaga, T. Sakai, Y. Akagi, U.-I. Chung, M. Shibayama, Structure characterization of tetra-PEG gel by small-angle neutron scattering, *Macromolecules* 42 (2009) 1344–1351.
- [242] D.J. Waters, K. Engberg, R. Parke-Houben, L. Hartmann, C.N. Ta, M.F. Toney, C.W. Frank, Morphology of photopolymerized end-linked poly(ethylene glycol) hydrogels by small-angle X-ray scattering, *Macromolecules* 43 (2010) 6861–6870.
- [243] M. Wallace, D.J. Adams, J.A. Iggo, Analysis of the mesh size in a supramolecular hydrogel by PFG-NMR spectroscopy, *Soft Matter* 9 (2013) 5483–5491.
- [244] K. Ishikiriya, M. Todoki, K. Motomura, Pore size distribution (PSD) measurements of silica gels by means of differential scanning calorimetry: I. Optimization for determination of PSD, *J. Colloid Interface Sci.* 171 (1995) 92–102.
- [245] M. Iza, S. Woerly, C. Danumah, S. Kaliaguine, M. Bousmina, Determination of pore size distribution for mesoporous materials and polymeric gels by means of DSC measurements: thermoporometry, *Polymer* 41 (2000) 5885–5893.
- [246] L. Pescosolido, L. Feruglio, R. Farra, S. Fiorentino, I. Colombo, T. Coviello, et al., Mesh size distribution determination of interpenetrating polymer network hydrogels, *Soft Matter* 8 (2012) 7708–7715.

-
- [247] M. Abrami, I. D'Agostino, G. Milcovich, S. Fiorentino, R. Farra, F. Asaro, et al., Physical characterization of alginate–Pluronic F127 gel for endoluminal NABDs delivery, *Soft Matter* 10 (2014) 729–737.
- [248] S. Kirchhof, A. Strasser, H.-J. Wittmann, V. Messmann, N. Hammer, A.M. Goepferich, F.P. Brandl, New insights into the cross-linking and degradation mechanism of Diels-Alder hydrogels, *J. Mater. Chem. B* 2 (2015) 449–457.
- [249] D.F. Martin, M.G. Maguire, G.-S. Ying, J.E. Grunwald, S.L. Fine, G.J. Jaffe, Ranibizumab and bevacizumab for neovascular age-related macular degeneration, *N. Engl. J. Med.* 364 (2011) 1897–1908.
- [250] J. Brandrup, E.H. Immergut, E.A. Grulke, Polymer handbook, 4th ed., Wiley, New York, (1999).
- [251] E. Merrill, K. Dennison, C. Sung, Partitioning and diffusion of solutes in hydrogels of poly(ethylene oxide), *Biomaterials* 14 (1993) 1117–1126.
- [252] G. Turco, I. Donati, M. Grassi, G. Marchioli, R. Lapasin, S. Paoletti, Mechanical Spectroscopy and Relaxometry on Alginate Hydrogels: A Comparative Analysis for Structural Characterization and Network Mesh Size Determination, *Biomacromolecules* 12 (2011) 1272–1282.
- [253] M.D. Correia, A.M. Souza, J.P. Sinnecker, R.S. Sarthour, B.C.C. Santos, W. Trevisan, I.S. Oliveira, Superstatistics model for T_2 distribution in NMR experiments on porous media, *J. Magn. Reson.* 244 (2014) 12–17.
- [254] S.W. Provencher, A constrained regularization method for inverting data represented by linear algebraic or integral equations, *Comput. Phys. Commun.* 27 (1982) 213–227.
- [255] X. Wang, Q. Ni, Determination of cortical bone porosity and pore size distribution using a low field pulsed NMR approach, *J. Orthop. Res.* 21 (2003) 312–319.
- [256] J. Schurz, Rheology of polymer solutions of the network type, *Prog. Polym. Sci.* 16 (1991) 1–53.

- [257] K. Brownstein, C. Tarr, Importance of classical diffusion in NMR studies of water in biological cells, *Phys. Rev. A* 19 (1979) 2446–2453.
- [258] M.M. Chui, R.J. Phillips, M.J. McCarthy, Measurement of the porous microstructure of hydrogels by nuclear magnetic resonance, *J. Colloid Interface Sci.* 174 (1995) 336–344.
- [259] G. Scherer, Hydraulic radius and mesh size of gels, *J. Sol-Gel Sci. Technol.* 1 (1994) 285–291.
- [260] T. Coviello, Guar gum/borax hydrogel: rheological, low field NMR and release characterizations, *Express. Polym. Lett.* 7 (2013) 733–746.
- [261] Y. Zhang, B.G. Amsden, Application of an Obstruction-Scaling Model To Diffusion of Vitamin B 12 and Proteins in Semidilute Alginate Solutions, *Macromolecules* 39 (2006) 1073–1078.
- [262] M. Holz, S.R. Heil, A. Sacco, Temperature-dependent self-diffusion coefficients of water and six selected molecular liquids for calibration in accurate ^1H NMR PFG measurements, *Phys. Chem. Chem. Phys.* 2 (2000) 4740–4742.
- [263] K.I. Momot, P.W. Kuchel, PFG NMR diffusion experiments for complex systems, *Concepts Magn. Reson.* 28A (2006) 249–269.
- [264] D. Venturoli, B. Rippe, Ficoll and dextran vs. globular proteins as probes for testing glomerular permselectivity: effects of molecular size, shape, charge, and deformability, *Am. J. Physiol. Renal Physiol.* 288 (2005) F605–13.
- [265] B. Amsden, An obstruction-scaling model for diffusion in homogeneous hydrogels, *Macromolecules* 32 (1999) 874–879.
- [266] J. Siepmann, F. Siepmann, Mathematical modeling of drug delivery, *Int. J. Pharm.* 364 (2008) 328–343.
- [267] L. Liu, P. Li, S.A. Asher, Entropic trapping of macromolecules by mesoscopic periodic voids in a polymer hydrogel, *Nature* 397 (1999) 141–144.

-
- [268] P.G. de Gennes, Reptation of a polymer chain in the presence of fixed obstacles, *J. Chem. Phys.* 55 (1971) 572.
- [269] S.K. Li, M.R. Liddell, H. Wen, Effective electrophoretic mobilities and charges of anti-VEGF proteins determined by capillary zone electrophoresis, *J. Pharm. Biomed. Anal.* 55 (2011) 603–607.
- [270] A.P. Chapman, PEGylated antibodies and antibody fragments for improved therapy: A review, *Adv. Drug Deliv. Rev.* 54 (2002) 531–545.
- [271] K.M. Ford, M. Saint-Geniez, T.E. Walshe, P.A. D'Amore, Expression and role of VEGF-a in the ciliary body, *Invest. Ophthalmol. Vis. Sci.* 53 (2012) 7520–7527.
- [272] C.P. Ryan, M.E.B. Smith, F.F. Schumacher, D. Grohmann, D. Papaioannou, G. Waksman, et al., Tunable reagents for multi-functional bioconjugation: reversible or permanent chemical modification of proteins and peptides by control of maleimide hydrolysis, *Chem. Commun.* 47 (2011) 5452–5454.
- [273] R.I. Nathani, V. Chudasama, C.P. Ryan, P.R. Moody, R.E. Morgan, R.J. Fitzmaurice, et al., Reversible protein affinity-labelling using bromomaleimide-based reagents, *Org. Biomol. Chem.* 11 (2013) 2408–2411.
- [274] R.P. Lyon, J.R. Setter, T.D. Bovee, S.O. Doronina, J.H. Hunter, M.E. Anderson, et al., Self-hydrolyzing maleimides improve the stability and pharmacological properties of antibody-drug conjugates, *Nat. Biotechnol.* 32 (2014) 1059–1062.
- [275] M. Abrishami, S. Zarei-Ghanavati, D. Soroush, M. Rouhbakhsh, M.R. Jaafari, B. Malaekheh-Nikouei, Preparation, characterization, and in vivo evaluation of nanoliposomes-encapsulated bevacizumab (avastin) for intravitreal administration, *Retina* 29 (2009) 699–703.
- [276] J.S. Andrew, E.J. Anglin, E.C. Wu, M.Y. Chen, L. Cheng, W.R. Freeman, M.J. Sailor, Sustained release of a monoclonal antibody from electrochemically prepared mesoporous silicon oxide, *Adv. Funct. Mater.* 20 (2010) 4168–4174.

- [277] F. Li, B. Hurley, Y. Liu, B. Leonard, M. Griffith, Controlled release of bevacizumab through nanospheres for extended treatment of age-related macular degeneration, *Open Ophthalmol. J.* 6 (2012) 54–58.
- [278] C.K. Pan, C. Durairaj, U.B. Kompella, O. Agwu, O.C.N. Scott, H. Quiroz-Mercado, et al., Comparison of long-acting bevacizumab formulations in the treatment of choroidal neovascularization in a rat model, *J. Ocul. Pharmacol. Ther.* 27 (2011) 219–224.
- [279] P. Tyagi, M. Barros, J.W. Stansbury, U.B. Kompella, Light-activated, in situ forming gel for sustained suprachoroidal delivery of bevacizumab, *Mol. Pharmaceutics* 10 (2013) 2858–2867.
- [280] C.-H. Wang, Y.-S. Hwang, P.-R. Chiang, C.-R. Shen, W.-H. Hong, G.-H. Hsiue, Extended release of bevacizumab by thermosensitive biodegradable and biocompatible hydrogel, *Biomacromolecules* 13 (2012) 40–48.
- [281] X. Xu, Y. Weng, L. Xu, H. Chen, Sustained release of Avastin[®] from polysaccharides cross-linked hydrogels for ocular drug delivery, *Int. J. Biol. Macromol.* 60 (2013) 272–276.

List of Figures

1.1.	Sustained release of entrapped antibodies.....	3
1.2.	Principle of DA reaction for <i>in situ</i> hydrogel formation.....	5
1.3.	Modification of eight-armed PEG.....	6
2.1.	Application sites of hydrogels in ophthalmology	12
2.2.	Chemical structures of selected polymers from natural sources commonly used for the preparation of hydrogels	13
2.3.	Chemical structures of synthetic polymers commonly used for the preparation of hydrogels.....	14
3.1.	Rheogram of a 15% (w/v) 4armPEG10k-hydrogel.....	44
3.2.	Dependence of gelation time (A) and stiffness (B) on concentration, branching factor and molecular weight of the macromonomers.....	44
3.3.	Correlation between the theoretical number of moles of elastically active chains (v_e) and the observed stiffness after cross-linking.	46
3.4.	Swelling and degradation of DA hydrogels as a function of polymer concentration and branching factor.....	49
3.5.	^1H -NMR spectra of 5% (w/v) 4armPEG10k-hydrogels in D_2O	50
3.6.	Correlation between the theoretical number of moles of elastically active chains (v_e) after cross-linking and the observed degradation time.....	51
4.1.	Hydrolytic stability of 8armPEG10k-maleimide at 37 °C and different pH-values (A), and at pH 7.4 and different temperatures (B).....	60
4.2.	Influence of the pH on the gel time (A) and stiffness (B) of DA hydrogels.....	62
4.3.	Swelling and degradation of 10% (w/v) 8armPEG10k-hydrogel.	65
4.4.	Comparison of the predicted ($3 \cdot t_{1/2}$) and observed degradation times at pH 7.4 and different temperatures.....	66
4.5.	Possible reaction pathways connecting different maleimide/furan-complexes in the presence of a water molecule and an OH^- -ion.	68

4.6. Semi-empirical MD simulations of the ring-opening reaction	69
5.1. Volumetric swelling ratio (A) and average mesh size (B) of 10% (w/v) 8armPEG10k hydrogels	79
5.2. (A) Absolute value of the complex shear modulus <i>vs.</i> oscillatory stress for 10% (w/v) 8armPEG10k hydrogels. (B) Storage and loss modulus <i>vs.</i> oscillatory frequency for 10% (w/v) 8armPEG10k hydrogels.....	80
5.3. (A) Signal intensity, related to the decay of the transverse component of the magnetization vector, <i>vs.</i> time. (B) Continuous distribution of the mesh size, $A(\xi)$, of 10% (w/v) 8armPEG10k hydrogels	84
5.4. (A) High (D_1) and low (D_2) self-diffusion coefficients of water molecules <i>versus</i> the square root of the diffusion time. (B) $A_1\%$ and $A_2\%$ represent the relative abundance of the fast and slow diffusing species, respectively	85
5.5. (A) Diffusion quotients of fluorescein isothiocyanate-labeled dextrans <i>vs.</i> time. (B) Predicted release of FDs from 10% (w/v) 8armPEG10k hydrogels.....	87
5.6. Release of fluorescein isothiocyanate-labeled dextrans (FDs) from 10% (w/v) 8armPEG10k hydrogels	88
5.7. Release of bevacizumab from 10% (w/v) 8armPEG10k hydrogels	90
6.1. Hydrolytic stability 8armPEG20k-Mal, 8armPEG20k-Ahx-Mal and 8armPEG20k-Lys-Ahx-Mal ₂	101
6.2. Gelation kinetics of 8armPEG20k- (A), 8armPEG20k-Ahx- (B) and 8armPEG20k-Lys-Ahx-hydrogels (C).....	103
6.3. Gel time (A) and stiffness (B) of different DA hydrogels	105
6.4. Swelling and degradation of 10% (w/v) 8armPEG20k-, 8armPEG20k-Ahx- and 8armPEG20k-Lys-Ahx-hydrogels	108
6.5. Network architecture of different DA hydrogels.	108
6.6. Cumulative release of bevacizumab from 10% (w/v) 8armPEG20k-, 8armPEG20k-Ahx- and 8armPEG20k-Lys-Ahx-hydrogels	110
7.1. DA hydrogels degraded due to rDA reaction and subsequent hydrolysis of maleimide to unreactive maleamic acid	121

List of Schemes

3.1	Chemical structures of 4armPEG-maleimide and 8armPEG-furan	37
3.2	Diels-Alder reaction of a PEG-maleimide and a furyl-substituted PEG	40
4.1	Potential degradation pathways of DA hydrogels	56
6.1	Cross-linking of 8armPEG20k-Fur and 8armPEG20k-Mal	96
6.2	Functional end-groups of 8armPEG20k-Ahx-Fur, 8armPEG20k-Ahx-Mal, 8armPEG20k-Lys-Ahx-Fur ₂ and 8armPEG20k-Lys-Ahx-Mal ₂	98
6.3	Functional end-groups of 1, 2a and 2b	112
6.4	Synthesis of 3 from 1 and Boc-6-aminohexanoic acid	113
6.5	Synthesis of 4 by deprotection of 3	114
6.6	Functional end-groups of 5a and 5b	114
6.7	Synthesis of 6 from 1 and Fmoc-Lys(Boc)-OH	115
6.8	Synthesis of 7 by deprotection of 6	115
6.9	Synthesis of 8 from 7 and Boc-6-aminohexanoic acid	116
6.10	Synthesis of 9 by deprotection of 8	117
6.11	Functional end-groups of 10a and 10b	117

List of Tables

2.1	Conventional hydrogel materials used for the preparation of corrective soft contact lenses	20
2.2	Silicone hydrogels used for the preparation of corrective soft contact lenses...	20
3.1	Calculated network mesh sizes of the prepared hydrogels.....	47
4.1	Pseudo-first-order rate constants (k_{obs}) of the ring-opening hydrolysis and half-lives ($t_{1/2}$) of 8armPEG10k-maleimide at 37 °C and different pH-values	61
4.2	Pseudo-first-order rate constants (k_{obs}) of the ring-opening hydrolysis and half-lives ($t_{1/2}$) of 8armPEG10k-maleimide at pH 7.4 and different temperatures	61
5.1	Transverse relaxation times (T_{2i}) of protons of water molecules entrapped in polymer meshes of size ξ_i	82
5.2	Mesh size of 10% (w/v) 8armPEG10k hydrogels	83
5.3	Relative molecular mass (M_r), hydrodynamic radius (R_h) and diffusion coefficient in water (D_0).....	82
6.1	Calculated rate constants (k_{obs}) of the ring-opening reaction and half-lives ($t_{1/2}$) of 8armPEG20k-Mal, 8armPEG20k-Ahx-Mal and 8armPEG20k-Lys-Ahx-Mal ₂	102
6.2	Second order rate constants (k) of the DA reaction in 8armPEG20k, 8armPEG20k-Ahx and 8armPEG20k-Lys-Ahx hydrogels.....	104
6.3	Average mesh size (ξ) of 8armPEG20k, 8armPEG20k-Ahx and 8armPEG20k-Lys-Ahx hydrogels derived from swelling data.....	107

Appendix

Abbreviations

ADH.....	adipic dihydrazide
Ahx.....	6-aminohexanoic acid
AMA.....	allyl methacrylate
AMD.....	age-related macular degeneration
ANOVA.....	analysis of variance
DA.....	Diels-Alder
DCC.....	<i>N,N'</i> -dicyclohexylcarbodiimide
DCM.....	dichloromethane
DIAD.....	diisopropyl azodicarboxylate
DIPEA.....	<i>N,N'</i> -diisopropylethylamine
DMAA.....	<i>N,N'</i> -dimethyl acrylamide
DMF.....	dimethylformamide
EDC.....	1-ethyl-3-(3-dimethylaminopropyl)carbodiimide
EGDMA.....	ethylene glycol dimethacrylate
EGF.....	epidermal growth factor
ESHU.....	poly(ethylene glycol)-poly-(serinol hexamethylene urethane)
ETPI.....	3,6-epoxy-1,2,3,6-tetrahydrophthalimide
¹ H-NMR.....	proton nuclear magnetic resonance
HA.....	hyaluronic acid
HOSu.....	<i>N</i> -hydroxysuccinimide
MC.....	methyl cellulose
HEMA.....	2-hydroxyethyl methacrylate
HPMC.....	(hydroxypropyl)methyl cellulose
IOL.....	intraocular lenses
Lys.....	lysine
MAA.....	methacrylic acid

Abbreviations

MAEBTP	4-(2-methacryloyloxyethyl)-2-(2H-benzotriazol-2-yl)phenol
MES	2-(<i>N</i> -Morpholino)ethanesulfonic acid
MPC	2-methacryloxyethyl phosphorylcholine
mPDMS	monofunctional polydimethylsiloxane
NCVE	<i>N</i> -carboxyvinyl ester
NHS	<i>N</i> -hydroxysuccinimide
NVP	<i>N</i> -vinylpyrrolidone
PAA	poly(acrylic acid)
PBVC	poly(dimethylsiloxyl)di-(silylbutanol)bis-(vinyl carbamate)
PCO	posterior capsule opacification
PDMS	poly(dimethylsiloxane)
PDR	proliferative diabetic retinopathy
PEG	poly(ethylene glycol)
4armPEG10k-OH	four-armed poly(ethylene glycol), molecular weight 10 kDa
8armPEG10k-OH	eight-armed poly(ethylene glycol), molecular weight 10 kDa
8armPEG20k-OH	eight-armed poly(ethylene glycol), molecular weight 20 kDa
PEPGDMA	poly(ethylene propylene glycol) dimethacrylate
pHEMA	poly(2-hydroxyethyl methacrylate)
PNIPAAm	poly(<i>N</i> -isopropylacrylamide)
PVA	poly(vinyl alcohol)
rDA	retro-Diels-Alder
RPC	retinal progenitor cells
RSC	retinal stem cells
SCL	soft contact lenses
SEMD	semi-empirical molecular dynamics
SiGMA	methylbis-(trimethylsiloxy)silylpropylglyceryl methacrylate
SMA	sodium methacrylate
STMP	trisodium trimetaphosphate
TBHMA	4-tert-butyl-2-hydroxycyclohexyl methacrylate
TRIM	1,1,1-tris(hydroxymethyl)propane trimethacrylate
TRIS	methacryloxypropyl tris(trimethylsiloxy silane)
USAN	United States adopted name
UV	ultraviolet
VEGF	vascular endothelial growth factor

Symbols

α	conversion of functional groups at the gel point
$a(T_2)$	unknown amplitude of the spectral component at relaxation time T_2
A_i	dimensionless pre-exponential factor
A_t	measured amplitudes of the echo with the gradient applied
A_0	measured amplitudes of the echo without the gradient applied
A_{0i}	fractions of water molecules characterized by D_i
c	concentration
c_{max}	maximum plasma concentration
C_n	Flory characteristic ratio
χ_1	Flory-Huggins interaction parameter for PEG in water
D_g	diffusion coefficient of the solute in the hydrogel
D_i	self-diffusion coefficient
D_0	diffusion coefficients in water
δ	chemical shift
δ	dihedral angle
η	viscosity of water
η_i	viscosity of the dashpot component
f	branching factor of the macromonomers
f	number of functional groups for cross-linking
G	shear modulus
G'	storage modulus
G''	loss modulus
$ G^* $	absolute value of the complex shear modulus
G_e	spring constant of the last, purely elastic Maxwell element
G_i	spring constant of the i^{th} Maxwell element
g	magnetic field gradient
γ	gyromagnetic ratio of the protons

Symbols

h	height of the gel cylinder
k	Boltzmann constant
k_{obs}	hydrolysis rate constants
k_Q	rate constant of the swelling process
k_ξ	rate constant of the mesh size increasing process
I_s	signal intensity
l	average bond length along the PEG backbone
λ_{em}	emission wavelength
λ_{ex}	excitation wavelength
λ_i	relaxation time of the i^{th} Maxwell element
$\langle \mathcal{M} \rangle$	relaxation sink strength (length / time)
M_t	absolute cumulative amounts released at time t
\bar{M}_c	average molecular weight between cross-links
m_p	mass of the polymer in the hydrogel
M_r	molecular mass of the PEG repeating unit
M_∞	absolute cumulative amounts released at infinity
N_A	Avogadro constant
n	number of considered Maxwell elements
ω	angular frequency
ρ_x	cross-link density
ϕ	polymer volume fraction of the hydrogel
Q	volumetric swelling ratio
q_n	roots of the Bessel function of the first kind of zero order
R	universal gas constant
R_f	radius of the polymer chain
R_h	hydrodynamic radius
r	radius of the gel cylinder
σ	oscillatory stress
T	temperature
T_2	transverse relaxation time
$\langle 1/T_2 \rangle$	average value of the inverse relaxation time
t	time
t_d	diffusion time of the water molecules
$t_{1/2}$	half-live time

ν_e	number of moles of elastically active chains in the hydrogel network
ν_{2c}	polymer fraction of the gel after cross-linking
ν_{2s}	polymer fraction of the gel in the swollen state
V_1	molar volume of the swelling agent
V_{gc}	gel volume after cross-linking
V_{gs}	gel volume after swelling
V_p	volume of the dry polymer
ξ	network mesh size
ξ_{avg}	average network mesh size

Curriculum Vitae

Personal data

Name: Susanne Kirchhof
Date of birth: 31th of January, 1985
Place of birth: Bobingen
Nationality: German
Marital Status: Single

Work Experience

02/2015 Teammanager
Vetter Pharma-Fertigung GmbH & Co. KG, Ravensburg

Professional training

08/2010 -01/2015 PhD program at the Department of Pharmaceutical Technology
University of Regensburg (Prof. Dr. Achim Goepferich)
07/2010 Approbation als Apotheker
(Acquisition of the license to practice as pharmacist)
11/2009 – 04/2010 Practical training, Herrenbach-Apotheke, Augsburg
05/2009 –10/2009 Practical training, F. Hoffmann-La Roche AG, Basel,
Switzerland
09/2007 – 02/2008 Erasmus semester, University of Vienna, Austria
10/2004 – 04/2009 Pharmaceutical studies, University of Regensburg

Education

06/2004	Allgemeine Hochschulreife (General qualification for university entrance)
09/1995 – 06/2004	Gymnasium Maria Stern, Augsburg (Grammar school)
09/1991 – 07/1995	Laurentius-Schule, Bobingen (Primary school)

List of Publications

Publications in scientific journals

Susanne Kirchhof, Michela Abrami, Viktoria Messmann, Nadine Hammer, Achim M. Goepferich, Mario Grassi, and Ferdinand P. Brandl, Diels-Alder hydrogels for controlled antibody release: Correlation between mesh size and release rate, *Mol. Pharm* 12 (2015) 3358-3368. **(Chapter 5)**

Susanne Kirchhof, Manuel Gregoritz, Viktoria Messmann, Nadine Hammer, Achim M. Goepferich and Ferdinand P. Brandl, Diels-Alder hydrogels with enhanced stability: First steps towards controlled release of bevacizumab. *Eur. J. Pharm. Biopharm. Eur. J. Pharm. Biopharm.* 96 (2015) 217-255. **(Chapter 6)**

Susanne Kirchhof, Achim M. Gopeferich and Ferdinand P. Brandl, Hydrogels in ophthalmic applications. *Eur. J. Pharm. Biopharm.* 95, (2015) 227–238. **(Chapter 1)**

Robert Hennig, Anika Vesper, **Susanne Kirchhof** and Achim M. Goepferich, Branched polymer-drug conjugates for multivalent blockade of angiotensin II receptors, *Mol. Pharm.* 12 (2015) 3292–3302.

Susanne Kirchhof, Andrea Strasser, Hans-Joachim Wittmann, Viktoria Messmann, Nadine Hammer, Achim M. Goepferich, Ferdinand P. Brandl, New insights into the cross-linking and degradation mechanism of Diels-Alder hydrogels, *J. Mater. Chem. B* 2 (2015) 449–457. **(Chapter 4)**

Nadine Hammer, Ferdinand P. Brandl, **Susanne Kirchhof** and Achim M. Goepferich, Protein Compatibility of Selected Cross-linking Reactions for Hydrogels, *Macromol. Biosci.* 15 (2015) 405–413.

Nadine Hammer, Ferdinand P. Brandl, **Susanne Kirchhof** and Achim M. Goepferich, Cleavable carbamate linkers for controlled protein delivery from hydrogels, *J. Control. Release* 183 (2014) 67–76.

Susanne Kirchhof, Ferdinand P. Brandl, Nadine Hammer, Achim M. Goepferich, Investigation of the Diels–Alder reaction as a cross-linking mechanism for degradable poly(ethylene glycol) based hydrogels, *J. Mater. Chem. B* 1 (2013) 4855–4864.

(Chapter 3)

Patent

Achim Goepferich, Ferdinand Brandl and **Susanne Kirchhof**. Production of hydrogels by means of Diels-Alder reaction. WO 2013/068397 A1 (2012).

Scientific talk

Ferdinand Brandl, **Susanne Kirchhof**, Nadine Hammer, Viktoria Messmann and Achim Goepferich. Development and pharmaceutical applications of Diels-Alder hydrogels. Deutsche Pharmazeutische Gesellschaft Annual Meeting, Greifswald, Germany (2012).

Conference abstracts

Nadine Hammer, Ferdinand Brandl, **Susanne Kirchhof**, and Achim Goepferich. Carbamate linkers for controlled protein release from hydrogels. 9th Worldmeeting on Pharmaceutics, Biopharmaceutics and Pharmaceutical Technology, Lisbon, Portugal (2014).

Susanne Kirchhof, Ferdinand Brandl, Nadine Hammer and Achim Goepferich. Degradable poly(ethylene glycol) based hydrogels crosslinked by Diels-Alder click-reaction. 9th Worldmeeting on Pharmaceutics, Biopharmaceutics and Pharmaceutical Technology, Lisbon, Portugal (2014).

Nadine Hammer, Ferdinand Brandl, **Susanne Kirchhof**, and Achim Goepferich. Degradation controlled protein release from Diels-Alder hydrogels. 246th American Chemical Society National Meeting & Exposition, Indianapolis, USA (2013).

Susanne Kirchhof, Ferdinand Brandl, Nadine Hammer and Achim Goepferich. Investigation of the degradation mechanism of Diels-Alder hydrogels. 246th American Chemical Society National Meeting & Exposition, Indianapolis, USA (2013).

Susanne Kirchhof, Ferdinand Brandl, Nadine Hammer, Viktoria Messmann, Joerg Tessmar and Achim Goepferich. Poly(ethylene glycol) based Diels-Alder hydrogels for biomedical applications. Society for Biomaterials Annual Meeting & Exposition, Boston, USA (2013).

Nadine Hammer, Ferdinand Brandl, **Susanne Kirchhof**, and Achim Goepferich. Protein Mobility in Diels-Alder Hydrogels. Controlled Release Society Local Chapter Meeting, Ludwigshafen, Germany (2013).

Susanne Kirchhof, Ferdinand Brandl, Nadine Hammer and Achim Goepferich. Diels-Alder hydrogels with defined mesh size for controlled drug delivery. Controlled Release Society Local Chapter Meeting, Ludwigshafen, Germany (2013).

Nadine Hammer, Ferdinand Brandl, **Susanne Kirchhof**, Viktoria Messmann, Joerg Tessmar and Achim Goepferich. Hydrogels for drug delivery: hydrolytically cleavable carbamate linkers for time controlled protein release. Deutsche Pharmazeutische Gesellschaft Annual Meeting, Greifswald, Germany (2012).

Susanne Kirchhof, Ferdinand Brandl, Nadine Hammer, Viktoria Messmann, Joerg Tessmar and Achim Goepferich. Hydrogels for drug delivery: influence of macromer branching on characteristics of poly(ethylene glycol) based hydrogels. Deutsche Pharmazeutische Gesellschaft Annual Meeting, Greifswald, Germany (2012).

Susanne Kirchhof, Ferdinand Brandl, Nadine Hammer, Joerg Tessmar and Achim Goepferich. Application of the Diels-Alder reaction as a new cross-linking mechanism for poly(ethylene glycol) based hydrogels. 244th American Chemical Society National Meeting & Exposition. Philadelphia, USA (2012).

Nadine Hammer, Ferdinand Brandl, **Susanne Kirchhof**, Joerg Tessmar and Achim Goepferich. Time controlled protein delivery by hydrolytically cleavable poly(ethylene glycol) linkers. 9th World Biomaterial Congress, Chengdu, China (2012)

Nadine Hammer, Ferdinand Brandl, **Susanne Kirchhof**, Joerg Tessmar and Achim Goepferich. Hydrogels for drug delivery: hydrolytically cleavable linkers for time

controlled protein release. Controlled Release Society Local Chapter Meeting, Würzburg, Germany (2012).

Susanne Kirchhof, Ferdinand Brandl, Nadine Hammer, Joerg Tessmar and Achim Goeperich. Investigation of novel poly(ethylene glycol) based hydrogels as delivery systems for peptides and proteins. Controlled Release Society Local Chapter Meeting, Würzburg, Germany (2012).

Eva Esser, **Susanne Kirchhof**, Ferdinand Brandl, Achim Goeperich and Joerg Tessmar. Biodegradable polymer films for adhesion prophylaxis – Influence of plasticizers and calcium on the stability and elasticity of alginate films. Deutsche Gesellschaft für Biomaterialien Annual Meeting, Gießen, Germany (2011).

Susanne Kirchhof, Ferdinand Brandl, Nadine Hammer, Joerg Tessmar and Achim Goeperich. Hydrogels for drug delivery: Investigation of the Diels-Alder click reaction as a new cross-linking mechanism. Deutsche Gesellschaft für Biomaterialien Annual Meeting, Gießen, Germany (2011).

Acknowledgments

An dieser Stelle möchte ich mich ganz herzlich bei allen bedanken, die mich in den letzten Jahren unterstützt und damit ganz maßgeblich zum Gelingen dieser Arbeit beigetragen haben.

Mein besonderer Dank gilt Herrn Prof. Dr. Achim Göpferich für die Möglichkeit an diesem spannenden Thema arbeiten zu dürfen, seine Unterstützung bei dessen Bearbeitung und die Möglichkeit zur Verwirklichung meiner eigenen Ideen. Die zahlreichen Diskussionen und Anregungen waren immer sehr hilfreich für mich. Darüber hinaus möchte ich mich auch für die vielfältigen Gelegenheiten bedanken, meine wissenschaftlichen Ergebnisse auf nationalen und internationalen Kongressen präsentieren zu dürfen.

Herrn Dr. Ferdinand Brandl danke ich sehr für die äußerst engagierte Betreuung der Arbeit und sein stetes Interesse am Fortgang der Experimente, selbst über den Atlantik hinweg. Seine vielfältigen Anregungen, die motivierenden Diskussionen und Ratschläge waren eine große Stütze im Laboralltag. Insbesondere bedanke ich mich für seine Hilfe bei Anfertigung zahlreicher Manuskripte.

Herrn Dr. Jörg Tessmar danke ich für seine Anregungen, sein Engagement und seine große Hilfsbereitschaft.

Frau PD Dr. Andrea Straßer und Herrn Dr. Hans-Joachim Wittmann danke ich für die SEMD-Simulierung des DA- und rDA-Komplexes.

Herrn Prof. Dr. Mario Grassi und Michela Abrami danke ich für die Durchführung der low field NMR-Messungen und die Hilfe bei der Auswertung von rheologischen Messungen.

Herrn Dr. Andreas Ohlmann danke ich für die gute Zusammenarbeit und tatkräftige Unterstützung bei der Durchführung von unzähligen Versuchen.

Frau PD Dr. Kerstin Galler und Andreas Eidt danke ich für die gute Kooperation im „Pulparegenerations“-Projekt.

Frau Viktoria Meßmann danke ich sehr für die äußerst engagierte und selbständige Unterstützung bei der Durchführung von Synthesen und Messungen. Viki, auf dich war immer Verlass!

Für die finanzielle Unterstützung des Projektes „Bioabbaubare Hydrogele für die lokale Verabreichung von Protein- und Nuklearsäurewirkstoffen im Auge“ (GO 565/16-1) möchte ich mich bei der Deutschen Forschungsgemeinschaft bedanken.

Nicht zuletzt gilt mein Dank allen aktuellen und ehemaligen Kollegen am Lehrstuhl für Pharmazeutische Technologie für die unkomplizierte Zusammenarbeit und die angenehme gemeinsame Zeit:

Insbesondere danke ich:

Dr. Eva Christina Wurster für die lustige Laborgemeinschaft, die Freundschaft und die nette Reisebegleitung bei größeren und kleineren Abenteuern.

Robert Hennig für die anregenden Diskussionen, die schönen Gespräche und natürlich für die täglichen Flurkonzerte – ich musste wirklich oft schmunzeln.

Michael Backofen für den Beistand bei Computerproblemen und die unkomplizierte Hilfsbereitschaft.

Eva Esser und Martina Kessler für die gemeinsame Zeit.

Nadine Hammer und Manuel Gregoritzka für die Zusammenarbeit im „Hydrogel“-Projekt.

Eva Wrobel für die unkomplizierte Unterstützung bei allen organisatorischen Angelegenheiten und die netten Gespräche zwischendurch.

Den technischen Assistenten Angelika Berié, Andrea Blaimer, Renate Lieb, Stefan Kolb und Edith Schindler für die tatkräftige und unkomplizierte Hilfe, wo immer sie nur konnten,

Meinen Auszubildenden Theresa Ferstl, Patrick Hudzikovski, David Jokl, Veronica Scheidler und Anna Weigl danke ich für die gute Zusammenarbeit und die hilfreiche Unterstützung bei der Durchführung der Synthesen und Versuche.

Mein besonderer Dank gilt meiner Familie und Florian, die mich immer in allen Belangen unterstützten, meine Ideen und Bestrebungen förderten und mir damit ermöglicht haben mein Ziel zu verwirklichen.

Erklärung

Hiermit erkläre ich, dass ich die vorliegende Arbeit selbst verfasst habe und keine anderen als die angegebenen Hilfsmittel verwendet habe.

Regensburg, den 31. Juli 2015

Susanne Kirchhof